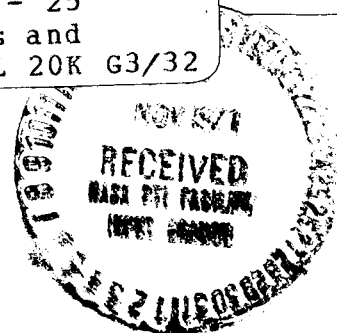


CR-121041

N72-12914 (NASA-CR-121041) RESPONSE OF AEROSPACE
STRUCTURES TO REENTRY AERODYNAMIC
EXCITATION Final Report, 26 Jun. 1970 - 25
Oct. D. Carlin, Jr. (Lockheed Missiles and
Space Co.) Oct. 1971 115 p CSCL 20K G3/32

Unclas
09774



Lockheed

HUNTSVILLE RESEARCH & ENGINEERING CENTER

LOCKHEED MISSILES & SPACE COMPANY

A GROUP DIVISION OF LOCKHEED AIRCRAFT CORPORATION

HUNTSVILLE, ALABAMA

Reproduced by
NATIONAL TECHNICAL
INFORMATION SERVICE
Springfield, Va. 22151

LOCKHEED MISSILES & SPACE COMPANY
HUNTSVILLE RESEARCH & ENGINEERING CENTER
HUNTSVILLE RESEARCH PARK
4800 BRADFORD DRIVE, HUNTSVILLE, ALABAMA

RESPONSE OF AEROSPACE
STRUCTURES TO REENTRY
AERODYNAMIC EXCITATION

FINAL REPORT

October 1971

Contract NAS8-26338

Prepared for National Aeronautics and Space Administration
Marshall Space Flight Center, Alabama 35812

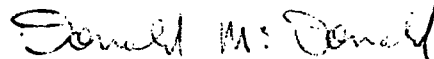
by

D. Carlin, Jr.

APPROVED:



W. L. Swanson, Supervisor
Acoustics Section



Donald McDonald, Manager
Structures & Mechanics Dept.



J. S. Farrior
Resident Director

FOREWORD

This report was prepared by Lockheed's Huntsville Research & Engineering Center, under Contract NAS8-26338, "Response of Aerospace Structures to Reentry Aerodynamic Excitation," for the George C. Marshall Space Flight Center of the National Aeronautics and Space Administration. The period of performance was from 26 June 1970 to 25 October 1971. The work was administered under the technical direction of the Astronautics Laboratory with J. B. Herring acting as the Contracting Officer's Representative.

ACKNOWLEDGEMENT

The author is grateful to Mr. R. A. Lott and Mr. B. W. George of Lockheed-Huntsville for their assistance in the aerodynamic excitation portion of this study.

SUMMARY

An extensive literature survey was conducted of aerodynamic excitation and associated structural response. A bibliography based on the survey is presented. Very little applicable data under actual reentry conditions was found. The survey did reveal many wind tunnel tests and some in-flight data.

A study was made of aerodynamic excitation and proposed space shuttle configurations and reentry trajectories. The study revealed that attached turbulent boundary layer, separated turbulent boundary layer and base pressure fluctuations are the regions of aerodynamic excitation most applicable to exterior panels of space shuttle-type vehicles. Prediction techniques are presented for these three aerodynamic environments.

An investigation was made of methods for predicting the response of panel structures to acoustic excitation. A normal mode approach was developed for the low frequency response and a statistical energy approach was utilized for the high frequency response.

A finite element model was made of a thermal protective system (TPS) test panel. The Structural Network Analysis Program (SNAP) was used to determine the natural frequencies and mode shapes of the panel. A computer program was generated to calculate the response of the panel to a reverberant acoustic field, using the normal mode approach developed for low frequency response. The power spectral densities of the response displacement and acceleration are presented.

CONTENTS

| Section | | Page |
|-------------|---|------|
| | FOREWORD | ii |
| | SUMMARY | iii |
| | LIST OF ILLUSTRATIONS | v |
| | NOMENCLATURE | ix |
| 1 | INTRODUCTION | 1 |
| 2 | REENTRY AERODYNAMIC EXCITATION | 2 |
| | 2.1 Attached Turbulent Boundary Layer | 2 |
| | 2.2 Separated Turbulent Boundary Layer | 4 |
| | 2.3 Base Pressure Fluctuations | 5 |
| 3 | STRUCTURAL RESPONSE | 7 |
| | 3.1 Low Frequency Response | 7 |
| | 3.2 High Frequency Response | 14 |
| 4 | RESPONSE OF TPS TEST PANEL | 18 |
| | REFERENCES | 22 |
| | BIBLIOGRAPHY | 24 |
| Appendixes: | | |
| A | Analysis of Attached Turbulent Boundary Layer | A-1 |
| B | Response Computer Program | B-1 |

LIST OF ILLUSTRATIONS

| Figure | | Page |
|--------|--|------|
| 1 | Overall Fluctuating Pressure Level for Attached Turbulent Boundary Layer | 32 |
| 2 | Power Spectral Density for Attached Turbulent Boundary Layer (from Blake, Ref. 2) | 33 |
| 3 | Broad-Band Convection Velocities for Attached Turbulent Boundary Layer (from Bull, Ref. 3) | 34 |
| 4 | Narrow-Band Convection Velocities for Attached Turbulent Boundary Layer (from Bies, Ref. 4) | 35 |
| 5 | Longitudinal Broad-Band Spatial Correlations for Attached Turbulent Boundary Layer (from Bull, Ref. 3) | 36 |
| 6 | Lateral Broad-Band Spatial Correlations for Attached Turbulent Boundary Layer (from Bull, Ref. 3) | 37 |
| 7 | Longitudinal Coherence Function for Attached Turbulent Boundary Layer (from Blake, Ref. 2) | 38 |
| 8 | Lateral Coherence Function for Attached Turbulent Boundary Layer (from Blake, Ref. 2) | 39 |
| 9 | Separated Turbulent Flow Ahead of Cone Frustum (from Chyu & Hanly, Ref. 5) | 40 |
| 10 | Longitudinal Variation of Fluctuating Pressure in Separated Turbulent Flow (from Chyu & Hanly, Ref. 5) | 40 |
| 11 | Overall Fluctuating Pressure Level for Separated Turbulent Boundary Layer | 41 |
| 12 | Power Spectral Density of Separated Turbulent Boundary Layer (from Chyu and Hanly, Ref. 5) | 42 |
| 13 | Longitudinal Coherence Function for Separated Turbulent Boundary Layer (from Chyu and Hanly, Ref. 5) | 43 |

LIST OF ILLUSTRATIONS (Continued)

| Figure | | Page |
|--------|--|------|
| 14 | Lateral Space Correlation for Separated Turbulent Boundary Layer (from Chyu and Hanly, Ref. 5) | 44 |
| 15 | Maximum Base Fluctuating Pressure by Altitude | 45 |
| 16 | Power Spectral Density of Base Pressure Fluctuations | 46 |
| 17 | TPS Test Panel | 47 |
| 18 | Original Model of TPS Test Panel, View 1 | 48 |
| 19 | Original Model of TPS Test Panel, View 2 | 49 |
| 20 | Original Model of TPS Test Panel, View 3 | 50 |
| 21 | First Mode of the Original Model, View 1 | 51 |
| 22 | First Mode of the Original Model, View 2 | 52 |
| 23 | First Mode of the Original Model, View 3 | 53 |
| 24 | Revised Model of TPS Test Panel, View 1 | 54 |
| 25 | Revised Model of TPS Test Panel, View 2 | 55 |
| 26 | Revised Model of TPS Test Panel, View 3 | 56 |
| 27 | First Mode of the Revised Model, View 1 | 57 |
| 28 | First Mode of the Revised Model, View 2 | 58 |
| 29 | First Mode of the Revised Model, View 3 | 59 |
| 30 | Second Mode of the Revised Model, View 1 | 60 |
| 31 | Second Mode of the Revised Model, View 2 | 61 |
| 32 | Second Mode of the Revised Model, View 3 | 62 |

LIST OF ILLUSTRATIONS (Continued)

| Figure | | Page |
|--------|---|------|
| 33 | Third Mode of the Revised Model, View 1 | 63 |
| 34 | Third Mode of the Revised Model, View 2 | 64 |
| 35 | Third Mode of the Revised Model, View 3 | 65 |
| 36 | Fourth Mode of the Revised Model, View 1 | 66 |
| 37 | Fourth Mode of the Revised Model, View 2 | 67 |
| 38 | Fourth Mode of the Revised Model, View 3 | 68 |
| 39 | Fifth Mode of the Revised Model, View 1 | 69 |
| 40 | Fifth Mode of the Revised Model, View 2 | 70 |
| 41 | Fifth Mode of the Revised Model, View 3 | 71 |
| 42 | Power Spectral Density of the Pressure Field in the Reverberation Chamber Test | 72 |
| 43 | Power Spectral Density of the Response Displacement at P, Linear Scale, 4% Modal Damping | 73 |
| 44 | Power Spectral Density of the Response Displacement at P, Log-Log Scale, 4% Modal Damping | 74 |
| 45 | Power Spectral Density of the Response Acceleration at P, Linear Scale, 4% Modal Damping | 75 |
| 46 | Power Spectral Density of the Response Acceleration at P, Log-Log Scale, 4% Modal Damping | 76 |
| 47 | Power Spectral Density of the Response Displacement at P, Linear Scale, 5% Modal Damping | 77 |
| 48 | Power Spectral Density of the Response Displacement at P, Log-Log Scale, 5% Modal Damping | 78 |
| 49 | Power Spectral Density of the Response Acceleration at P, Linear Scale, 5% Modal Damping | 79 |

LIST OF ILLUSTRATIONS (Continued)

| Figure | | Page |
|--------|---|------|
| 50 | Power Spectral Density of the Response Acceleration at P, Log-Log Scale, 5% Modal Damping | 80 |
| A-1 | Broad Band Convection Velocities | A-14 |
| A-2 | Mean-Square Spectra of Wall Pressure Fluctuations | A-15 |
| A-3 | Variation of the rms Pressure Fluctuations Along the Tunnel Wall, $M_{\infty} = 0.42$ | A-16 |
| A-4 | Variation of the rms Pressure Fluctuations Along the Tunnel Wall, $M_{\infty} = 0.59$ | A-17 |
| A-5 | Narrow Band Convective Velocities | A-18 |

NOMENCLATURE

| | |
|-------------|--|
| \bar{a}^2 | mean-square acceleration |
| A | area of the panel |
| c | speed of sound in the acoustic medium |
| C_o | conversion constant |
| d | derivative |
| F | forcing function |
| G | power spectral density |
| h | height of cone frustrum |
| H | transfer function |
| i | $\sqrt{-1}$ |
| j_r^2 | joint acceptance squared |
| j_{rs}^2 | cross-joint acceptance squared |
| k_1 | unknown constant |
| K | kinetic energy |
| L_r | generalized force of the r^{th} mode |
| m_o | distributed mass |
| m_p | mass of the panel |
| m_r | generalized mass of the r^{th} mode |
| n | number of modes |
| n_a | modal density of acoustic medium |
| n_p | modal density of panel |
| p | root mean-square of the fluctuating pressure |

| | |
|-------------------|--|
| P | point on panel where response was calculated |
| q | freestream dynamic pressure |
| R | correlation function |
| $R_{\alpha\beta}$ | spatial correlation |
| t | time |
| u | panel coordinate |
| U_c | instantaneous broad-band convection velocity |
| \overline{U}_c | average broad-band convection velocity |
| $U_c(\omega)$ | narrow-band convection velocity |
| U_∞ | freestream velocity |
| v | panel coordinate |
| V | volume of acoustic medium |
| x | distance coordinate in the longitudinal direction |
| \overline{x} | vector panel coordinate |
| y | panel displacement |
| z | distance coordinate in the lateral direction |
| Z_r | modal impedance |
| γ | coherence function |
| δ^* | boundary layer displacement thickness |
| δ_j | frequency band width in radians per second |
| ζ_r | modal damping value |
| η_p | average modal loss factor for a panel mode |
| η_{pa} | average coupling loss factor for energy flow from a panel mode to an acoustic mode |
| λ | distance |
| ξ | generalized coordinate |

| | |
|------------|--|
| ρ | density |
| ϕ | phase angle of cross-spectral density |
| Φ | power spectral density of fluctuating pressure |
| ψ_r | mode shape of the r^{th} mode |
| ω | frequency in radians per second |
| ω_r | natural frequency of the r^{th} mode |

Subscripts

| | |
|----------|--|
| a | acoustic medium |
| c | convection |
| j | frequency interval index |
| l | panel coordinate location where response is calculated |
| m | modal average |
| p | panel |
| r | mode index |
| s | mode index |
| α | force and coordinate index |
| β | force and coordinate index |
| ∞ | freestream |

Superscripts

| | |
|---|--|
| * | complex conjugate (except δ^*) |
|---|--|

Section 1

INTRODUCTION

With the advent of the space shuttle concept for manned space flight, a new regime of aerodynamic excitation has evolved, that of the reentry noise environment of a lifting body. In order to cope with this new environment, information was needed on the nature and magnitude of this excitation and the expected response of space shuttle-type structure to this excitation. To help supply this information, Lockheed undertook this study of the response of aerospace structures to reentry aerodynamic excitation.

An extensive literature survey was made of aerodynamic noise data and associated structural response. A listing of the applicable documents reviewed is given in the Bibliography. The survey revealed very little usable data under actual reentry conditions. Consequently, the prediction techniques developed for reentry aerodynamic excitation are based primarily on the results of wind tunnel tests and flight measurements taken on airplanes. Analytical methods were then developed to calculate the expected response of the external panels of space shuttle-type vehicles to this excitation. The methods developed are also applicable for predicting the response of the structure to the expected acoustic excitation during liftoff and the response of test panels of the proposed exterior surface to reverberation chamber tests. The response analysis methods were used to predict the response of a Haynes 25 alloy L-605 thermal protection system test panel in a reverberation chamber test.

Section 2

REENTRY AERODYNAMIC EXCITATION

An extensive literature review of aerodynamic noise data and analyses of proposed space shuttle configurations and reentry trajectories revealed that the primary regions of aerodynamic excitation applicable to panels on the space shuttle are attached turbulent boundary layer, separated turbulent boundary layer and base pressure fluctuations. The attached turbulent boundary layer excitation is applicable to the bottom surfaces of the shuttle at the high angles of attack associated with high Mach numbers and to most protuberance-free surfaces at low angles of attack associated with low Mach numbers. Panels immediately in front of contour discontinuities and protuberances are excited by separated turbulent boundary layer. The base pressure fluctuations are applicable to the top surface of the shuttle at the high angles of attack associated with high Mach numbers.

Of these three excitation sources, the attached turbulent boundary layer has been the subject of the most extensive studies. The studies concerning separated turbulent boundary layer and base pressure fluctuations are less numerous and less detailed. In all cases, the primary sources of reliable data are wind tunnel tests. Most flight data suffer from instrumentation problems and/or unknown flow conditions and parameters. Consequently, in developing the prediction technique for the various flow conditions, flight measurements were used only in determining the overall fluctuating pressure levels. The power spectra, correlation functions and convection velocities were obtained from wind tunnel tests.

2.1 ATTACHED TURBULENT BOUNDARY LAYER

An analysis was made of the attached turbulent boundary layer. A detailed description of the boundary layer and the problems encountered in measuring boundary layer parameters and fluctuating pressures is given in Appendix A.

The literature review revealed considerable scatter in the measured data of attached turbulent boundary layers. Possible sources of this scatter include differences in microphone size, microphone mounting and surface roughness, wind tunnel noise and variations in flow parameters. Due to these wide variations in the data and the lack of data in certain Mach number ranges, a purely empirical approach could not be used for predicting the boundary-layer excitation. A combination of theoretical and empirical techniques was used.

The prediction techniques for the attached turbulent boundary layer were taken from the studies of Houbolt (Ref. 1), Blake (Ref. 2), Bull (Ref. 3) and Bies (Ref. 4). Houbolt was selected for this theory on the effect of Mach number on the overall fluctuating pressure level. Blake was selected because of his superior test conditions and instrumentation. Blake's experiments were conducted in the low turbulence acoustic wind tunnel at MIT and he used pinhole microphones to provide high frequency data without extensive transducer-size corrections. In many areas, Blake's results were in close agreement with previous investigators. Bull was selected as one of the earlier investigations whose results were verified by Blake and others. Bies made an empirical study of the aerodynamic noise data available up to 1966.

Houbolt's curve for overall fluctuating pressure level, expressed as the ratio (p/q) of the mean-square fluctuating pressure level to freestream dynamic pressure as a function of Mach number, is shown in Fig. 1 (lower curve). Houbolt's curve provides a good fit for the available data on very smooth surfaces. However, investigators have measured (p/q) 's of up to 0.02 for rough-surfaced space launch vehicles at subsonic Mach numbers. The proposed prediction curve for p/q for attached turbulent boundary layers is shown in Fig. 1 (upper curve). This curve was obtained by using an empirical factor of 0.02 instead of 0.007 as used by Houbolt for the subsonic turbulent boundary layer. All the reliable attached turbulent boundary layer data uncovered in the literature search fall on or beneath this prediction curve.

Figure 2 gives the power spectral density $\Phi(\omega)$ in terms of p/q from Fig. 1, freestream velocity (U_∞) and boundary layer displacement thickness (δ^*). This

curve was taken from Blake's curve (Ref. 2) for the attached turbulent boundary layer over a rough wall. The basic shape of the spectrum is in general agreement with the work of other investigators.

Figures 3 and 4 give the convection velocities of the flow in the longitudinal direction. The broad-band convection velocities were taken from the work of Bull (Ref. 3) and the narrow-band convection velocities were taken from the empirical data of Bies (Ref. 4).

Figures 5 and 6 give the longitudinal and lateral broad-band spatial correlations. These results of Bull (Ref. 3) are in close agreement with the work of a number of other investigators.

Figures 7 and 8 give the longitudinal and lateral coherence functions. The coherence function is the magnitude of the cross-power spectral density function. Figure 7 also gives the phase angle of the cross-power spectral density function for the longitudinal direction. These data from Blake (Ref. 2) are in agreement with the work of other investigators.

2.2 SEPARATED TURBULENT BOUNDARY LAYER

Several investigators have studied the separated turbulent boundary layer associated with contour discontinuities and protuberances. Chyu and Hanley investigated the separated flow on an ogive cylinder in front of a 45-degree cone frustum. Other investigators — Speaker and Ailman (Ref. 6) and Kistler (Ref. 7) — studied the separated flow due to forward-facing and aft-facing steps along wind tunnel walls.

Figures 9 and 10 are taken from Chyu and Hanly's investigation. These figures show the mechanism of the separated flow and the general level of the fluctuating pressures. It is noted that the levels are higher than the levels for the attached turbulent boundary layer. The power spectrum of the fluctuating pressure of the separated turbulent boundary layer has a higher percentage of its energy concentrated in the lower frequencies than the power spectrum of

the fluctuating pressure of the attached turbulent boundary layer. The oscillating shock wave, indicated by the sharp peak in the p/q curves in Fig. 10, is a very localized phenomenon, with most of the power concentrated in the very low frequencies.

The prediction techniques developed for the separated turbulent boundary layer are taken primarily from Chyu and Hanly (Ref. 5). The data associated with the steps were used only for enveloping the overall fluctuating pressure level, since these conditions are not expected on space shuttle configurations.

Figure 11 gives the overall fluctuating pressure level as a function of Mach number. This curve envelopes all the data found in the literature search on separated turbulent boundary due to contour discontinuities and protuberances.

Figures 12, 13 and 14 show the properties of the separated turbulent boundary layer based on the results of Chyu and Hanly. The power spectral density is shown in Fig. 12. Figure 13 presents the longitudinal coherence function. The lateral space correlation is shown in Fig. 14. The boundary layer displacement thickness indicated on these plots is the displacement thickness of the attached turbulent boundary layer immediately ahead of the separated region.

2.3 BASE PRESSURE FLUCTUATIONS

There are much less data available on base pressure fluctuations than there are on turbulent boundary layer. Most studies give only the overall fluctuating pressure level or the overall level and the power spectrum. A number of studies exist on the base pressure fluctuations of cone-shaped vehicles at low angles of attack. However, there are no data available at this time of the fluctuating pressure on the leeward side of a space shuttle-type vehicle at high angles of attack (50 to 60 degrees). Houbolt provided a means for determining a limiting value of the base fluctuating pressures at high altitudes. Houbolt theorized that since the pressure could never be negative, the root mean square fluctuating pressure at a point must be less

than 0.408 times the mean static pressure at the point. Since the static pressure at the base is generally less than the freestream static pressure, the maximum base fluctuating pressure can be determined as a function of altitude. Figure 15 shows this relationship. Since the space shuttle will pass through the high hypersonic Mach number range at altitudes over 150,000 ft, Fig. 15 indicates that base fluctuating pressures will not be a problem in this Mach number range.

The prediction technique developed for base pressure fluctuations at supersonic velocities are based on the results of Robinson, Gambucci and George (Ref. 8), Eldred (Ref. 9), Wiley and Seidl (Ref. 10), and Lockheed Missiles & Space Company (Ref. 11). The data indicated that the overall fluctuating pressure level is a function of freestream static pressure (p_∞), instead of freestream dynamic pressure as in the case of turbulent boundary layer. It is proposed that a constant p/p_∞ of 0.05 be used for all base pressure fluctuations. This value would envelope all the data found in the literature search.

Figure 16 gives the proposed prediction curve for the power spectral density of the base pressure fluctuations. There is an unknown constant, k_1 , associated with this curve that will have to be determined for the shuttle configuration. This results from the lack of a suitable non-dimensionalizing factor for the top of a shuttle-type vehicle. The spectrums presented in the literature were taken from bodies of revolution and used the diameter for the non-dimensionalizing factor. The basic shape of the spectrum, including rolloff rate, agrees with the results of Robinson, Gambucci and George (Ref. 8) and Eldred (Ref. 9).

Section 3

STRUCTURAL RESPONSE

Three general methods were initially considered for predicting the response of exterior panels on space shuttle-type vehicles to reentry aerodynamic excitation. They were: (1) classical dynamic equations of motion (normal mode approach), (2) statistical energy analysis, and (3) empirical and semi-empirical methods. However, two factors resulted in the elimination of empirical and semi-empirical methods from consideration. These factors are the complete lack of panel response data under reentry conditions and the complete change in panel structure from the Saturn vehicles to the shuttle-type vehicles that precluded use of Saturn test and ascent data. Consequently, solutions of the classical dynamic equations of motion are utilized to calculate the response in the low frequency modes and the statistical energy analysis is used to determine the high frequency response.

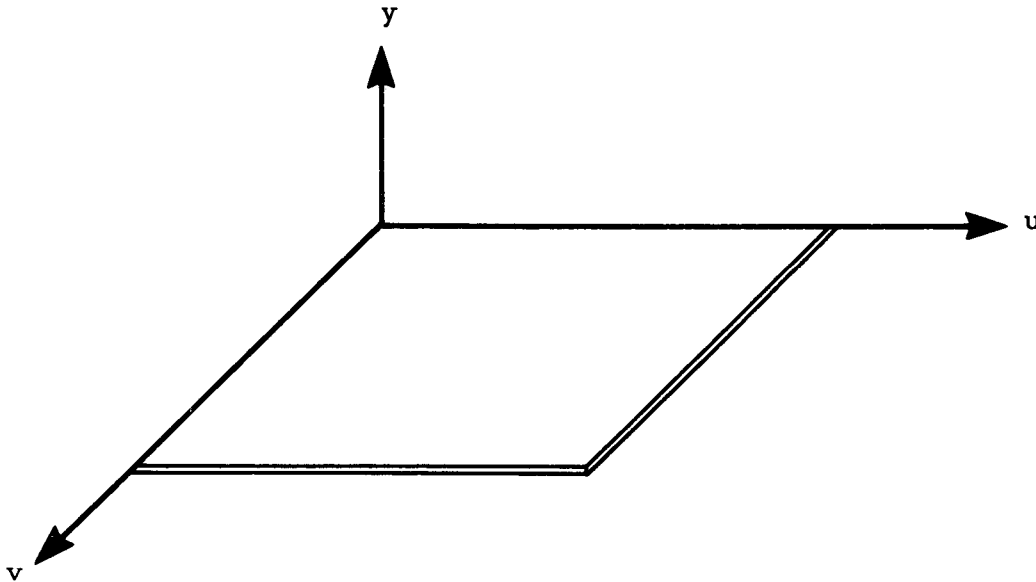
3.1 LOW FREQUENCY RESPONSE

The normal mode approach, utilizing the classical dynamic equations of motion, is used for the low frequency response. The method requires detailed information on natural frequencies, mode shapes and modal damping factors of the surface panels and the power spectral density and spatial correlation of the excitation field.

The natural frequencies and mode shapes are calculated with the Structural Network Analysis Computer Program (SNAP). SNAP is a finite-element program developed by Lockheed-Huntsville. The structure to be analyzed is modeled as a network of connected beam, plate, membrane and shell elements. The program computes the undamped vibrational frequencies and mode shapes using an iterative procedure analogous to the Stodola method of beam analysis. The instructions for utilizing SNAP are given in Ref. 12.

In using the normal mode method, it is assumed that the modes are uncoupled, so that the total response of the structure can be determined by adding up the responses of the individual modes. Although this assumption is theoretically true only for undamped structures, it is a good approximation for lightly-damped structures. A problem that arises in using the normal mode approach is the determination of the modal damping values. They must be either determined experimentally or estimated.

To derive the expression for the power spectral density of the response of a panel to an acoustic excitation field, we define a coordinate system for the panel. The following sketch shows the coordinate system.



Let $\bar{x} = (u, v)$ be the vector coordinate of a point on the panel. Let n be the number of modes to be utilized in the analysis.

First, we consider the response of the panel to a single forcing function, $F(t)$, applied at the point \bar{x}_1 . Equations of motion can be set up by the use of Lagrange's equations. Expressed in a set of normal coordinates, $\xi_1, \xi_2, \dots, \xi_n$, such that the response of the system at a time t is given by

$$y(\bar{x}, t) = \sum_{r=1}^n \xi_r(t) \psi_r(\bar{x}) \quad (1)$$

Lagrange's equation gives

$$\ddot{\xi}_r(t) + 2\zeta_r \omega_r \dot{\xi}_r(t) + \omega_r^2 \xi_r(t) = \frac{1}{m_r} L_r(t) \quad (2)$$

where

$\psi_r(\bar{x})$ = mode shape of the r^{th} mode

ζ_r = damping value for the r^{th} mode

ω_r = natural frequency of the r^{th} mode in radians per second

$m_r = \int_A m_o(\bar{x}) \psi_r^2(\bar{x}) d\bar{x}$ = generalized mass of the r^{th} mode

$L_r(t) = \psi_r(\bar{x}_1) F(t)$ = generalized force of the r^{th} mode

$m_o(\bar{x})$ = distributed mass of the panel

\int_A indicates integration over the total area of the panel.

Solving Eq. (2), we obtain

$$\xi_r(t) = \frac{\psi_r(\bar{x}_1) F(t)}{m_r(\omega_r^2 - \omega^2 + 2i \zeta_r \omega_r \omega)} \quad (3)$$

Substituting Eq. (3) into Eq. (1), we obtain for the response at the point \bar{x}_ℓ

$$y(\bar{x}_\ell, t) = H_{\ell 1}(\omega) F(t) \quad (4)$$

where

$$H_{\ell 1}(\omega) = \sum_{r=1}^n \frac{\psi_r(\bar{x}_1) \psi_r(\bar{x}_\ell)}{m_r (\omega_r^2 - \omega^2 + 2i \zeta_r \omega_r \omega)} \quad (5)$$

$H_{\ell 1}(\omega)$ is known as the transfer function. If $F(t)$ is a random forcing function, the power spectral density, $G_y(\bar{x}_\ell, \omega)$, of the displacement, $y(\bar{x}_\ell)$, is given by

$$G_y(\bar{x}_\ell, \omega) = |H_{\ell 1}(\omega)|^2 G_F(\omega) \quad (6)$$

where

$G_F(\omega)$ = power spectral density of the forcing function $F(t)$.

Next, we consider a number of forces, $F_1(t)$, $F_2(t)$, ..., $F_k(t)$, acting at the points, \bar{x}_1 , \bar{x}_2 , ..., \bar{x}_k , respectively. In this case, the relation shown in Eq. (6) becomes more complex due to possible correlations between the forcing functions as well as the increased number of forcing functions. For this case, the power spectral density of the response at \bar{x}_1 becomes

$$G_y(\bar{x}_\ell, \omega) = \sum_{\alpha=1}^k \sum_{\beta=1}^k H_{\ell \alpha}^*(\omega) H_{\ell \beta}(\omega) G_{\alpha \beta}(\omega) \quad (7)$$

where

$G_{\alpha \beta}(\omega)$ = cross-power spectral density of F_α and F_β .

* Indicates the complex conjugate.

We now return to the case of interest, where the forcing function is an acoustic excitation field. For this case, the double summation of Eq. (7) becomes a double integral to give

$$G_y(\bar{x}_\ell, \omega) = \int_A \int_A H_{\ell\alpha}^*(\omega) H_{\ell\beta}(\omega) G_{\alpha\beta}(\omega) d\bar{x}_\alpha d\bar{x}_\beta. \quad (8)$$

Modal impedance, $Z_r(\omega)$, of the r^{th} mode is defined by

$$Z_r(\omega) = m_r(\omega_r^2 - \omega^2 + 2i \zeta_r \omega_r \omega). \quad (9)$$

Combining Eqs. (5), (8) and (9) and simplifying gives

$$G_y(\bar{x}_\ell, \omega) = \sum_{r=1}^n \sum_{s=1}^n \frac{\psi_r(\bar{x}_\ell) \psi_s(\bar{x}_\ell)}{Z_r^*(\omega) Z_s(\omega)} \int_A \int_A \psi_r(x_\alpha) \psi_s(x_\beta) G_{\alpha\beta}(\omega) d\bar{x}_\alpha d\bar{x}_\beta. \quad (10)$$

Separating Eq. (10) into equal-mode terms and unequal-mode terms and multiplying by $\frac{A^2 \Phi(\omega)}{A^2 \Phi(\omega)}$, where $\Phi(\omega)$ is the power spectral density of the acoustic excitation field, gives

$$\begin{aligned} G_y(\bar{x}_\ell, \omega) = & A^2 \Phi(\omega) \sum_{r=1}^n \frac{\psi_r^2(\bar{x}_\ell)}{|Z_r(\omega)|^2} \int_A \int_A \frac{\psi_r(\bar{x}_\alpha) \psi_r(\bar{x}_\beta)}{A^2} \frac{G_{\alpha\beta}(\omega)}{\Phi(\omega)} d\bar{x}_\alpha d\bar{x}_\beta \\ & + A^2 \Phi(\omega) \sum_{r=1}^n \sum_{\substack{s=1 \\ s \neq r}}^n \frac{\psi_r(\bar{x}_\ell) \psi_s(\bar{x}_\ell)}{Z_r^*(\omega) Z_s(\omega)} \int_A \int_A \frac{\psi_r(\bar{x}_\alpha) \psi_s(\bar{x}_\beta)}{A^2} \frac{G_{\alpha\beta}(\omega)}{\Phi(\omega)} d\bar{x}_\alpha d\bar{x}_\beta. \end{aligned} \quad (11)$$

The joint acceptance squared, $j_r^2(\omega)$, is a measure of the correlation between the pressure field and the mode deflection. It is given by

$$j_r^2(\omega) = \int_A \int_A \frac{\psi_r(\bar{x}_\alpha) \psi_r(\bar{x}_\beta)}{A^2} \frac{G_{\alpha\beta}(\omega)}{\Phi(\omega)} d\bar{x}_\alpha d\bar{x}_\beta . \quad (12)$$

The cross-joint acceptance squared, $j_{rs}^2(\omega)$, is defined by

$$j_{rs}^2(\omega) = \int_A \int_A \frac{\psi_r(\bar{x}_\alpha) \psi_s(\bar{x}_\beta)}{A^2} \frac{G_{\alpha\beta}(\omega)}{\Phi(\omega)} d\bar{x}_\alpha d\bar{x}_\beta . \quad (13)$$

Substituting Eqs. (12) and (13) into Eq. (11) gives

$$\begin{aligned} G_y(\bar{x}_\ell, \omega) = & A^2 \Phi(\omega) \sum_{r=1}^n \frac{\psi_r^2(\bar{x}_\ell) j_r^2(\omega)}{|Z_r(\omega)|^2} \\ & + A^2 \Phi(\omega) \sum_{r=1}^n \sum_{\substack{s=1 \\ s \neq r}}^n \frac{\psi_r(\bar{x}_\ell) \psi_s(\bar{x}_\ell) j_{rs}^2(\omega)}{Z_r^*(\omega) Z_s(\omega)} . \end{aligned} \quad (14)$$

Since the cross-joint acceptance is generally very small compared with the joint acceptance, the second term in Eq. (14) is dropped to give

$$G_y(\bar{x}_\ell, \omega) = A^2 \Phi(\omega) \sum_{r=1}^n \frac{\psi_r^2(\bar{x}_\ell) j_r^2(\omega)}{|Z_r(\omega)|^2} . \quad (15)$$

Although the cross-power spectral density function, $G_{\alpha\beta}(\omega)$, in Eq. (12) is a complex function, the imaginary part integrates to zero. Therefore, $G_{\alpha\beta}(\omega)$

can be replaced by its real component. But the real component of $G_{\alpha\beta}(\omega)$ divided by $\Phi(\omega)$ defines the spatial correlation function, $R_{\alpha\beta}(\omega)$. Therefore, Eq. (12) simplifies to

$$j_r^2(\omega) = \frac{1}{A^2} \int_A \int_A \psi_r(\bar{x}_\alpha) \psi_r(\bar{x}_\beta) R_{\alpha\beta}(\omega) d\bar{x}_\alpha d\bar{x}_\beta . \quad (16)$$

Taking the absolute value of Eq. (9) and squaring gives

$$|Z_r(\omega)|^2 = m_r^2 \left[(\omega_r^2 - \omega^2)^2 + 4\zeta_r^2 \omega_r^2 \omega^2 \right] . \quad (17)$$

The power spectral density of the acceleration response, $G_{\ddot{y}}(\bar{x}_\ell, \omega)$, is given by

$$G_{\ddot{y}}(\bar{x}_\ell, \omega) = C_o \omega^4 G_y(\bar{x}_\ell, \omega) \quad (18)$$

where C_o is a conversion constant that depends on the units of the power spectral densities. If G_y is in inches²/radian and $G_{\ddot{y}}$ is desired in g²/radian, then $C_o = 0.6709 \times 10^{-5}$.

A Fortran computer program has been written to calculate the power spectral density of the displacement response and the acceleration response of a panel, utilizing the output tape from SNAP for the natural frequencies and mode shapes. The program is based on Eqs. (15) through (18), with the double integration being approximated by a double summation. A listing of the program is given in Appendix B.

3.2 HIGH FREQUENCY RESPONSE

Statistical energy analysis is used to estimate the high frequency response of the exterior panels on space shuttle-type vehicles. The statistical energy approach to response estimation was developed to handle high frequency vibrations. The method basically works with averages and eliminates the need for detailed information on natural frequencies and mode shapes. Lyon and Maidanik first postulated the technique in Ref. 13. Further work in this field was done by a number of other investigators, including Smith and Lyon (Ref. 14), Scharton (Ref. 15), and Ungar (Ref. 16). The following methods developed for space-shuttle panels are based on Ungar's results.

We consider a panel exposed to a diffuse sound field in a reverberation chamber. The total kinetic energy, $K_a(\omega_j, \delta_j)$, in the chamber in a frequency band, δ_j , centered at frequency ω_j is given by

$$K_a(\omega_j, \delta_j) = \frac{p^2(\omega_j, \delta_j) V}{2\rho_a c^2} \quad (19)$$

where

c = speed of sound in the acoustic medium

$p^2(\omega_j, \delta_j)$ = mean-square fluctuating pressure in the frequency band, δ_j , centered at frequency ω_j

V = volume of the acoustic medium

ρ_a = density of the acoustic medium.

The average kinetic energy per acoustic mode, $\langle K_a(\omega_j, \delta_j) \rangle_m$, in the frequency band, δ_j , centered at frequency ω_j is given by

$$\langle K_a(\omega_j, \delta_j) \rangle_m = \frac{K_a(\omega_j, \delta_j)}{n_a(\omega_j) \delta_j} \quad (20)$$

where

$n_a(\omega_j)$ = modal density of the acoustic medium at frequency ω_j .

The modal density, $n_a(\omega_j)$, of the acoustic medium is given by

$$n_a(\omega_j) = \frac{V \omega_j^2}{2\pi^2 c^3} \quad (21)$$

Substituting Eqs. (19) and (21) into Eq. (20) and simplifying gives

$$\langle K_a(\omega_j, \delta_j) \rangle_m = \frac{\pi^2 c p^2(\omega_j, \delta_j)}{\rho_a \omega_j^2 \delta_j} \quad (22)$$

The total kinetic energy, $K_p(\omega_j, \delta_j)$, of the panel in a frequency band, δ_j , centered at frequency ω_j is given by

$$K_p(\omega_j, \delta_j) = \frac{m_p \bar{a}^2(\omega_j, \delta_j)}{2\omega_j^2} \quad (23)$$

where

$\bar{a}^2(\omega_j, \delta_j)$ = mean-square acceleration of the panel in the frequency band, δ_j , centered at frequency ω_j .

m_p = mass of the panel.

The average kinetic energy per panel mode, $\langle K_p(\omega_j, \delta_j) \rangle_m$, in the frequency band, δ_j , centered at frequency ω_j is given by

$$\langle K_p(\omega_j, \delta_j) \rangle_m = \frac{K_p(\omega_j, \delta_j)}{n_p(\omega_j) \delta_j} \quad (24)$$

where

$n_p(\omega_j)$ = modal density of the panel at frequency ω_j .

Substituting Eq. (23) into Eq. (24) gives

$$\langle K_p(\omega_j, \delta_j) \rangle_m = \frac{m_p^{-2}(\omega_j, \delta_j)}{2\omega_j^2 n_p(\omega_j) \delta_j} \quad (25)$$

Ungar (Ref. 16) has shown that for two coupled sets of modes where energy is supplied to one mode set and no energy is supplied to the other set, the ratio of the average modal kinetic energy of the two sets can be expressed in terms of a coupling loss factor and a modal loss factor. Applying Ungar's formulation to the present problem gives

$$\frac{\langle K_p(\omega_j, \delta_j) \rangle_m}{\langle K_a(\omega_j, \delta_j) \rangle_m} = \frac{\eta_{pa}(\omega_j, \delta_j)}{\eta_{pa}(\omega_j, \delta_j) + \eta_p(\omega_j, \delta_j)} \quad (26)$$

where

$\eta_{pa}(\omega_j, \delta_j)$ = average coupling loss factor for energy flow from a panel mode to an acoustic mode in the frequency interval, δ_j , centered at frequency ω_j

$\eta_p(\omega_j, \delta_j)$ = average modal loss factor for a panel mode in the frequency interval, δ_j , centered at frequency ω_j .

Substituting Eqs. (22) and (25) into Eq. (26) and simplifying gives

$$\bar{a}^2(\omega_j, \delta_j) = \frac{2\pi^2 c_n(\omega_j) \eta_{pa}(\omega_j, \delta_j) p^2(\omega_j, \delta_j)}{m_p \rho_a [\eta_{pa}(\omega_j, \delta_j) + \eta_p(\omega_j, \delta_j)]} . \quad (27)$$

Equation (27) provides a method for determining the acceleration response of a panel excited by a reverberant acoustic field. To apply this formula, one must be able to divide the frequency range of interest for the response into a number of frequency intervals. These intervals must be chosen so that the structural modes in a given interval have similar modal loss factors. All structural modes in the given interval must have equivalent coupling to all acoustic modes in the interval, and the coupling loss factors must be similar. For each frequency interval, one must have a good estimate of the modal density of the panel, the average modal loss factor of the panel modes, and the average coupling loss factor for energy flow from a panel mode to an acoustic mode.

Section 4

RESPONSE OF TPS TEST PANEL

A test panel of a proposed thermal protective system (TPS) configuration was fabricated at Marshall Space Flight Center for reverberation chamber tests. The test panel, which is made of Haynes 25 Alloy L-605, is shown in Fig. 17. It consists of two individual corrugated panels which overlap each other by one inch. Only one half of one of the panels is shown in Fig. 17. The panel is symmetrical about the A-A axis. The panel is attached to a corrugated standoff-panel along one edge and a series of flexible clips along the other edge. Only half of each clip is shown. The clips are symmetrical about the B-B axis, with the other panel attached to the other half of each clip. Each panel has a series of horizontal stiffeners parallel to the corrugations. The stiffeners are attached to the panel by a series of spot welds. The panel and stiffeners are attached to the standoff-panel and clips by bolts (not shown). The standoff-panels and clips are bolted to large aluminum channels perpendicular to the corrugations.

To determine the low frequency response of this panel in the reverberation chamber, a finite element model of the panel was developed. In the model, the panel is represented as a series of plate elements and the standoff-panel, clips and stiffeners are represented as a series of beam elements. The points of connection between the aluminum channels and the standoff-panel and clips are considered fixed in the model. Since the two individual panels are connected at fixed points on the clips and by a sliding overlap, they can be considered decoupled. Therefore, it is sufficient to model only one of the panels. A plane-of-symmetry technique is used so that only one-half of each individual panel is modeled. The original model is shown in Figs. 18, 19 and 20.

The model was analyzed by the Structural Network Analysis Program (SNAP) to determine the natural frequencies and mode shapes of the low

frequency modes. However, four out of the first five modes turned out to be local modes of one cantilever overhang of the panel. The first mode is shown in Figs. 21, 22 and 23. Since the local cantilever modes do not appreciably affect the response near the center of the panel, the model was changed to eliminate the overhangs. The revised model is shown in Figs. 24, 25 and 26.

The revised model was analyzed by SNAP to determine the first five modes. All five modes are panel modes. They are shown in Figs. 27 through 41.

A computer program was written to compute the response at any designated point on the panel. The program uses the output tape from SNAP for the natural frequencies and mode shapes. The spatial correlation used for the reverberant field is given by

$$R_{\alpha\beta}(\omega) = \frac{\sin(\lambda_{\alpha\beta} \omega/c)}{\lambda_{\alpha\beta} \omega/c} \quad (28)$$

where

$\lambda_{\alpha\beta}$ = distance between points α and β .

A description of the program is given in Appendix B.

The acoustic test criteria for the reverberation chamber in one-third octave bands is given in the following table. The power spectral density (PSD) of the acoustic test criteria was determined from the one-third octave band data. The PSD is shown in Fig. 42 on a log-log scale.

TABULATION OF ACOUSTIC TEST CRITERIA

One-Third Octave Band Acoustical Specification in dB re 2×10^{-5} N/M²

| Geometric Mean Freq. (Hz) | dB |
|---------------------------------|-------|
| 5.0 | 135.0 |
| 6.3 | 136.0 |
| 8.0 | 137.0 |
| 10.0 | 137.5 |
| 12.5 | 138.5 |
| 16.0 | 139.5 |
| 20.0 | 140.0 |
| 25.0 | 140.5 |
| 31.5 | 141.0 |
| 40.0 | 141.5 |
| 50.0 | 142.5 |
| 63.0 | 144.5 |
| 80.0 | 146.5 |
| 100.0 | 147.5 |
| 125.0 | 148.5 |
| 160.0 | 148.5 |
| 200.0 | 147.5 |
| 250.0 | 146.5 |
| 315.0 | 145.5 |
| 400.0 | 144.0 |
| 500.0 | 143.0 |
| 630.0 | 142.5 |
| 800.0 | 142.5 |
| 1000.0 | 141.5 |
| 1250.0 | 141.0 |
| 1600.0 | 140.5 |
| 2000.0 | 139.5 |
| 2500.0 | 138.5 |
| 3150.0 | 137.5 |
| 4000.0 | 137.0 |
| 5000.0 | 136.0 |
| 6300.0 | 135.0 |
| 8000.0 | 134.0 |
| 10000.0 | 133.0 |

Overall SPL

158.0

The response program was utilized to calculate the response of the panel at the point P (Fig. 17), which is over a stiffener near the center of the panel. The revised model of the panel (without overhangs) was used. Two separate runs were made, one using 4% damping for all modes and one using 5% damping for all modes. The results obtained with 4% damping are shown in Figs. 43 through 46. The results of the 5% damping run are given in Figs. 47 through 50. These figures give the power spectral densities of the response displacement and acceleration using both linear and log-log scales. The overall variance and the root mean square (RMS) of the response is also given on each figure.

The response power spectral density is dominated by the response of the second mode, at approximately 198 Hz. Analysis of the mode shapes of the panel and the spatial correlation of the acoustic field reveals that the joint acceptance squared is much higher for the second mode than for any of the other modes. This effect overshadows other factors, such as the higher acoustic excitation level at the natural frequency of the first mode.

Comparison of the results of the two runs shows the effect of damping. Due to the predominance of the second mode, the damping value of the second mode is the primary determining factor for the height of the resonant peak and the RMS of the response.

REFERENCES

1. Houbolt, J.C., "On the Estimation of Pressure Fluctuations in Boundary Layers and Wakes," ARAP Report No. 90, Princeton, N.J., June 1966.
2. Blake, W.K., "Turbulent Boundary Layer Wall Pressure Fluctuations on Smooth and Rough Walls," Report No. 70208-1, Massachusetts Institute of Technology, Cambridge, Mass. , January 1969.
3. Bull, M.K., "Properties of the Fluctuating Wall-Pressure Field of a Turbulent Boundary Layer," AGARD Report 455, Paris, France, April 1963.
4. Bies, D.A., "Review of Flight and Wind Tunnel Measurements of Boundary Layer Pressure Fluctuations and Induced Structural Response," NASA CR-626, Washington, D.C., October 1966.
5. Chyu, W.J., and R.J. Hanly, "Power and Cross-Spectra and Space-Time Correlations of Surface Fluctuating Pressures at Mach Numbers between 1.6 and 2.5," NASA TN D-5440, Washington, D.C., September 1969.
6. Speaker, W.V., and C.M. Ailman, "Spectra and Space-Time Correlations of the Fluctuating Pressures at a Wall Beneath a Supersonic Turbulent Boundary Layer Perturbed by Steps and Shock Waves," NASA CR-486, Washington, D.C. June 1966.
7. Kistler, A.L., "Fluctuating Wall Pressure under a Separated Supersonic Flow," J. Acoust. Soc. Am., Vol. 36, March 1964, pp. 543-550.
8. Robinson, R.C., B.J. Gambucci, and R.E. George, "Fluctuating Pressures on the Afterbodies of Five Blunt Atmosphere Entry Vehicles," NASA TN D-4591, Washington, D.C., May 1968.
9. Eldred, K. McK., "Base Pressure Fluctuations," J. Acoust. Soc. Am., Vol. 33, January 1961, pp. 59-63.
10. Wiley, D.R., and M.G. Seidl, "Aerodynamic Noise Tests on X-20 Scale Models, Vol. II, Summary and Analysis Report," AFFDL-TR-65-192, Vol. II, Wright-Patterson Air Force Base, Ohio, November 1965.
11. Lockheed Missiles & Space Company, "Trends in Base Pressure Fluctuations Level Variations — Saturn V Hinge Moment Model Wind Tunnel Test," LMSC-HREC A782411, Huntsville, Ala., March 1966.

12. Whetstone, W. D., "Structural Network Analysis Program, User's Manual, Dynamic Analysis Version V70E," LMSC-HREC D225101, Lockheed Missiles & Space Company, Huntsville, Ala., May 1971.
13. Lyon, R. H., and G. Maidanik, "Power Flow Between Linearly Coupled Oscillators," J. Acoust. Soc. Am., Vol. 34, May 1962, pp. 623-639.
14. Smith, P. W., Jr., and R. H. Lyon, "Sound and Structural Vibration," NASA CR-160, Washington, D. C., March 1965.
15. Scharton, T. D., "Random Vibration of Coupled Oscillators and Coupled Structures," Doctoral Thesis, Massachusetts Institute of Technology, Cambridge, Mass., October 1965.
16. Ungar, E. E., "Fundamentals of Statistical Energy Analysis of Vibrating Systems," AFFDL-TR-66-52, Wright-Patterson Air Force Base, Ohio, May 1966.

BIBLIOGRAPHY

Ailman, C. M., "Wind Tunnel Investigation of the Fluctuating Pressures at the Surface of 2.75% Saturn Models," Paper presented at Second International Conference on Acoustical Fatigue, Dayton, Ohio, April 1964.

Ailman, C. M., "On Predicting Fluctuating Pressures at a Wall Beneath a Turbulent Boundary Layer," Paper presented to the Acoustical Society of America, New York, N. Y., 19-21 April 1967.

AVCO Corporation, "Endoatmospheric Decoy Technology Program Postflight Data Report - Payload D-9," AVSD-0312-69-CR, AVCO Corp., Wilmington, Mass., July 1969.

AVCO Corporation, "RVTO Phase 1A Reentry Data Final Report for WT1A-L2 and WT1A-S3 Vehicles," AVMSD-0113-69-RR, AVCO Corp., Wilmington, Mass., May 1969.

AVCO Corporation, "RVTO Phase 1A Reentry Data Final Report for WT1A-L3 and WT1A-S4 Vehicles," AVMSD-0120-69-CR, AVCO Corp., Wilmington, Mass., June 1969.

Barnoski, R. L., and J. R. Maurer, "Distributed System Response Characteristics in Random Pressure Fields," NASA CR-1660, Washington, D. C., September 1970.

Barnoski, R. L., A. G. Piersol, W. F. Van der Laan, P. H. White, and E. F. Winter, "Summary of Random Vibration Prediction Procedures," NASA-CR-1302, Washington, D. C., April 1969.

Barrett, R. E., "Techniques for Predicting Localized Vibratory Environments of Rocket Vehicles," NASA TN D-1836, Washington, D. C., October 1963.

Barrett, R. E., "Statistical Techniques for Describing Localized Vibratory Environments of Rocket Vehicles," NASA TN D-2158, Washington, D. C., July 1964.

Batten, R. L., "Compilation of Atlas E and F Series Vehicle Flight Environmental Vibration Data, Part I," GD/A-DDE65-016, General Dynamics Corp., San Diego, Calif., March 1965.

Belcher, P. M., "Predictions of Boundary-Layer-Turbulence Spectra and Correlations for Supersonic Flight," Paper presented at the 5th Congress International D'Acoustique, Liege, Belgium, September 1965.

Benedetti, F. J., and F. A. Smith, "Reentry Vibration and Acoustic Data Measured on a High Ballistic Coefficient Vehicle," TOR-669 (S6810-21)-1, Aerospace Corporation, San Bernardino, Calif., February 1966.

Bies, D. A., "A Wind Tunnel Investigation of Panel Response to Boundary Layer Pressure Fluctuations at Mach 1.4 and Mach 3.5," NASA CR-501, Washington, D. C., May 1966.

Bies, D. A., "Review of Flight and Wind Tunnel Measurements of Boundary Layer Pressure Fluctuations and Induced Structural Response," NASA CR-626, Washington, D. C., October 1966.

Blake, W. K., "Turbulent Boundary Layer Wall Pressure Fluctuations on Smooth and Rough Walls," Report No. 70208-1, Massachusetts Institute of Technology, Cambridge, Mass., January 1969.

Bull, M. K., "Properties of the Fluctuating Wall-Pressure Field of a Turbulent Boundary Layer," AGARD Rept. 455, Paris, France, April 1963.

Bull, M. K., "Wall-Pressure Fluctuations Associated with Subsonic Turbulent Boundary Layer Flow," J. Fluid Mech., Vol. 28, Part 4, 1967, pp. 719-754.

Bull, M. K., and J. L. Willis, "Some Results of Experimental Investigations of the Surface Pressure Field Due to a Turbulent Boundary Layer," ASD-TDR-62-425, Wright-Patterson Air Force Base, Ohio, August 1962.

Bull, M. K., J. F. Wilby, and D. R. Blackman, "Wall Pressure Fluctuations in Boundary Layer Flow and Response of Simple Structures to Random Pressure Fields," A. A. S. U. Rept. No. 243, University of Southampton, Hampshire, England, July 1963.

Chandiramani, K. L., and R. W. Pyle, Jr., "Structural Response of Saturn V Launch Vehicle to Inflight Acoustic and Aerodynamic Environments," Rept. 1418, Bolt, Beranek and Newman, Inc., Cambridge, Mass., July 1966.

Chandiramani, K. L., S. E. Widnall, R. H. Lyon, and P. A. Franken, "Structural Response to Inflight Acoustic and Aerodynamic Environments," Rept. 1417, Bolt, Beranek and Newman, Inc., Cambridge, Mass., July 1966.

Chevalier, H. L., and J. E. Robertson, "Pressure Fluctuations Resulting from an Alternating Separation and Attachment at Transonic Speeds," AEDC-TDR-63-204, Arnold Air Force Station, Tenn., November 1963.

Chrysler Corporation, "Apollo-Saturn IB Flight Technology Acoustics," TN HSM-N24-67, Chrysler Corporation, Huntsville, Ala., March 1967.

Chyu, W. J., and R. J. Hanly, "Power and Cross-Spectra and Space-Time Correlations of Surface Fluctuating Pressures at Mach Numbers Between 1.6 and 2.5," NASA TN D-5440, Washington, D. C., September 1969.

Coe, C. F., "Surface-Pressure Fluctuations Associated with Aerodynamic Noise," NASA SP-207, Washington, D. C., July 1969, pp. 409-424.

Coe, C. F., "The Effects of Some Vibrations in Launch-Vehicle Nose Shape on Steady and Fluctuating Pressures at Transonic Speeds," NASA TM X-646, Washington, D. C., March 1962.

Coe, C. F., "Steady and Fluctuating Pressures at Transonic Speeds on Two Space-Vehicle Payload Shapes," NASA TM X-503, Washington, D. C., March 1961.

Coe, C. F., and J. B. Nute, "Steady and Fluctuating Pressures at Transonic Speeds on Hammerhead Launch Vehicles," NASA TM X-778, Washington, D. C., December 1962.

Corcos, G. M., "The Structure of the Turbulent Pressure Field in Boundary Layer Flows," Institute of Engineering Research Report, Series 183, No. 4, University of California, Berkeley, Calif., March 1963.

Corcos, G. M., "Resolution of Pressure in Turbulence," J. Acoust. Soc. Am., Vol. 35, February 1963, pp. 192-199.

Dyer, I., P. A. Franken, and E. E. Ungar, "Noise Environments of Flight Vehicles," Noise Control, January/February 1960, pp. 31-40.

el Baroudi, M. Y., G. R. Ludwig, and H. S. Ribner, "An Experimental Investigation of Turbulence-Excited Panel Vibration and Noise (Boundary-Layer Noise)," AGARD Report 465, Paris, France, April 1963.

Eldred, K. McK., "Base Pressure Fluctuations," J. Acoust. Soc. Am., Vol. 33, January 1961, pp. 59-63.

Ffowcs Williams, J. E., "Surface-Pressure Fluctuations Induced by Boundary-Layer Flow at Finite Mach Number," J. Fluid Mech., Vol. 22, Part 3, 1965, pp. 507-519.

Fotieo, G., W. H. Roberts and J. P. White, "Vibration Characteristics of a Hypersonic Missile Interceptor," J. Environ. Sci., Vol. 12, February 1969, pp. 10-15.

Franken, P. A., et al., "Methods of Space Vehicle Noise Prediction," WADC TR 58-343, Vol. II, Wright-Patterson Air Force Base, Ohio, September 1960.

Franken, P. A., E. M. Kerwin, Jr., et al., "Methods of Flight Vehicle Noise Prediction," WADC TR 58-343, Vol. I, Wright-Patterson Air Force Base, Ohio, October 1958.

George, B. W., "Launch Vehicle Inflight Acoustic Environment Predictions," Paper presented at the 72nd Meeting of the Acoustical Society of America, Los Angeles, Calif., November 1966.

Gibson, J. S., "Boundary Layer Noise Measurements on a Large Turbofan Aircraft," Paper presented to the Acoustical Society of America, St. Louis, Mo., November 1965.

Gruner, W. J., "Comparative Analysis of Acoustic Testing Techniques," Technical Report HSM-R30-69, Chrysler Corporation, Huntsville, Ala., July 1969.

Hilton, D. A., E. M. Bracalente, and H. H. Hubbard, "In-Flight Aerodynamic Noise Measurements on a Scout Launch Vehicle," NASA TN D-1818, Washington, D. C., July 1963.

Himelblau, H., C. M. Fuller, and T. D. Scharon, "Assessment of Space Vehicle Aeroacoustic-Vibration Prediction, Design, and Testing," NASA CR-1596, Washington, D. C., July 1970.

Houbolt, J. C., "On the Estimation of Pressure Fluctuations in Boundary Layers and Wakes," ARAP Report No. 90, Princeton, N. J., June 1966.

Jacobs, L. D., and D. R. Lagerquist, "A Finite Element Analysis of Simple Panel Response to Turbulent Boundary Layers," AFFDL-TR-67-81, Wright-Patterson Air Force Base, Ohio, July 1967.

Johnson, R. I., M. N. Macourek, and H. Saunders, "Boundary Layer Acoustic Measurements in Transitional and Turbulent Flow at $M = 4.0$," AIAA Paper No. 69-344, AIAA 4th Aerodynamic Testing Conference, Cincinnati, Ohio, April 1969.

Kistler, A. L., "Fluctuating Wall Pressure Under a Separated Supersonic Flow," J. Acoust. Soc. Am., Vol. 36, March 1964, pp. 543-550.

Kistler, A. L., "Surface Pressure Fluctuations Produced by Attached and Separated Supersonic Boundary Layers," AGARD Report 458, Paris, France, April 1963.

Kistler, A. L., and W. S. Chen, "The Fluctuating Pressure Field in a Supersonic Turbulent Boundary Layer," J. Fluid Mech., Vol. 16, Part 1, 1963, pp. 41-64.

Kordes, E. E., and C. S. Tanner, "Preliminary Results of Boundary-Layer Noise Measured on the X-15 Airplane," Paper presented at the Second International Conference on Acoustical Fatigue, Dayton, Ohio, April 1964.

Laufer, J., "Aerodynamic Noise in Supersonic Wind Tunnels," J. Aerospace Sci., September 1961.

Laufer, J., J. E. Ffowcs Williams, and S. Childress, "Mechanism of Noise Generation in the Turbulent Boundary Layer," AGARDograph 90, Paris, France, November 1964.

Lee, T. N., and W. L. Swanson, "Computer Programs for Prediction of Structural Vibrations Due to Fluctuating Pressure Environments," Technical Report HSM-R28-69, Chrysler Corporation, Huntsville, Ala., July 1969.

Leech, F. J., and V. E. Sackschewsky, "Boundary Layer Noise Measurements of the F-102 Aircraft," MRL-TDR-62-71, Wright-Patterson Air Force Base, Ohio, August 1962.

Leissa, A. W., "Vibration of Plates," NASA SP-160, Washington, D. C., 1969.

Lewis, T. L., and N. J. McLeod, "Flight Measurements of Boundary-Layer Noise on the X-15," NASA TN D-3364, Washington, D. C., March 1966.

Lilley, G. M., "Pressure Fluctuations in an Incompressible Turbulent Boundary Layer," Rept. 133, College of Aeronautics, Cranfield, England, 1960.

Lockheed Missiles & Space Company, "SA-201 External Acoustic Data," LMSC-HREC A782441, Lockheed Missiles & Space Company, Huntsville, Ala., March 1966.

Lockheed Missiles & Space Company, "Trends in Base Pressure Fluctuations Level Variations - Saturn V Hinge Moment Model Wind Tunnel Test," LMSC-HREC A782411, Lockheed Missiles & Space Company, Huntsville, Ala., March 1966.

Lowson, M. V., "Prediction of Boundary Layer Pressure Fluctuations," AFFDL-TR-67-167, Wright-Patterson Air Force Base, Ohio, January 1968.

Ludwig, G. R., "An Experimental Investigation of the Sound Generated by Thin Steel Panels Excited by Turbulent Flow (Boundary Layer Noise)," UTIA Report No. 87, Institute of Aerophysics, University of Toronto, Toronto, Canada, November 1962.

Maidanik, G., "Response of Ribbed Panels to Reverberant Acoustic Fields," J. Acoust. Soc. Am., Vol. 34, June 1962, pp. 809-826.

Martin Company, "Compilation of Shock, Vibration, and Acoustic Data from Titan Vehicles, Vol. II - Titan I Acoustic and Vibration Data," NASA CR-62001, Washington, D. C., January 1965.

Mayes, W. H., D. A. Hilton, and C. A. Hardesty, "In-Flight Noise Measurements for Three Project Mercury Vehicles," NASA TN D-997, Washington, D. C., January 1962.

Murphy, J. S., D. A. Bies, W. W. Speaker, and P. A. Franken, "Wind Tunnel Investigation of Turbulent Boundary Layer Noise as Related to Design Criteria for High Performance Vehicles," NASA TN D-2247, Washington, D. C., April 1964.

Noonan, W. E., and J. R. Daiber, "Acoustic Tests of a Flexible Spacecraft Model," NASA CR-1618, Washington, D. C., June 1970.

Pate, S. R., and M. D. Brown, "Acoustic Measurements in Supersonic Transitional Boundary Layers," AEDC-TR-69-182, Arnold Air Force Station, Tenn., October 1969.

Rader, W. P., "Titan III Acoustic/Vibration Test Program, Phase I," SSD-CR-64-196, Martin Company, Denver, Colo., November 1964.

Reich, H. K., "Flight Vibration Survey of B-58 Aircraft," ASD-TDR-62-384, Wright-Patterson Air Force Base, Ohio, April 1962.

Revell, J. D., and R. E. Gleason, "Turbulent Wall Pressure Fluctuations Under Separated Supersonic and Hypersonic Flows," AFFDL-TR-65-77, Wright-Patterson Air Force Base, Ohio, August 1965.

Robertson, J. E., "Unsteady Pressure Phenomena for Basic Missile Shapes at Transonic Speeds," Paper presented at the AIAA Aerospace Sciences Meeting, New York, N. Y., January 1964.

Robinson, R. C., B. J. Gambucci, and R. E. George, "Fluctuating Pressures on the Afterbodies of Five Blunt Atmosphere Entry Vehicles," NASA TN D-4591, Washington, D. C., May 1968.

Runyan, H. L., "Some Recent Information on Aircraft Vibration Due to Aerodynamic Sources," Paper presented at the Acoustical Society of America Meeting, Ottawa, Canada, May 1968.

Saunders, H., and D. E. Nestler, "Prediction of the Boundary Layer Acoustic Pressure Levels of a Blunt Nose Reentry Vehicle at High Mach Numbers," The Shock and Vibration Bulletin, Bulletin 35, Part 7, April 1966, pp. 19-23.

Scharton, T. D., "Random Vibration of Coupled Oscillators and Coupled Structures," Doctoral Thesis, Massachusetts Institute of Technology, Cambridge, Mass., October 1965.

Schiffer, R. A., "Correlation of Launch-Vehicle Wind-Tunnel Aerodynamic Noise with Spacecraft Flight Vibration Data (Revision No. 1)," TR 32-619, Jet Propulsion Laboratory, Pasadena, Calif., September 1964.

Schlichting, H., Boundary Layer Theory, (6th ed.), McGraw-Hill, New York, 1968.

Schloemer, H. H., "Effects of Pressure Gradients on Turbulent Boundary-Layer Wall-Pressure Fluctuations," J. Acoust. Soc. Am., Vol. 42, July 1967, pp. 93-113.

Serafini, J. S., "Wall-Pressure Fluctuations and Pressure-Velocity Correlations in Turbulent Boundary Layers," AGARD Report 453, Paris, France, April 1963.

Shattuck, R. D., "Sound Pressures and Correlations of Noise on the Fuselage of a Jet Aircraft in Flight," NASA TN D-1086, Washington, D. C., August 1961.

- Smith, F. A., and F. J. Benedetti, "Prediction of Reentry Vibration," TDR-669 (S6810-21)-1, Aerospace Corporation, San Bernardino, Calif., September 1965.
- Smith, R. D., "Response of a Conical Shell Frustrum - Three Degree of Freedom Harmonic Oscillator System to a Convecting Random Pressure Field," B-62-68-6, Lockheed Missiles & Space Company, Palo Alto, Calif., October 1968.
- Speaker, W. V., and C. M. Ailman, "Spectra and Space-Time Correlations of the Fluctuating Pressures at a Wall Beneath a Supersonic Turbulent Boundary Layer Perturbed by Steps and Shock Waves," NASA CR-486, Washington, D. C., June 1966.
- Speaker, W. V., and C. M. Ailman, "Static and Fluctuating Pressures in Regions of Separated Flow," AIAA Paper No. 66-456, Los Angeles, Calif., June 1966.
- Strawderman, W. A., and R. S. Brand, "Turbulent-Flow-Excited Vibration of a Simply Supported, Rectangular Flat Plate," J. Acoust. Soc. Am., Vol. 45, January 1969, pp. 177-192.
- Sutherland, L. C., J. C. Furlong, and J. Sugamele, "Revised Analysis X-20 Vibration and Acoustic Environment," D2-8109-1, The Boeing Company, Seattle, Wash., January 1964.
- Townsend, J. C., "Estimation of the Sound Levels Produced by a Body in Reentry," Aerophysics Engineering TM-167, General Electric Company, Philadelphia, Pa., December 1960.
- TRW Systems Group, "Reentry Measurements Instrumentation Package (RMIP) Project Flight No. 1 Data Validation Report," 06488-6228-R3-00, TRW Systems Group, Redondo Beach, Calif., December 1968.
- TRW Systems Group, "Reentry Measurements Instrumentation Package (RMIP) Project RMIP No. 7 Data Validation Report," 06488-6394-R3-00, TRW Systems Group, Redondo Beach, Calif., April 1970.
- TRW Systems Group, "RMV Reentry Acoustic Data," 06488-6348-R3-00, TRW Systems Group, Redondo Beach, Calif., December 1969.
- Ungar, E. E., "Fundamentals of Statistical Energy Analysis of Vibrating Systems," AFFDL-TR-66-52, Wright-Patterson Air Force Base, Ohio, May 1966.
- Weathers, L. R., "The Reliability of Fluctuating Pressure Data Obtained from Wind Tunnel Testing of a 2.75 Percent Scale Model Saturn I Vehicle," TM-AA-4-65-4, Brown Engineering Company, Inc., Huntsville, Ala., April 1965.
- Wiksten, D. B., "Dynamic Environment of the Ranger Spacecraft: I through IX (Final Report)," TR 32-909, Jet Propulsion Laboratory, Pasadena, Calif., May 1966.

Wilby, J. F., W. V. Bhat, and F. L. Gloyna, "Airplane Fuselage Response to Turbulent Boundary Layers," 70-WA/DE-10, American Society of Mechanical Engineers, New York, N. Y., December 1970.

Wiley, D. R., and M. G. Seidl, "Aerodynamic Noise Tests on X-20 Scale Models, Volume II, Summary and Analysis Report," AFFDL-TR-65-192, Vol. II, Wright-Patterson Air Force Base, Ohio, November 1965.

Willmarth, W. W., "Turbulent Boundary Measurements of the Fluctuating Pressure at the Wall Beneath a Thick Turbulent Boundary Layer," J. Fluid Mech., Vol. 21, Part 1, January 1965, pp. 107-109.

Willmarth, W. W., and C. E. Wooldridge, "Measurements of the Fluctuating Pressure at the Wall Beneath a Thick Turbulent Boundary Layer," J. Fluid Mech., Vol. 14, Part 2, October 1962, pp. 187-210.

Willmarth, W. W., and C. E. Wooldridge, "Measurements of the Correlation Between the Fluctuating Velocities and the Fluctuating Wall Pressure in a Thick Turbulent Boundary Layer," AGARD Report 456, Paris, France, April 1963.

Willmarth, W. W., and F. W. Roos, "Resolution and Structure of the Wall Pressure Field Beneath a Turbulent Boundary Layer," J. Fluid Mech., Vol. 22, Part 1, 1965, pp. 81-94.

Wills, J. A. B., "On Convection Velocities in Turbulent Shear Flows," AGARD Report 457, Paris, France, April 1963.

Zeman, J. L., and J. L. Bogdanoff, "Statistical Approach to Complex Random Vibration," J. Acoust. Soc. Am., Vol. 50, September 1971, pp. 1019-1027.

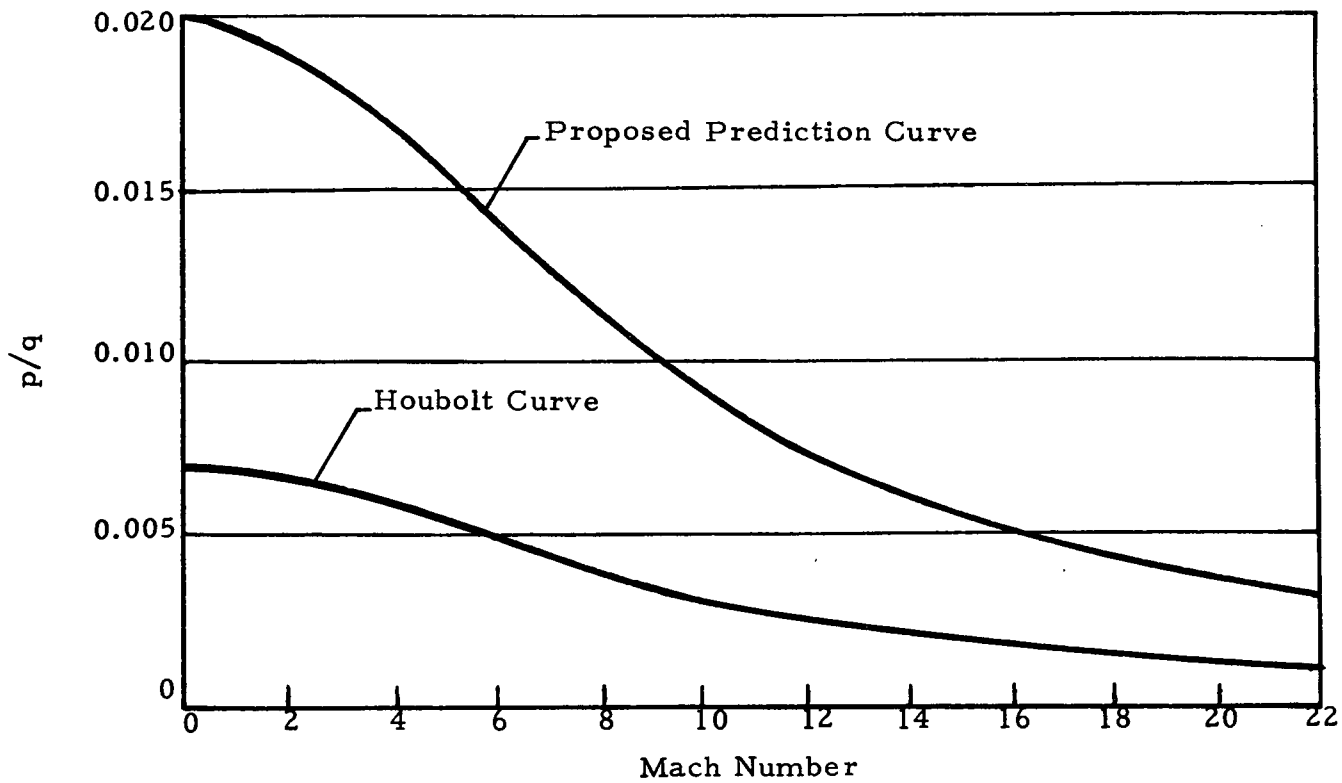


Fig. 1 - Overall Fluctuating Pressure Level for Attached Turbulent Boundary Layer

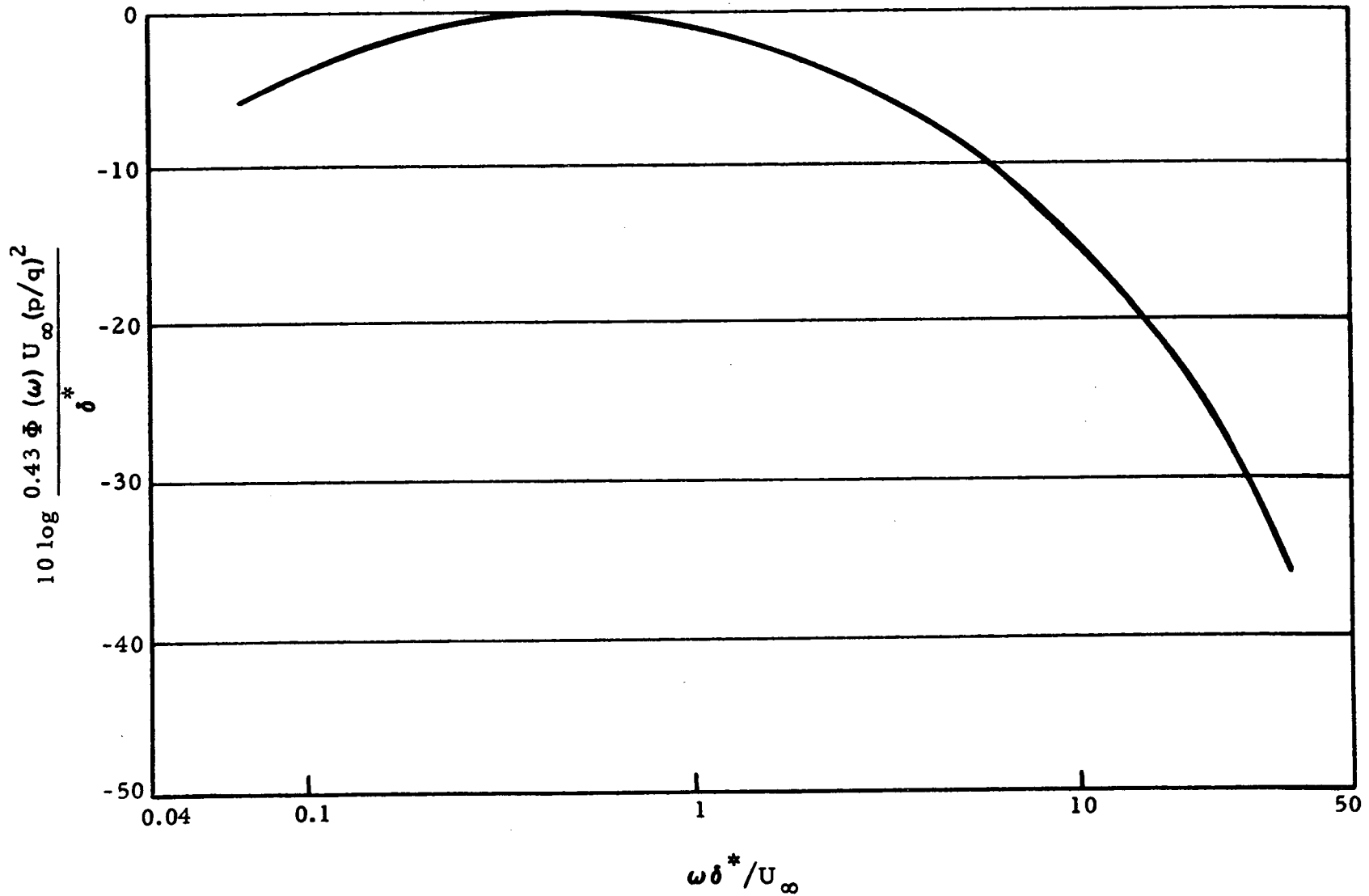


Fig. 2 - Power Spectral Density for Attached Turbulent Boundary Layer (from Blake, Ref. 2)

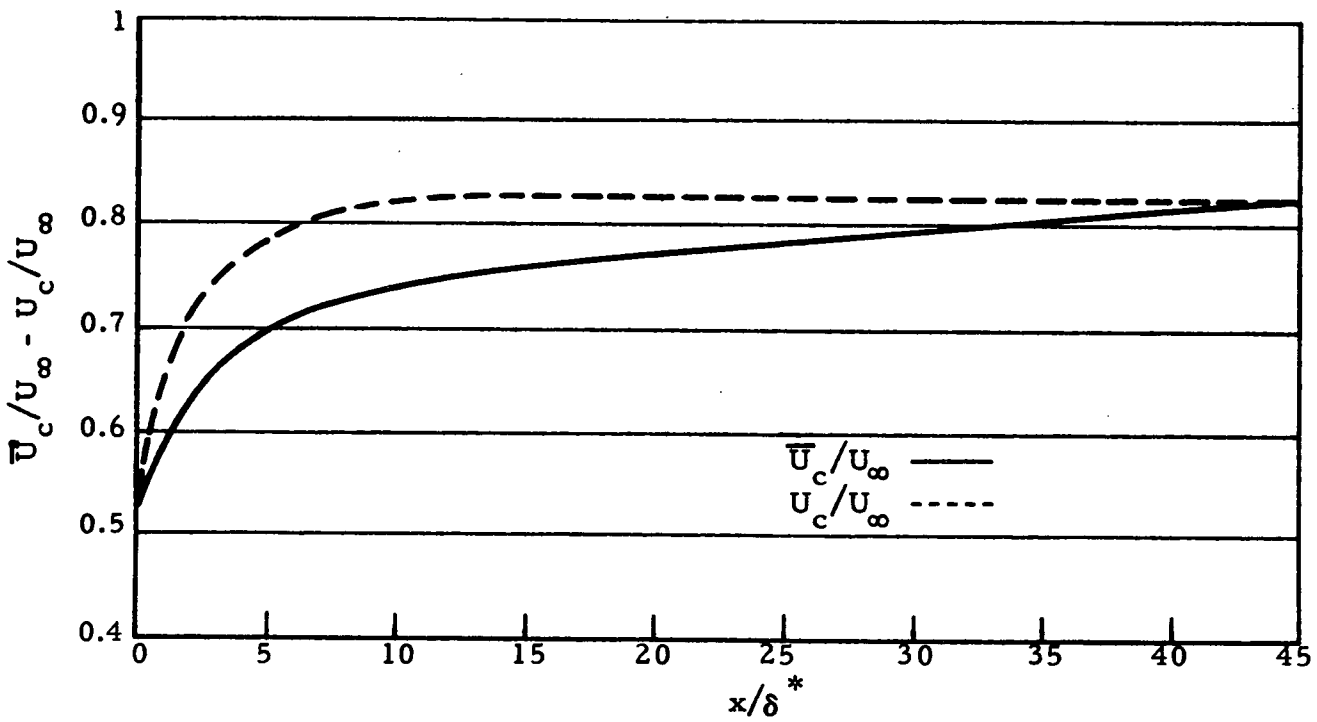


Fig. 3 - Broad-Band Convection Velocities for Attached Turbulent Boundary Layer (from Bull, Ref. 3)

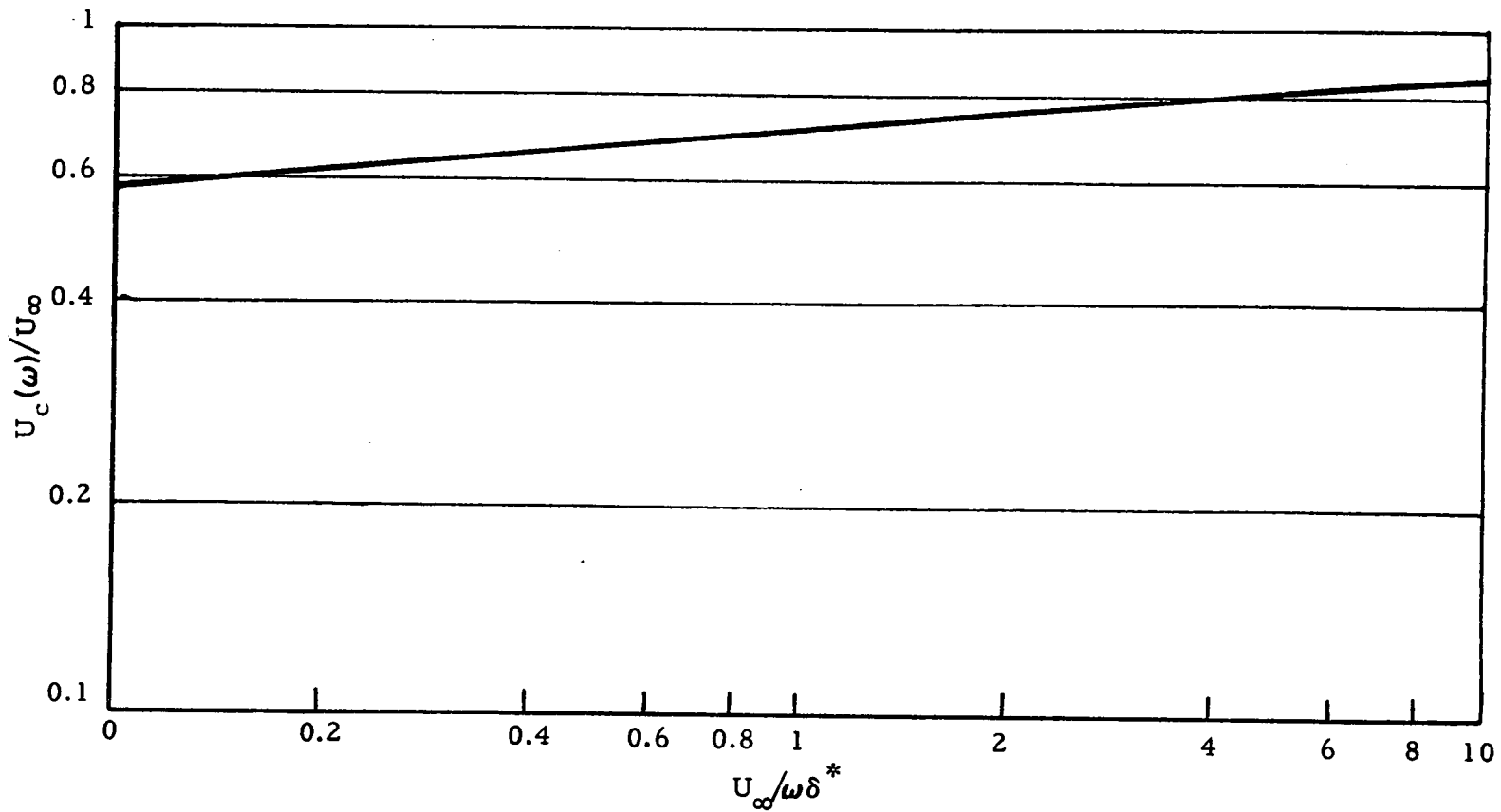


Fig. 4 - Narrow-Band Convection Velocities for Attached Turbulent Boundary Layer (from Bies, Ref. 4)

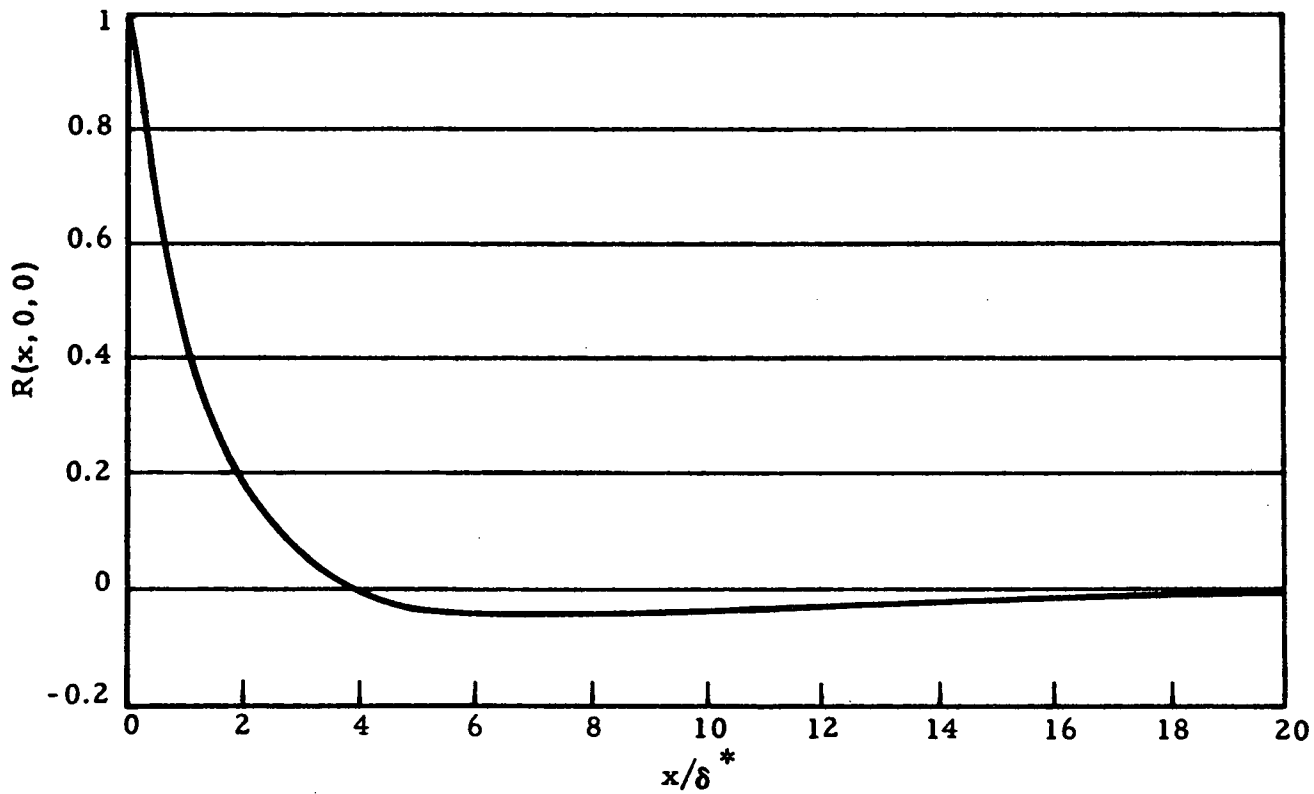


Fig. 5 - Longitudinal Broad-Band Spatial Correlations for Attached Turbulent Boundary Layer (from Bull, Ref. 3)

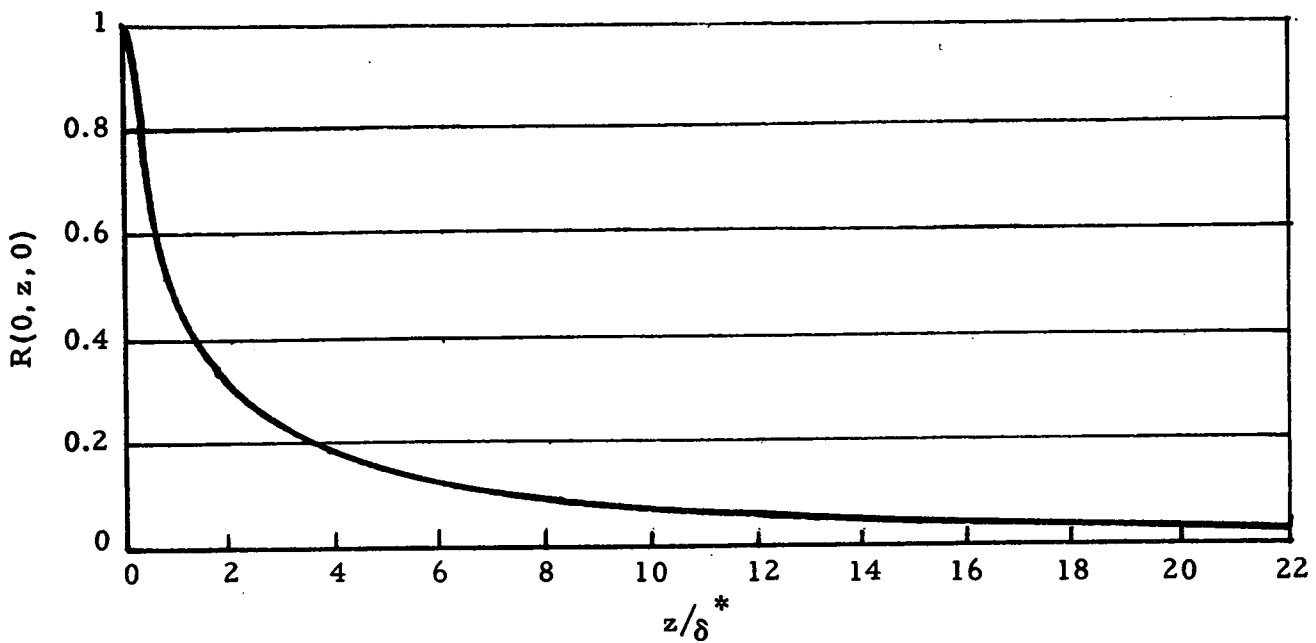


Fig. 6 - Lateral Broad-Band Spatial Correlations for Attached Turbulent Boundary Layer (from Bull, Ref. 3)

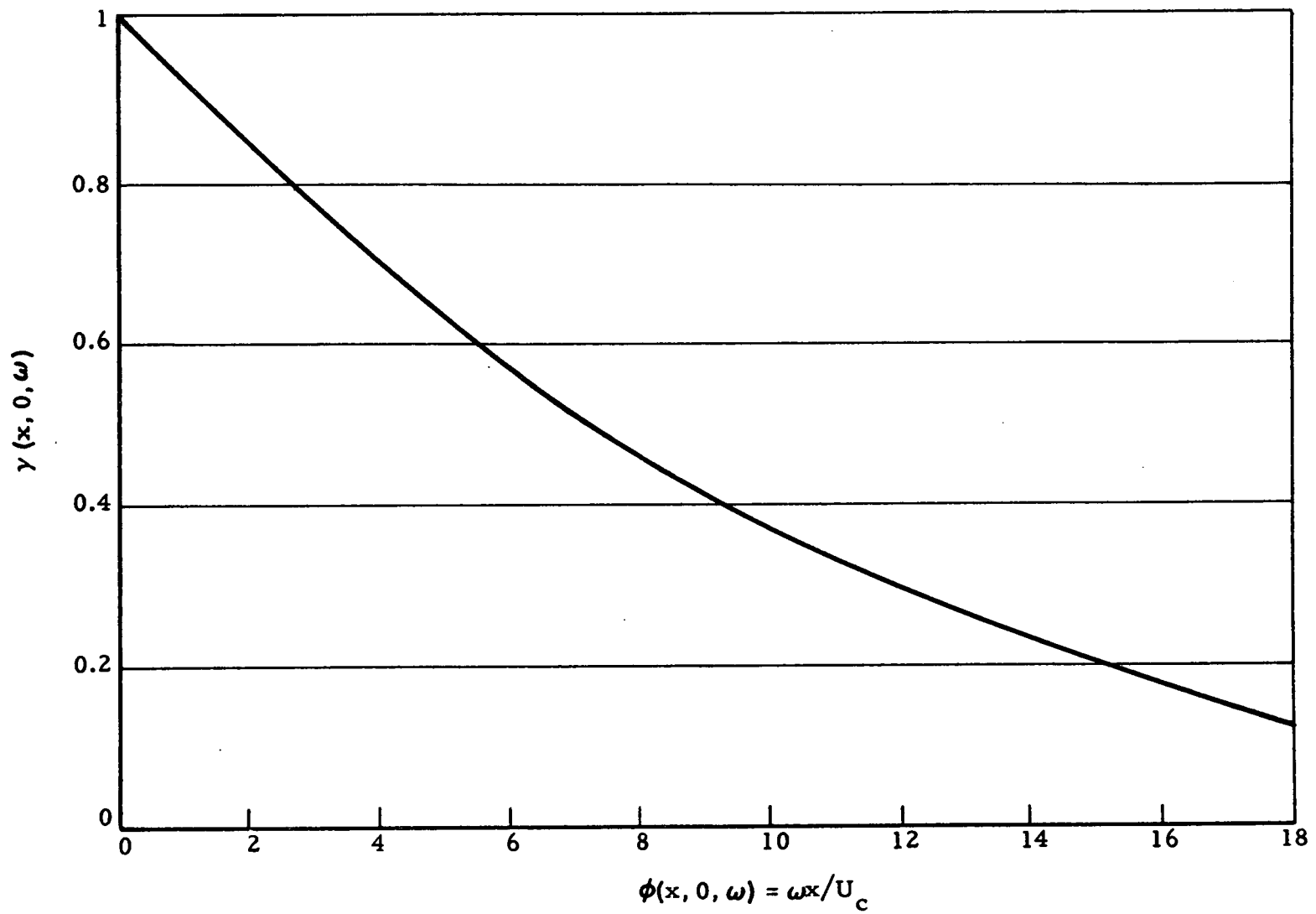


Fig. 7 - Longitudinal Coherence Function for Attached Turbulent Boundary Layer (from Blake, Ref. 2)

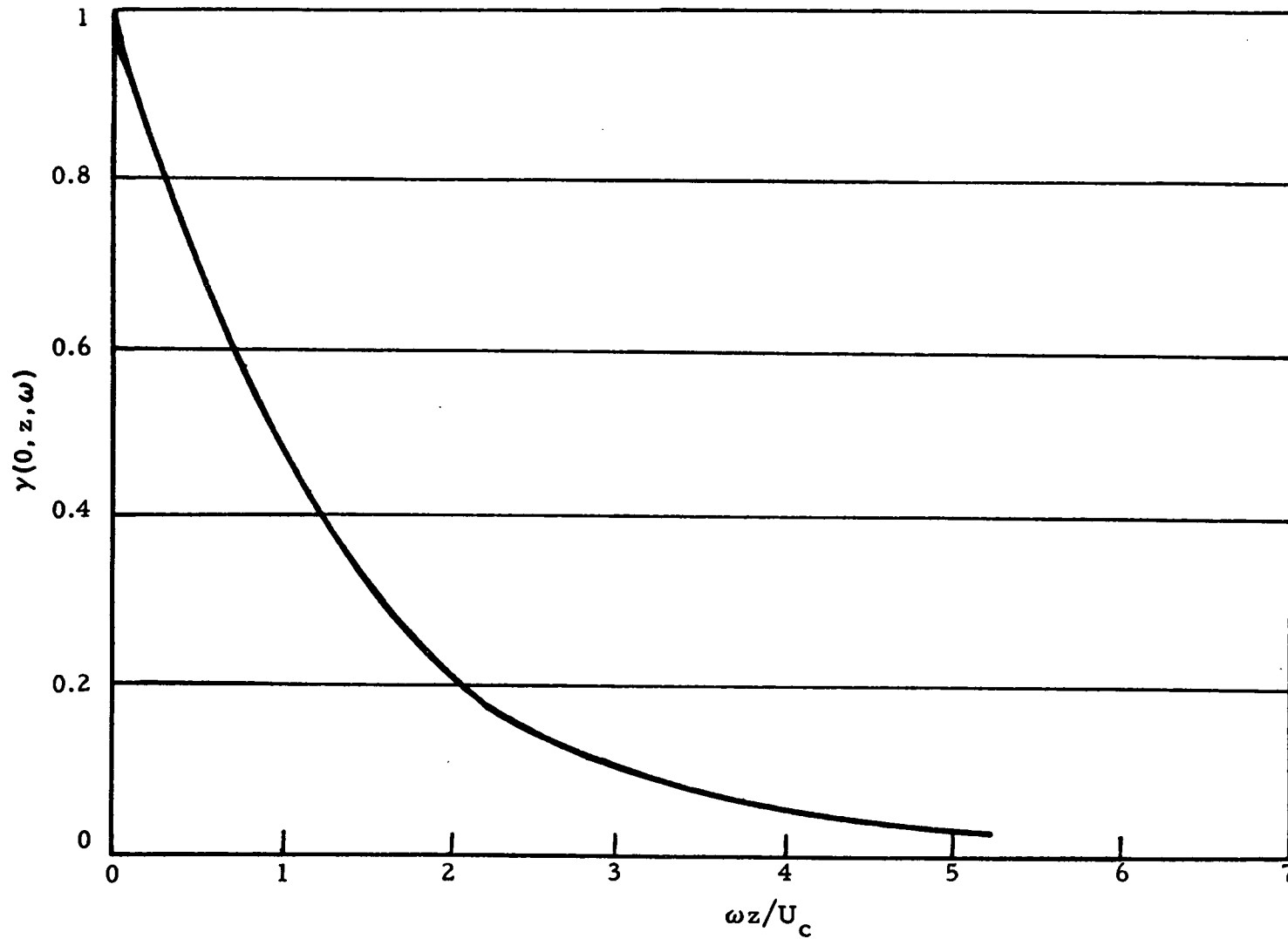


Fig. 8 - Lateral Coherence Function for Attached Turbulent Boundary Layer (from Blake, Ref. 2)

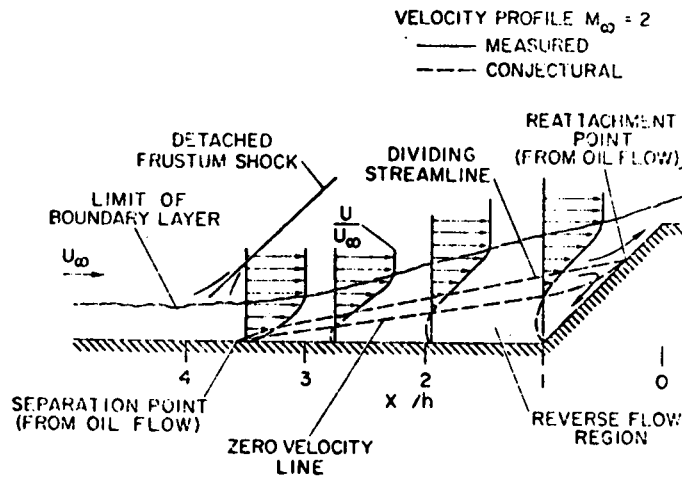


Fig. 9 - Separated Turbulent Flow Ahead of Cone Frustum (from Chyu & Hanly, Ref. 5)

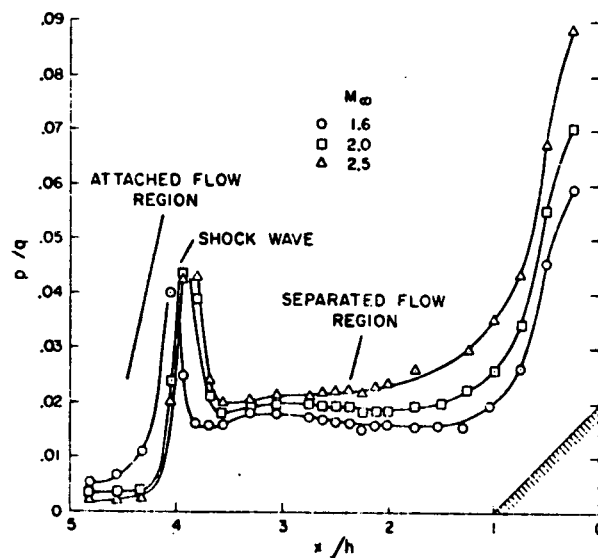


Fig. 10- Longitudinal Variation of Fluctuating Pressure in Separated Turbulent Flow (from Chyu & Hanly, Ref. 5)

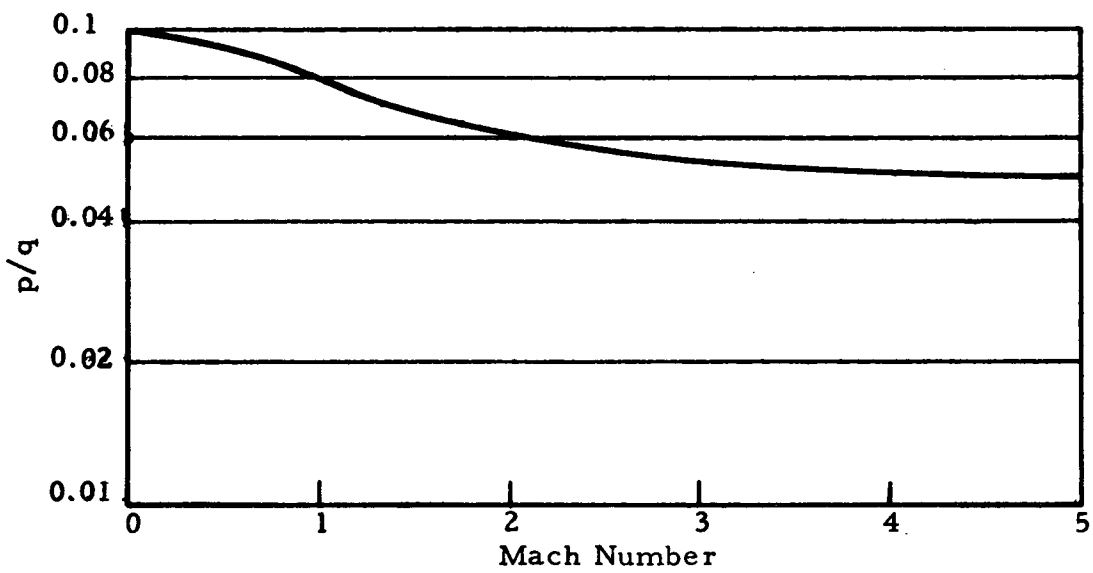


Fig. 11 - Overall Fluctuating Pressure Level for Separated Turbulent Boundary Layer

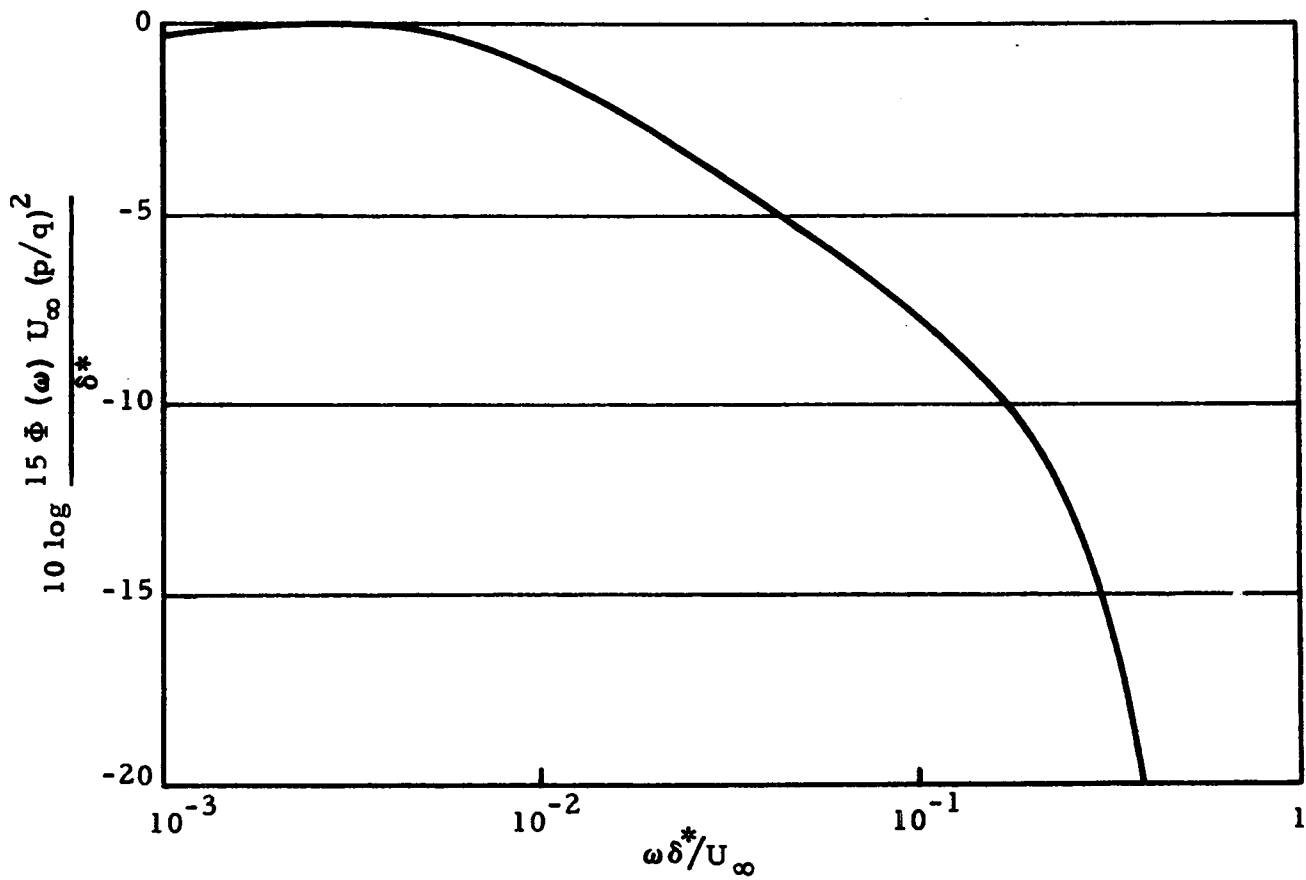


Fig. 12 - Power Spectral Density of Separated Turbulent Boundary Layer (from Chyu and Hanly, Ref. 5)

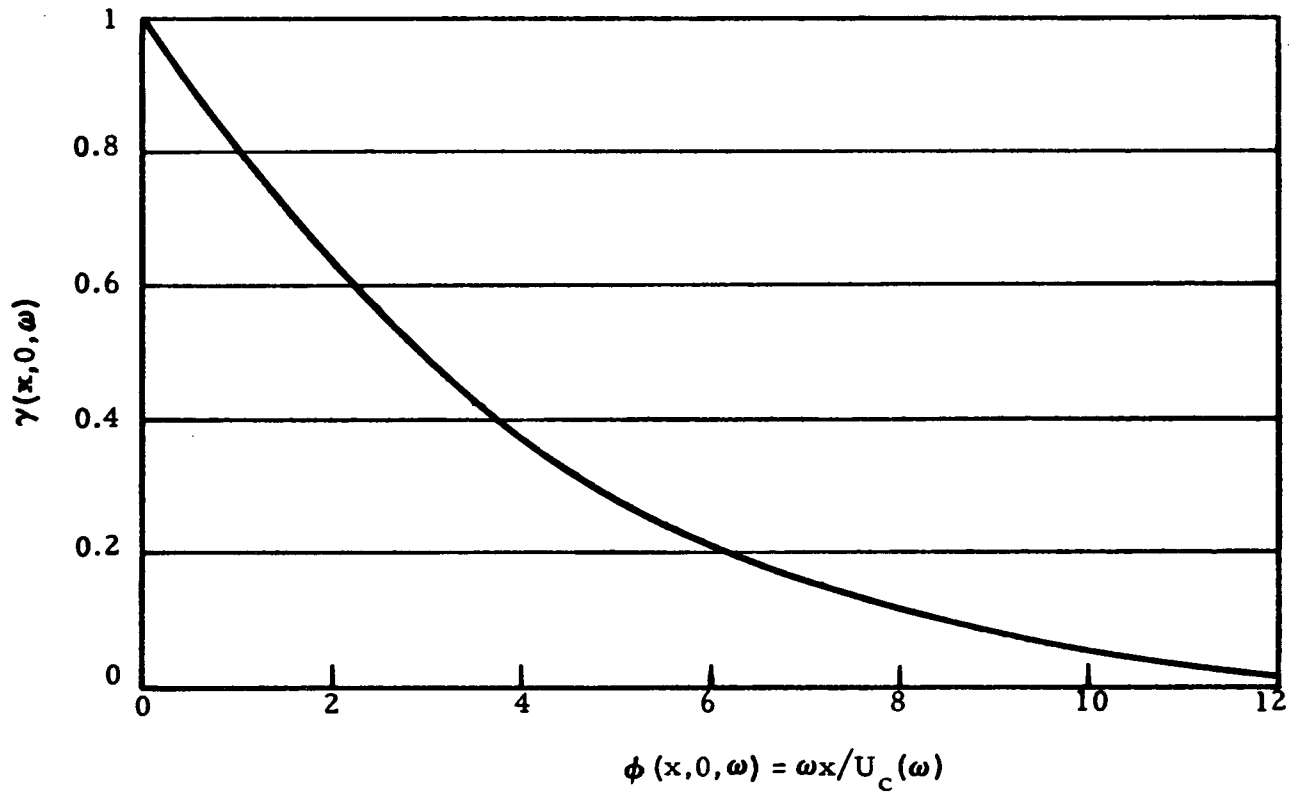


Fig. 13 - Longitudinal Coherence Function for Separated Turbulent Boundary Layer (from Chyu and Hanly, Ref. 5)

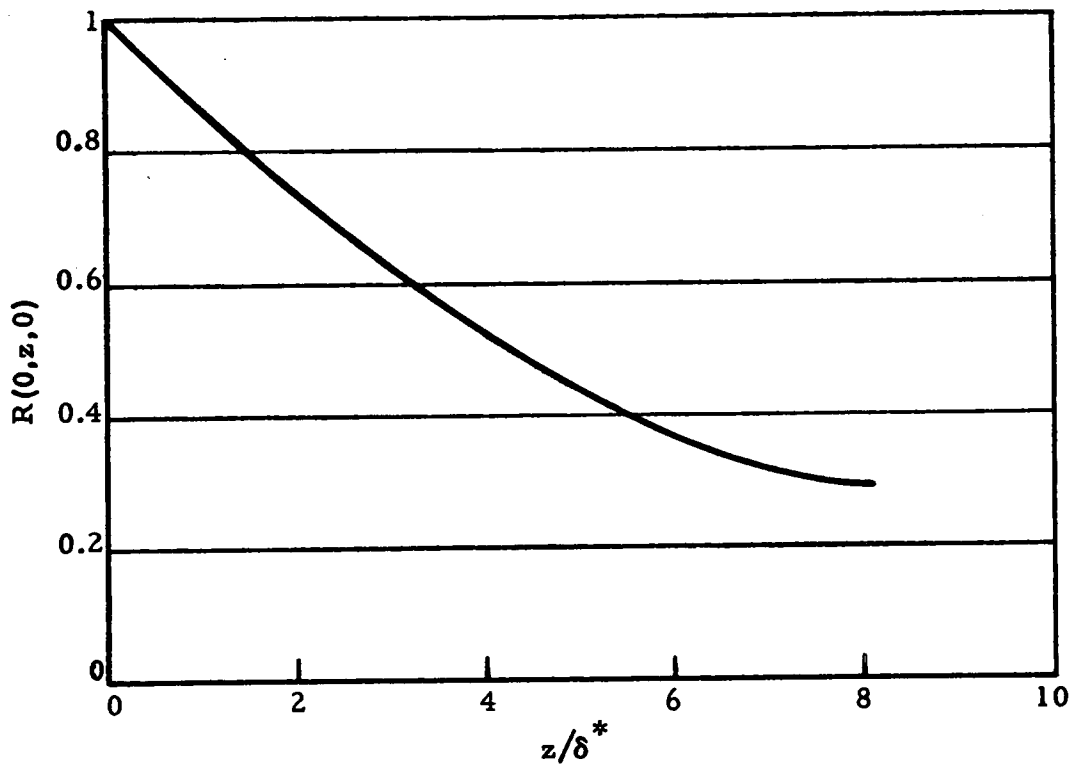


Fig. 14 - Lateral Space Correlation for Separated Turbulent Boundary Layer (from Chyu and Hanly, Ref. 5)

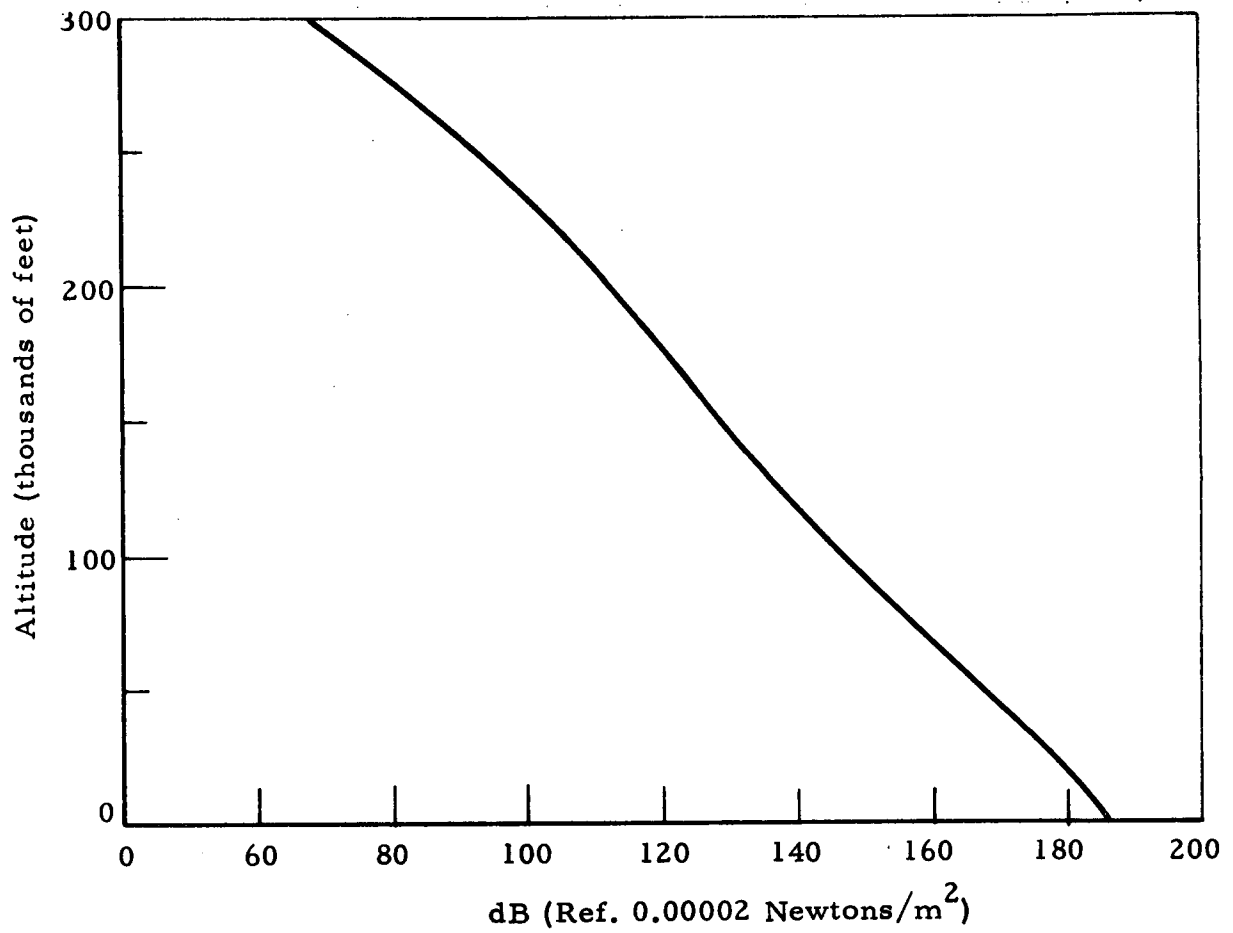


Fig. 15 - Maximum Base Fluctuating Pressure by Altitude

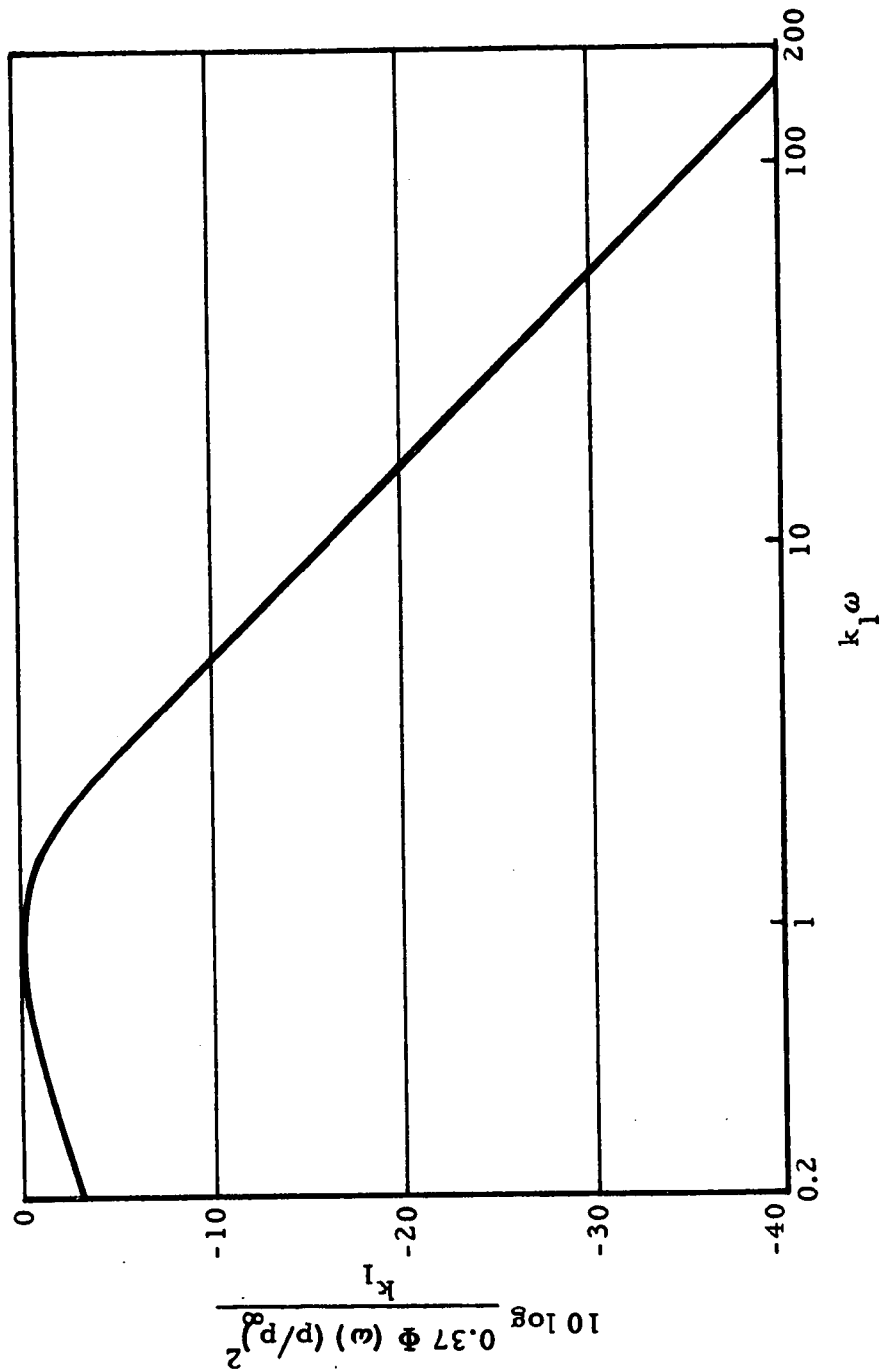


Fig. 16 - Power Spectral Density of Base Pressure Fluctuations

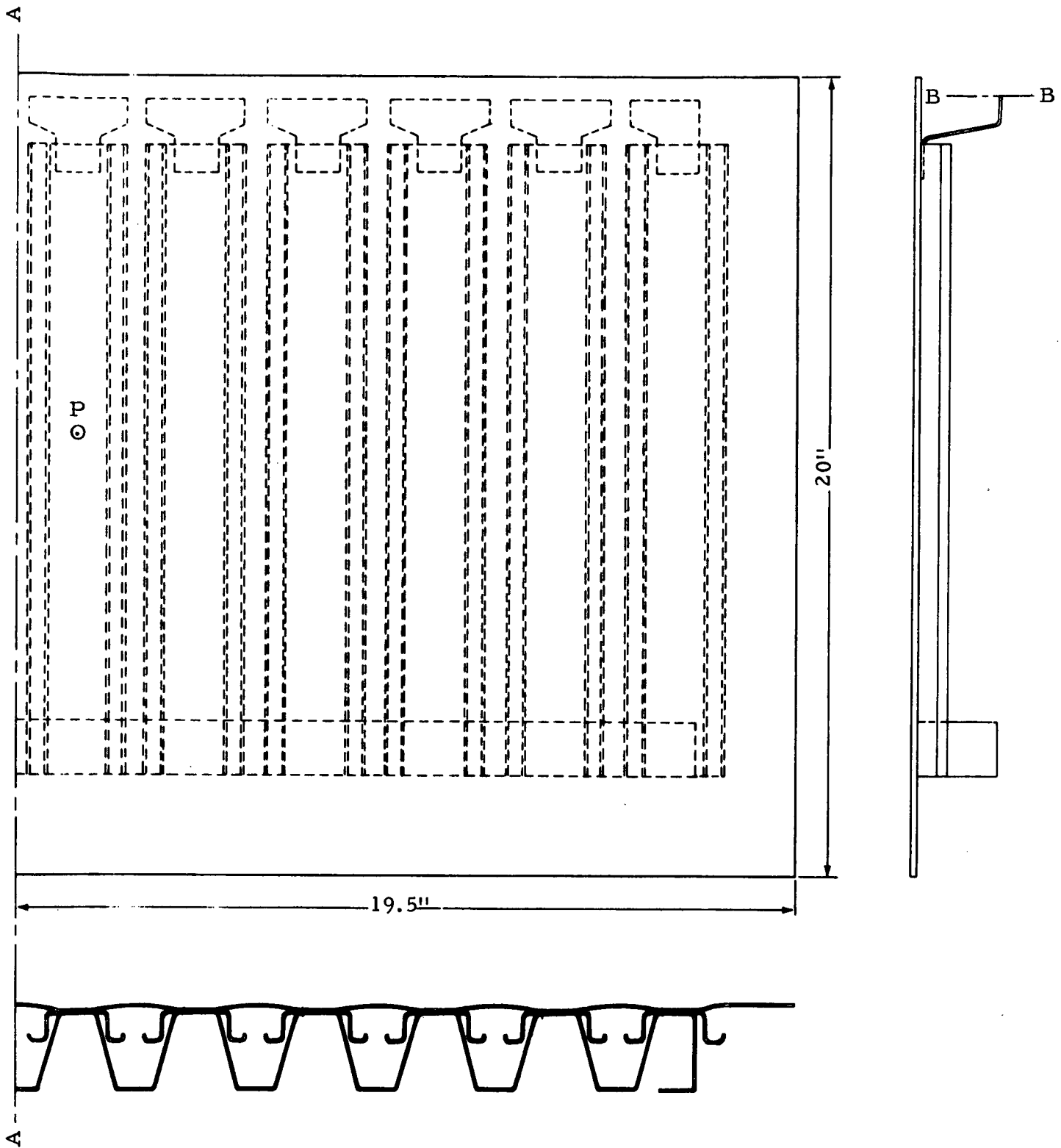


Fig. 17 - TPS Test Panel

UNDEFORMED STRUCTURE



**PLOT 1
VIEW 1**

TPS TEST PANEL * L-805 HAYNES 25

SCALE 1

Fig. 18 - Original Model of TPS Test Panel, View 1

UNDEFORMED STRUCTURE



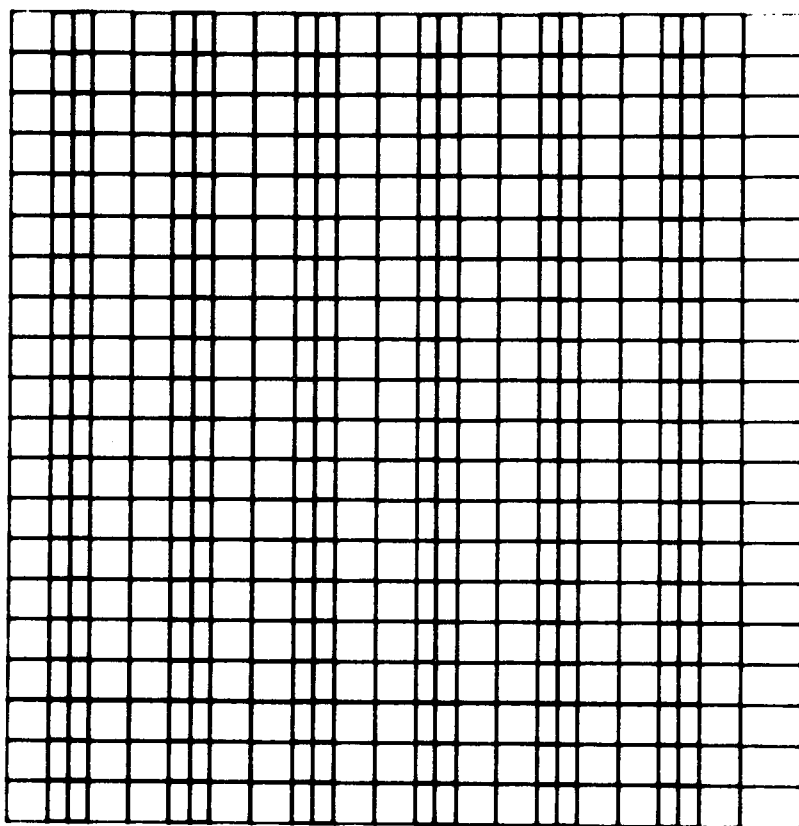
**PLOT 1
VIEW 2**

TPS TEST PANEL * L-605 HAYNES 25

9 SCALE 1

Fig.19 - Original Model of TPS Test Panel, View 2

UNDEFORMED STRUCTURE



**PLOT 1
VIEW 3**

TPS TEST PANEL * L-605 HAYNES 25

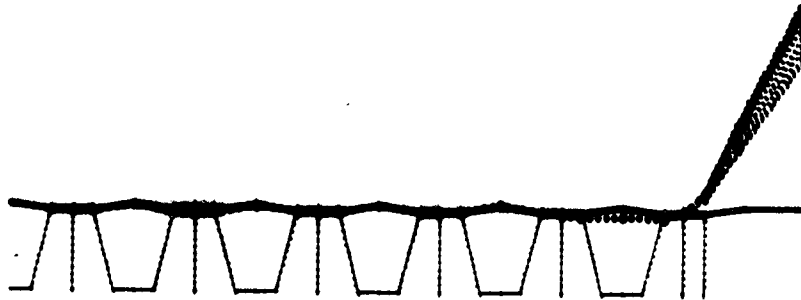
SCALE 1

Fig.20 - Original Model of TPS Test Panel, View 3

MODE 1

FREQUENCY = $.519346 \times 10^{+02}$ CPS

ITERATION 3



PLOT 1
VIEW 1

TPS TEST PANEL * L-805 HAYNES 25

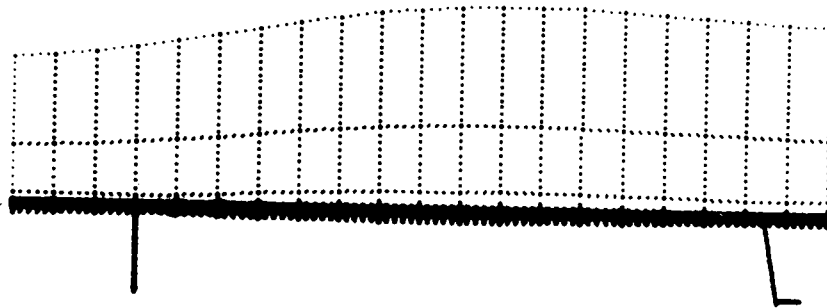
9 SCALE 1

Fig.21 - First Mode of the Original Model, View 1

MODE 1

FREQUENCY = $.519346 \times 10^{+02}$ CPS

ITERATION 3



PLOT 1
VIEW 2

TPS TEST PANEL * L-805 HAYNES 25

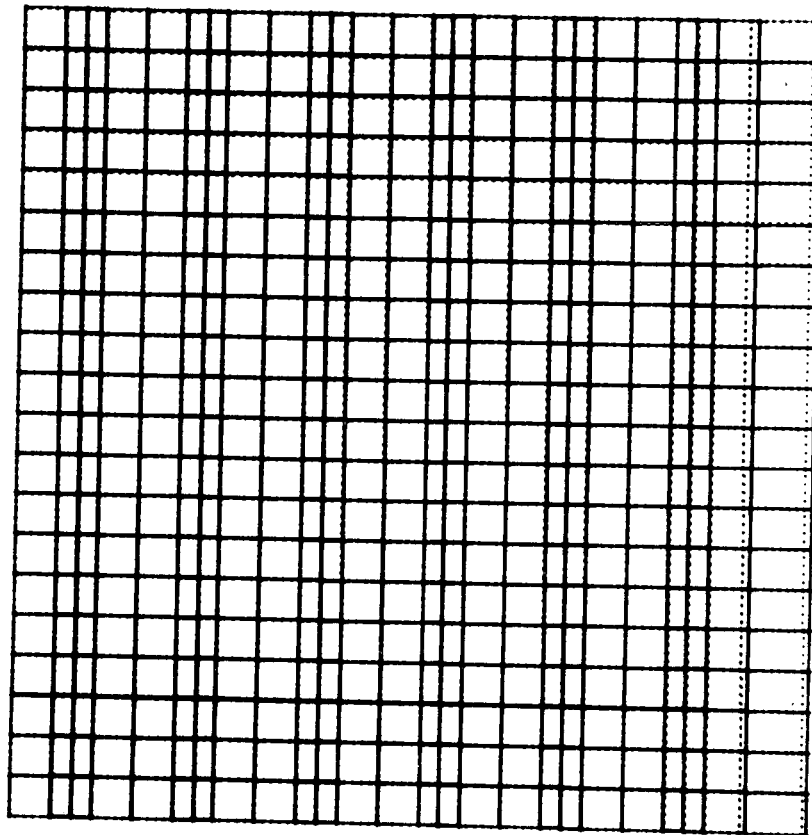
9 SCALE 1

Fig. 22 - First Mode of the Original Model, View 2

MODE 1

FREQUENCY = $.519346 \times 10^{+02}$ CPS

ITERATION 3



PLOT 1
VIEW 3

TPS TEST PANEL * L-805 HAYNES 25

9 SCALE 1

Fig. 23 - First Mode of the Original Model, View 3

UNDEFORMED STRUCTURE



PLOT 1
VIEW 1

TPS TEST PANEL * L-605 HAYNES 25

0 3
SCALE

Fig.24 - Revised Model of TPS Test Panel, View 1

UNDEFORMED STRUCTURE



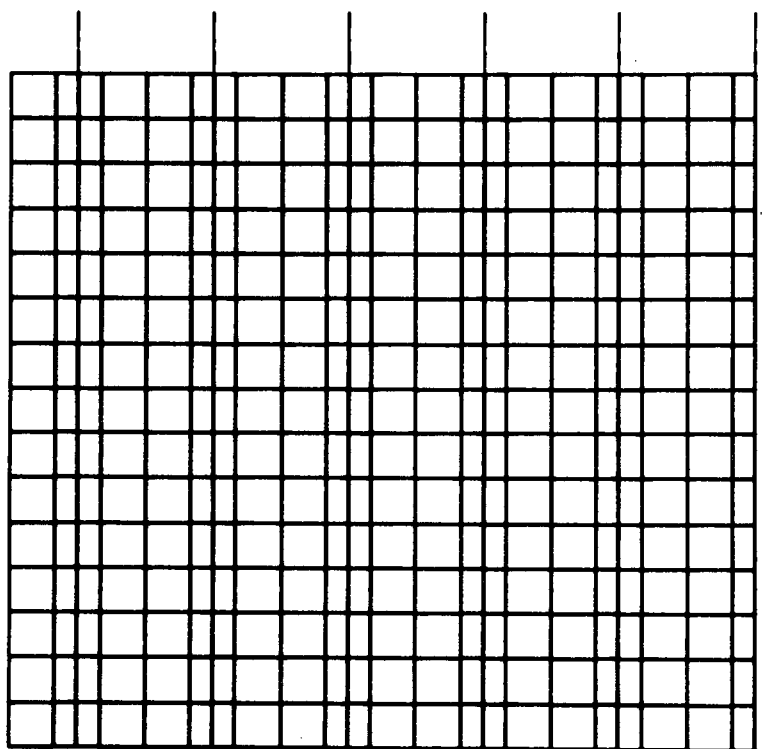
PLOT 1
VIEW 2

TPS TEST PANEL * L-605 HAYNES 25

0 3
SCALE

Fig. 25 - Revised Model of TPS Test Panel, View 2

UNDEFORMED STRUCTURE



PLOT 1
VIEW 3

TPS TEST PANEL * L-605 HAYNES 25

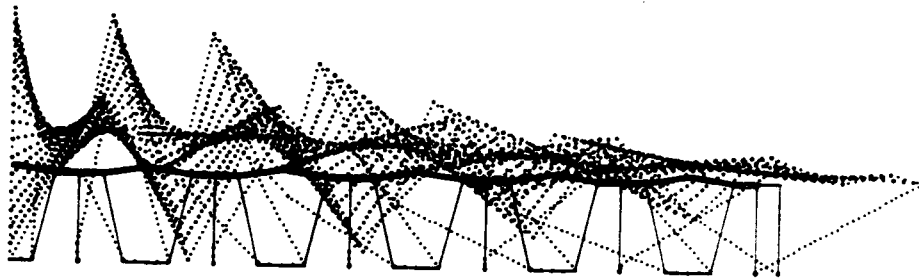
0 3
SCALE

Fig.26 - Revised Model of TPS Test Panel, View 3

MODE 1

FREQUENCY = $.113098 \times 10^{+03}$ CPS

ITERATION 6



PLOT 1
VIEW 1

TPS TEST PANEL * L-605 HAYNES 25

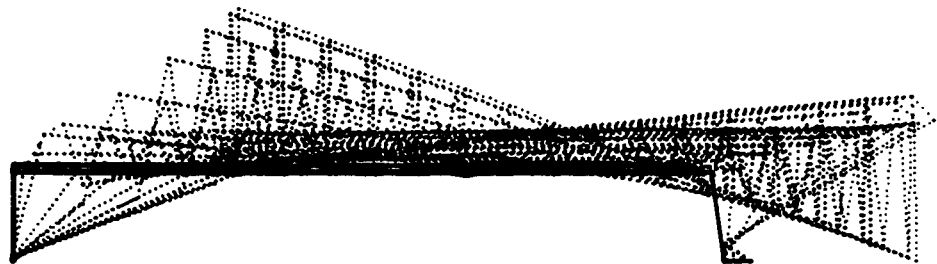
0 SCALE 3

Fig.27 - First Mode of the Revised Model, View 1

MODE 1

ITERATION 6

FREQUENCY = $.113098 \times 10^{+03}$ CPS



PLOT 1
VIEW 2

TPS TEST PANEL * L-605 HAYNES 25

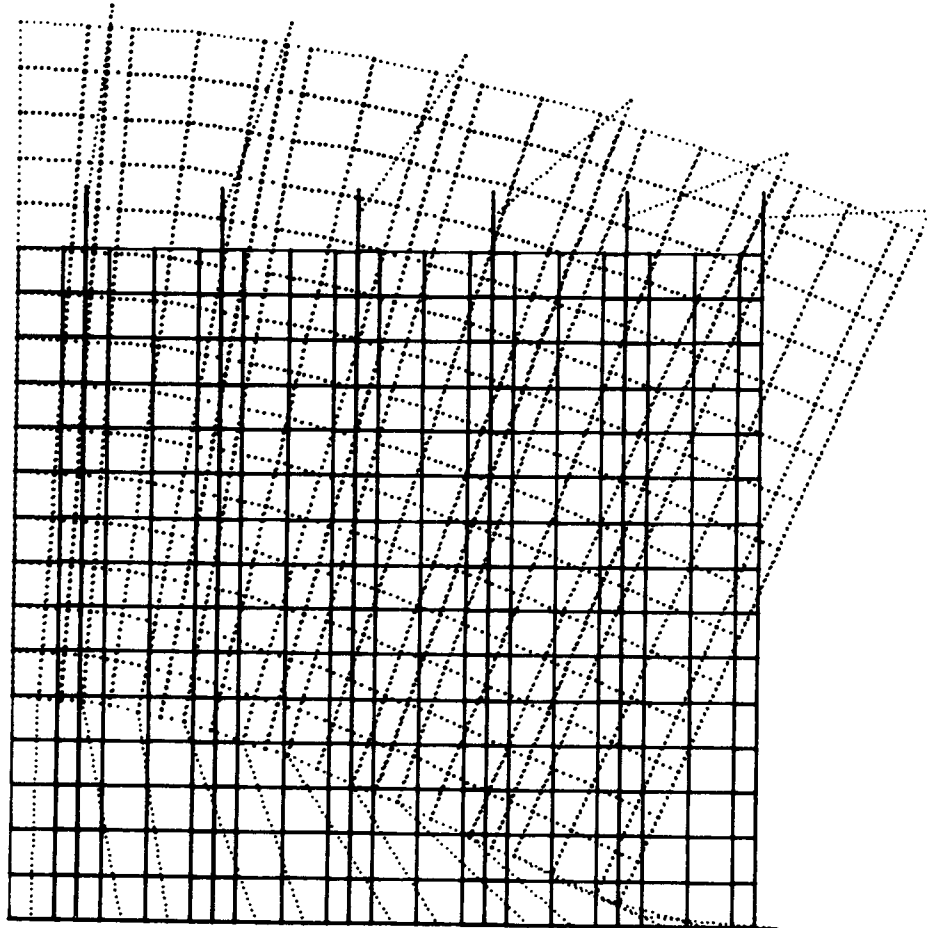
0 SCALE 3

Fig.28 - First Mode of the Revised Model, View 2

MODE 1

FREQUENCY = $.113098 \times 10^{+03}$ CPS

ITERATION 6



PLOT 1
VIEW 3

TPS TEST PANEL * L-605 HAYNES 25

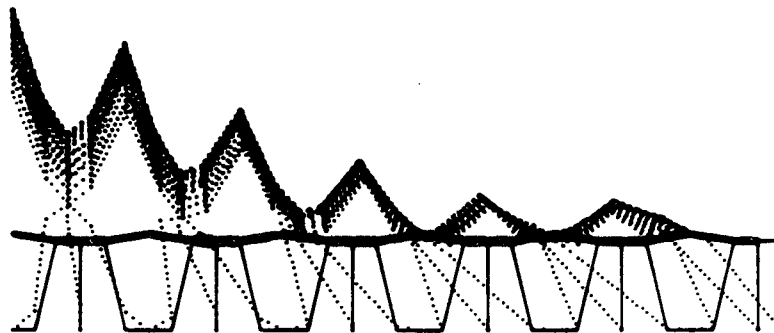
0 SCALE 3

Fig.29 - First Mode of the Revised Model, View 3

MODE 2

FREQUENCY = $.197759 \times 10^{+03}$ CPS

ITERATION 2
0



PLOT 1
VIEW 1

TPS TEST PANEL * L-605 HAYNES 25

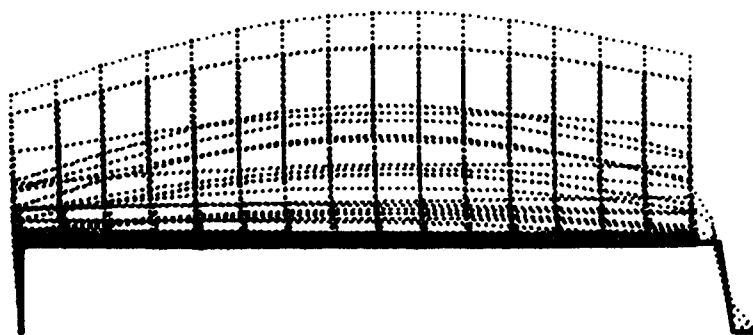
0 3
SCALE

Fig. 30 - Second Mode of the Revised Model, View 1

MODE 2

FREQUENCY = $.197759 \times 10^{+03}$ CPS

ITERATION 2
0



PLOT 1
VIEW 2

TPS TEST PANEL * L-605 HAYNES 25

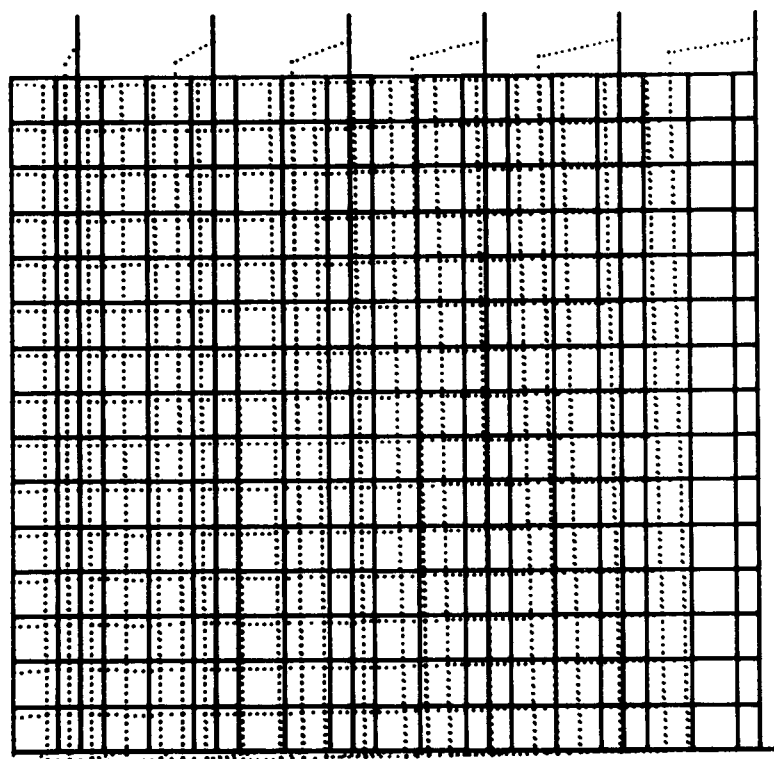
0  3
SCALE

Fig. 31 - Second Mode of the Revised Model, View 2

MODE 2

ITERATION 2
0

FREQUENCY = $.197759 \times 10^{+03}$ CPS



PLOT 1
VIEW 3

TPS TEST PANEL * L-605 HAYNES 25

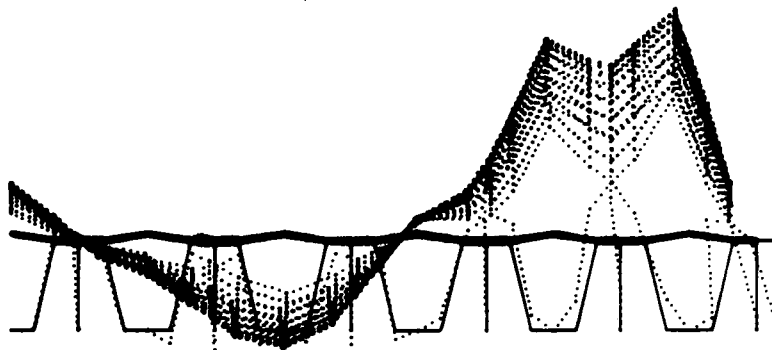
0 3
SCALE

Fig. 32 - Second Mode of the Revised Model, View 3

MODE 3

FREQUENCY = $.212658 \times 10^{+03}$ CPS

ITERATION 2
0



PLOT 1
VIEW 1

TPS TEST PANEL * L-605 HAYNES 25

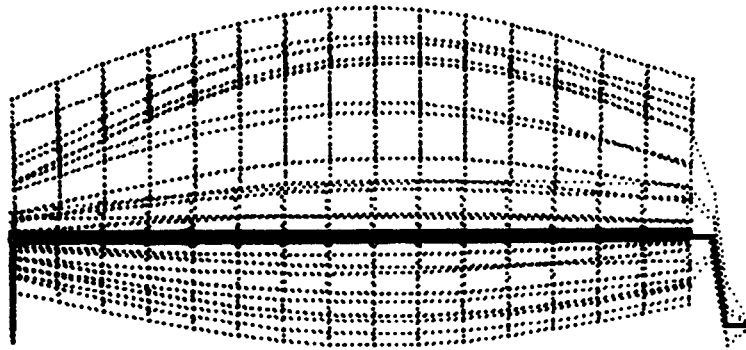
0 SCALE 3

Fig. 33 - Third Mode of the Revised Model, View 1

MODE 3

FREQUENCY = $.212658 \times 10^{+03}$ CPS

ITERATION 2
0



PLOT 1
VIEW 2

TPS TEST PANEL * L-605 HAYNES 25

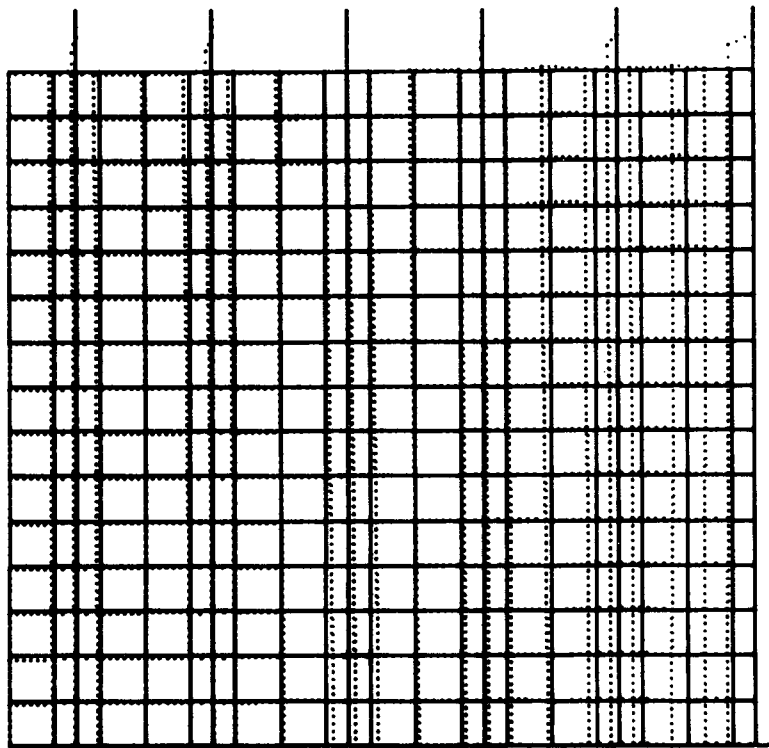
0 SCALE 3

Fig. 34 - Third Mode of the Revised Model, View 2

MODE 3

FREQUENCY = $.212658 \times 10^{+03}$ CPS

ITERATION 2
0



PLOT 1
VIEW 3

TPS TEST PANEL * L-605 HAYNES 25

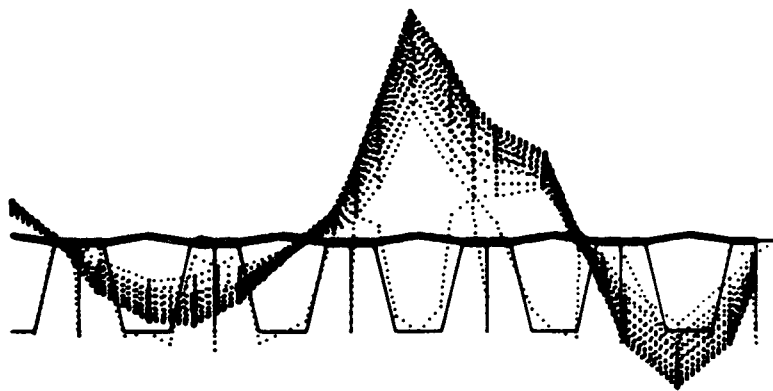
0  3
SCALE

Fig.35 - Third Mode of the Revised Model, View 3

MODE 4

FREQUENCY = $.215982 \times 10^{+03}$ CPS

ITERATION 2
0



PLOT !
VIEW !

TPS TEST PANEL * L-605 HAYNES 25

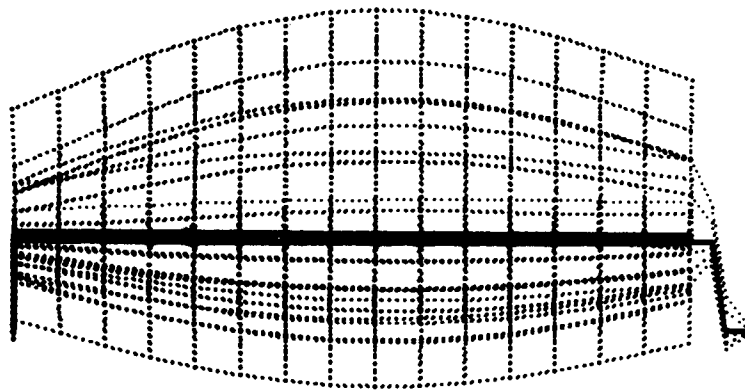
0 3
SCALE

Fig. 36 - Fourth Mode of the Revised Model, View 1

MODE 4

FREQUENCY = $.215982 \times 10^{+03}$ CPS

ITERATION 2
0



PLOT 1
VIEW 2

TPS TEST PANEL * L-605 HAYNES 25

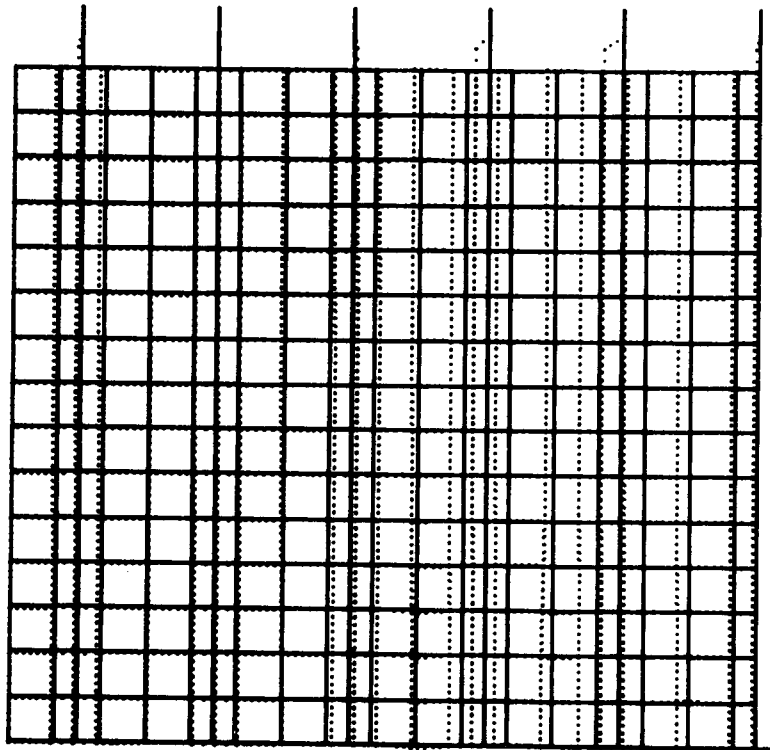
0  3
SCALE

Fig.37 - Fourth Mode of the Revised Model, View 2

MODE 4

FREQUENCY = $.215982 \times 10^{+03}$ CPS

ITERATION 2
0



PLOT 1
VIEW 3

TPS TEST PANEL * L-605 HAYNES 25

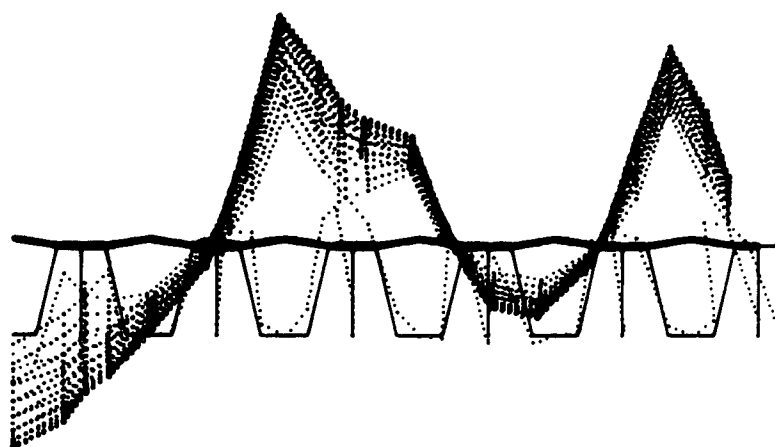
0 3
SCALE

Fig. 38 - Fourth Mode of the Revised Model, View 3

MODE 5

FREQUENCY = $.215822 \times 10^{+03}$ CPS

ITERATION 2
0



PLOT 1
VIEW 1

TPS TEST PANEL * L-605 HAYNES 25

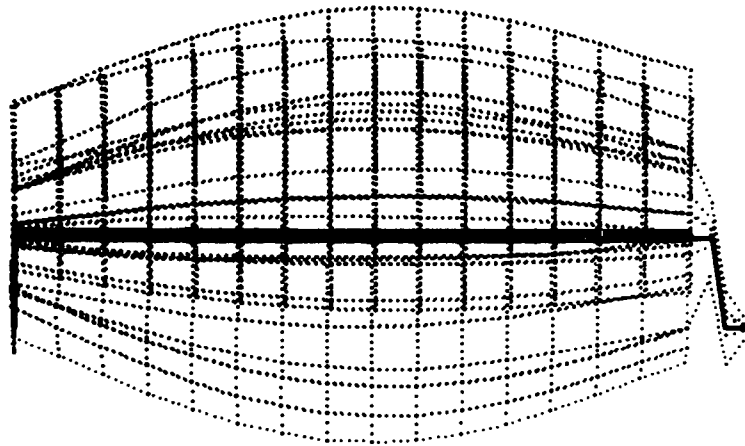
0 SCALE 3

Fig. 39 - Fifth Mode of the Revised Model, View 1

MODE 5

FREQUENCY = $.215822 \times 10^{+03}$ CPS

ITERATION 2
0



PLOT 1
VIEW 2

TPS TEST PANEL * L-605 HAYNES 25

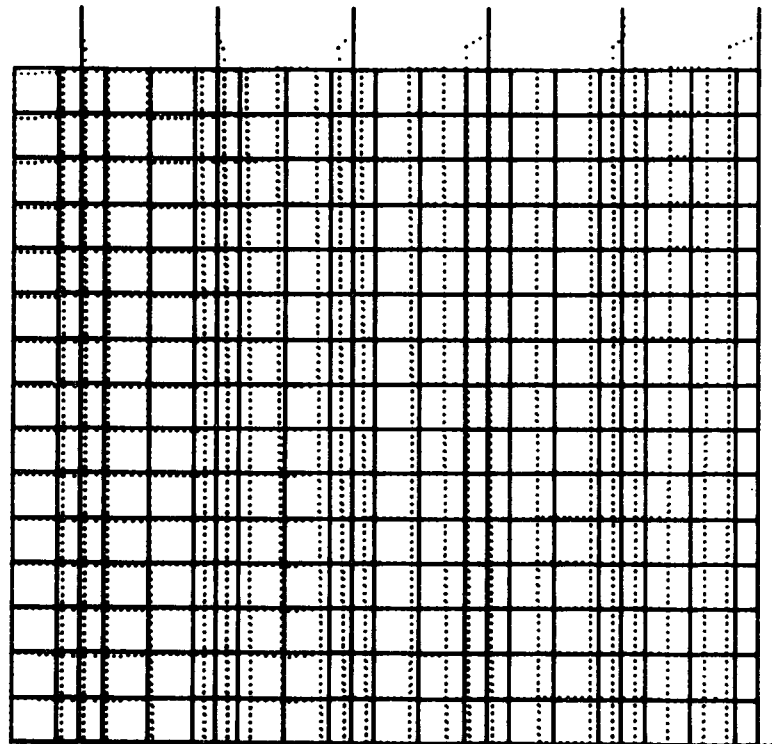
0 3
SCALE

Fig. 40 - Fifth Mode of the Revised Model, View 2

MODE 5

FREQUENCY = $.215822 \times 10^{+03}$ CPS

ITERATION 2
0



PLOT 1
VIEW 3

TPS TEST PANEL * L-605 HAYNES 25

0 3
SCALE

Fig. 41 - Fifth Mode of the Revised Model, View 3

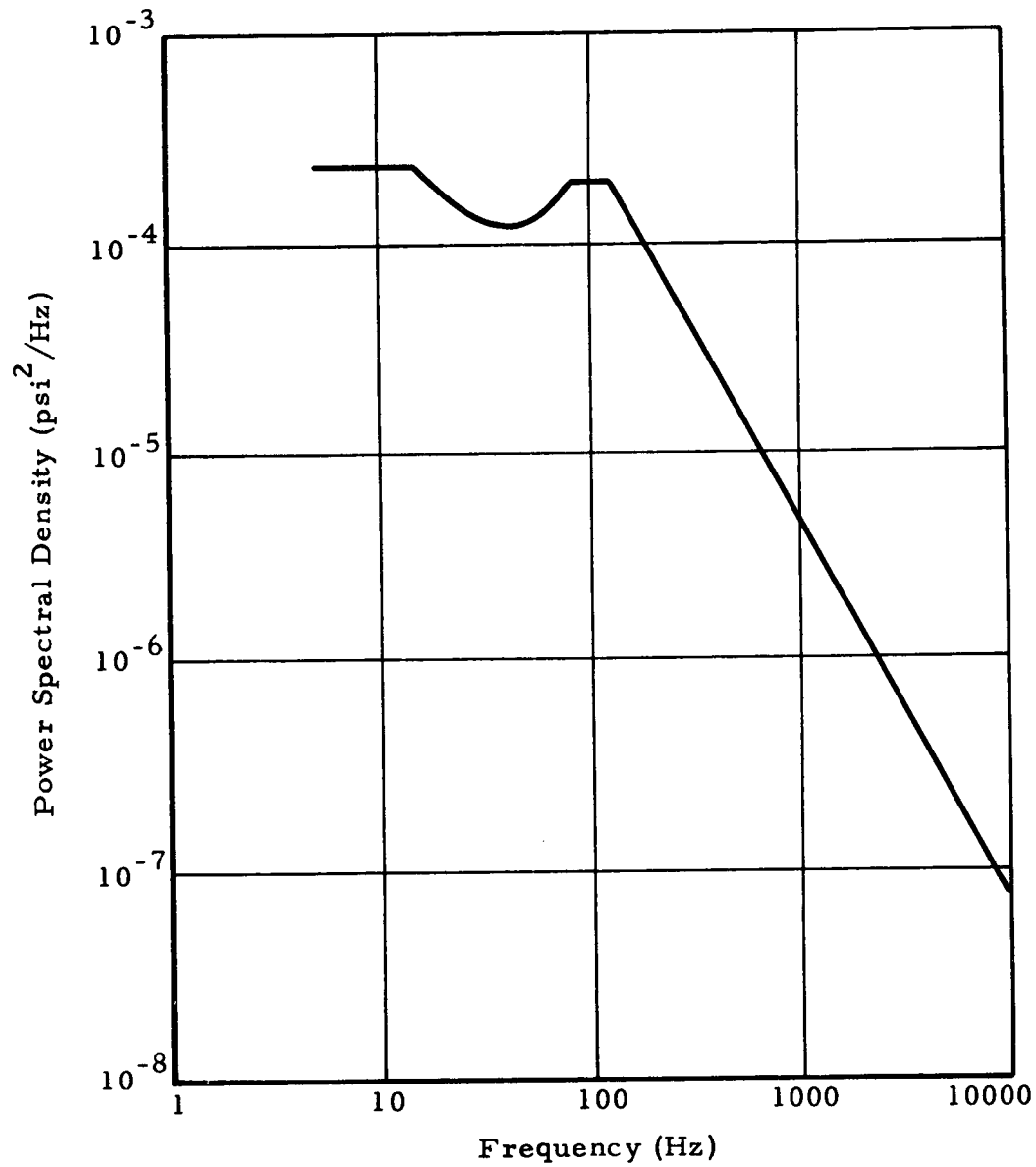


Fig. 42 Power Spectral Density of the Pressure Field in the Reverberation Chamber Test

TPS PANEL HAYNES 25 ALLOY L-605
DISPLACEMENT RESPONSE IN INCHES JOINT 53

VAR = 0.74332 E-04
RMS = 0.86216 E-02

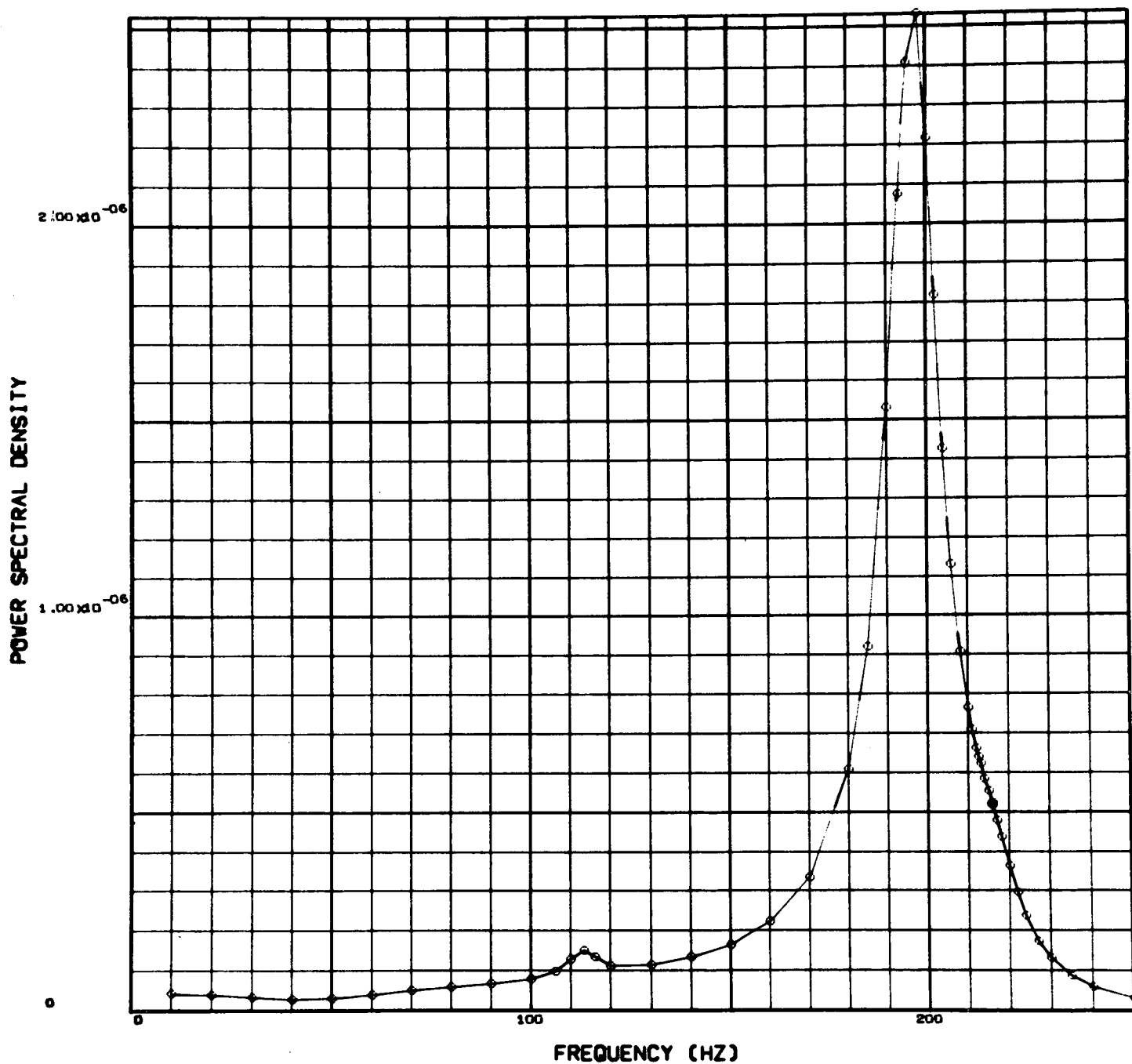


Fig. 43 - Power Spectral Density of the Response Displacement at P,
Linear Scale, 4% Modal Damping

TPS PANEL HAYNES 25 ALLOY L-605
DISPLACEMENT RESPONSE IN INCHES JOINT 53

VAR = 0.74332 E-04
RMS = 0.86216 E-02

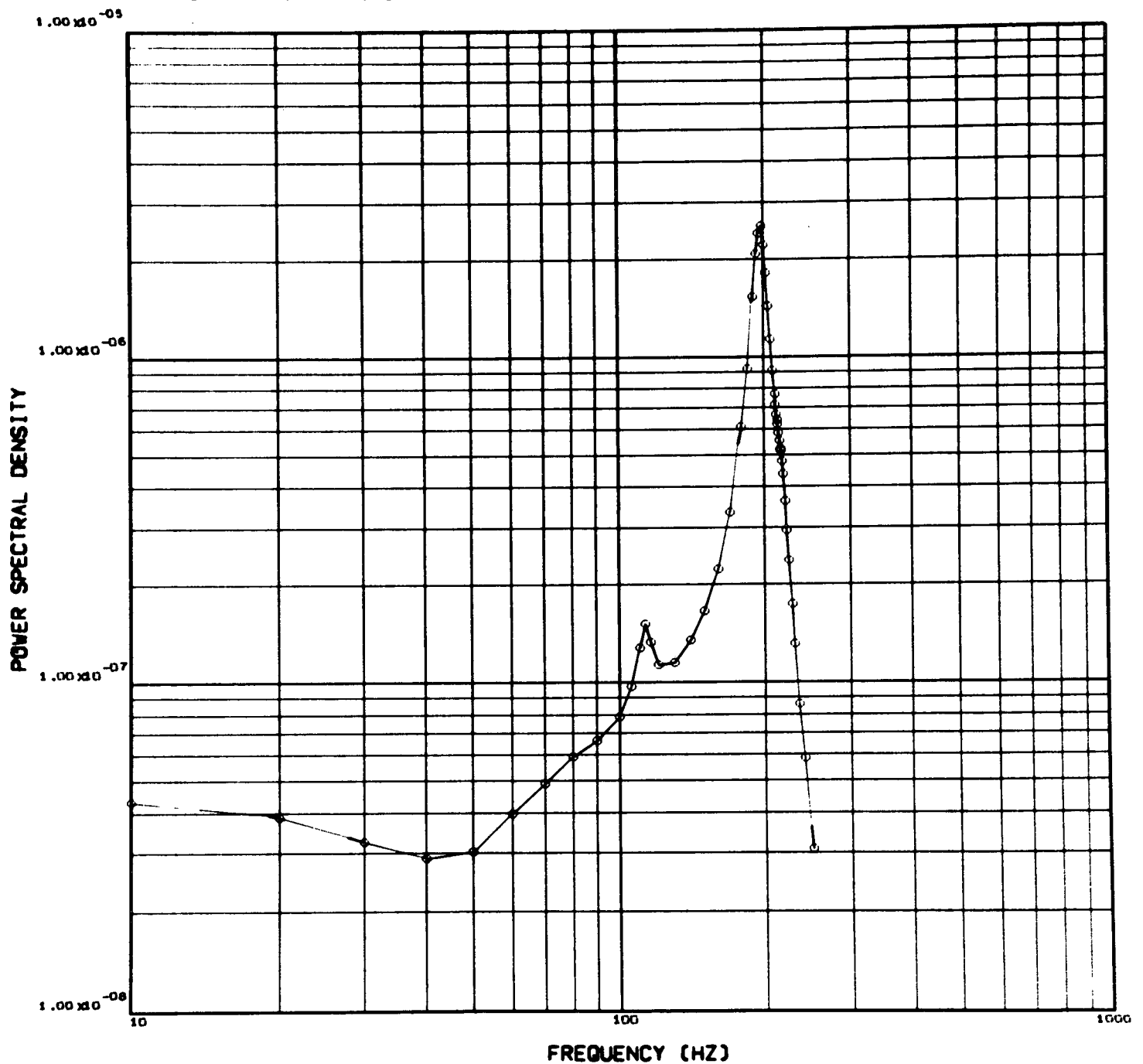


Fig. 44 - Power Spectral Density of the Response Displacement at P, Log-Log Scale, 4% Modal Damping

TPS PANEL HAYNES 25 ALLOY L-605
ACCELERATION RESPONSE IN G'S JOINT 53

VAR = 0.10345 E 04
RMS = 0.32164 E 02

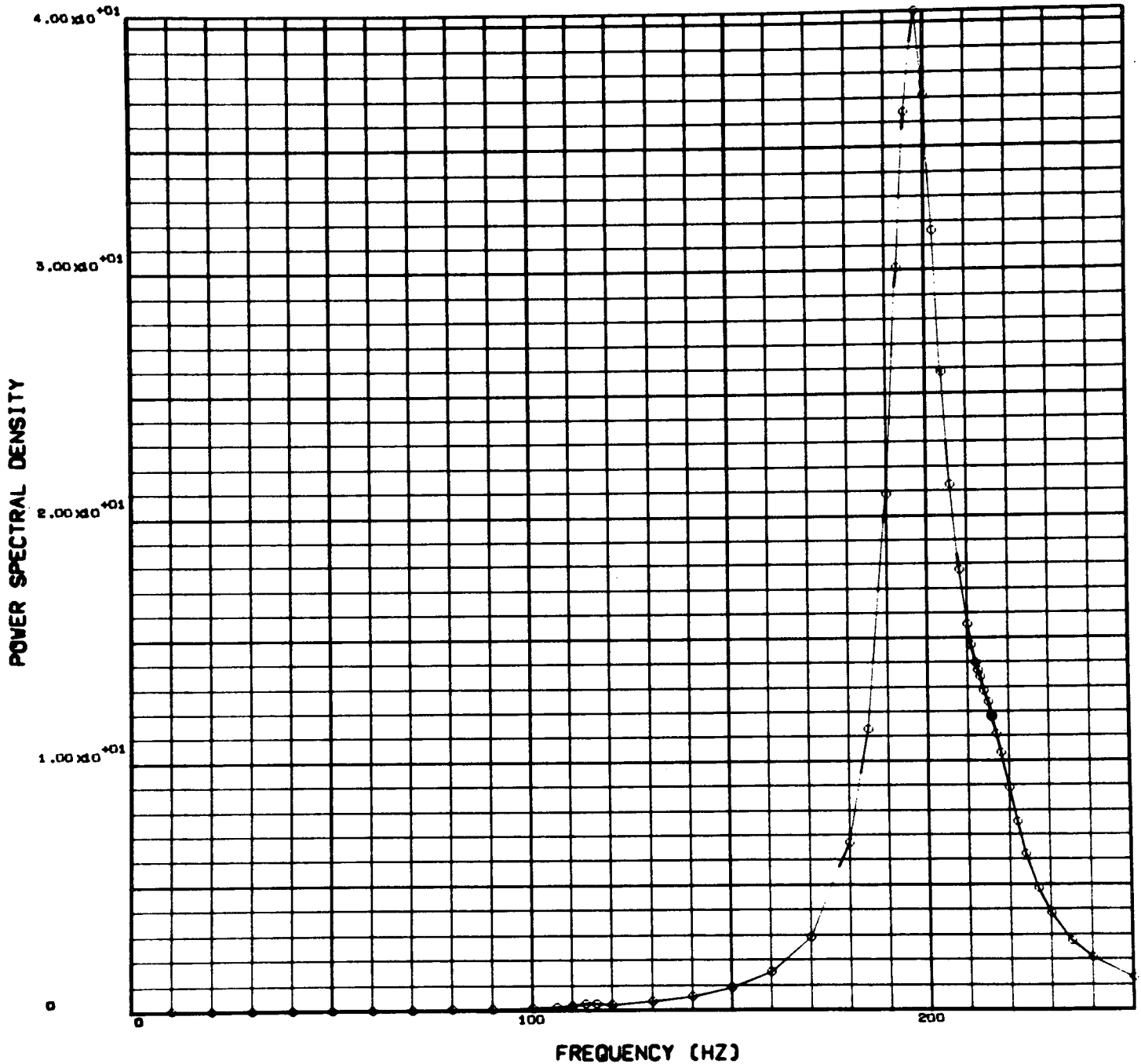


Fig. 45 - Power Spectral Density of the Response Acceleration at P,
Linear Scale, 4% Modal Damping

TPS PANEL HAYNES 25 ALLOY L-605
ACCELERATION RESPONSE IN G'S JOINT 53

VAR = 0.10345 E 04
RMS = 0.32164 E 02

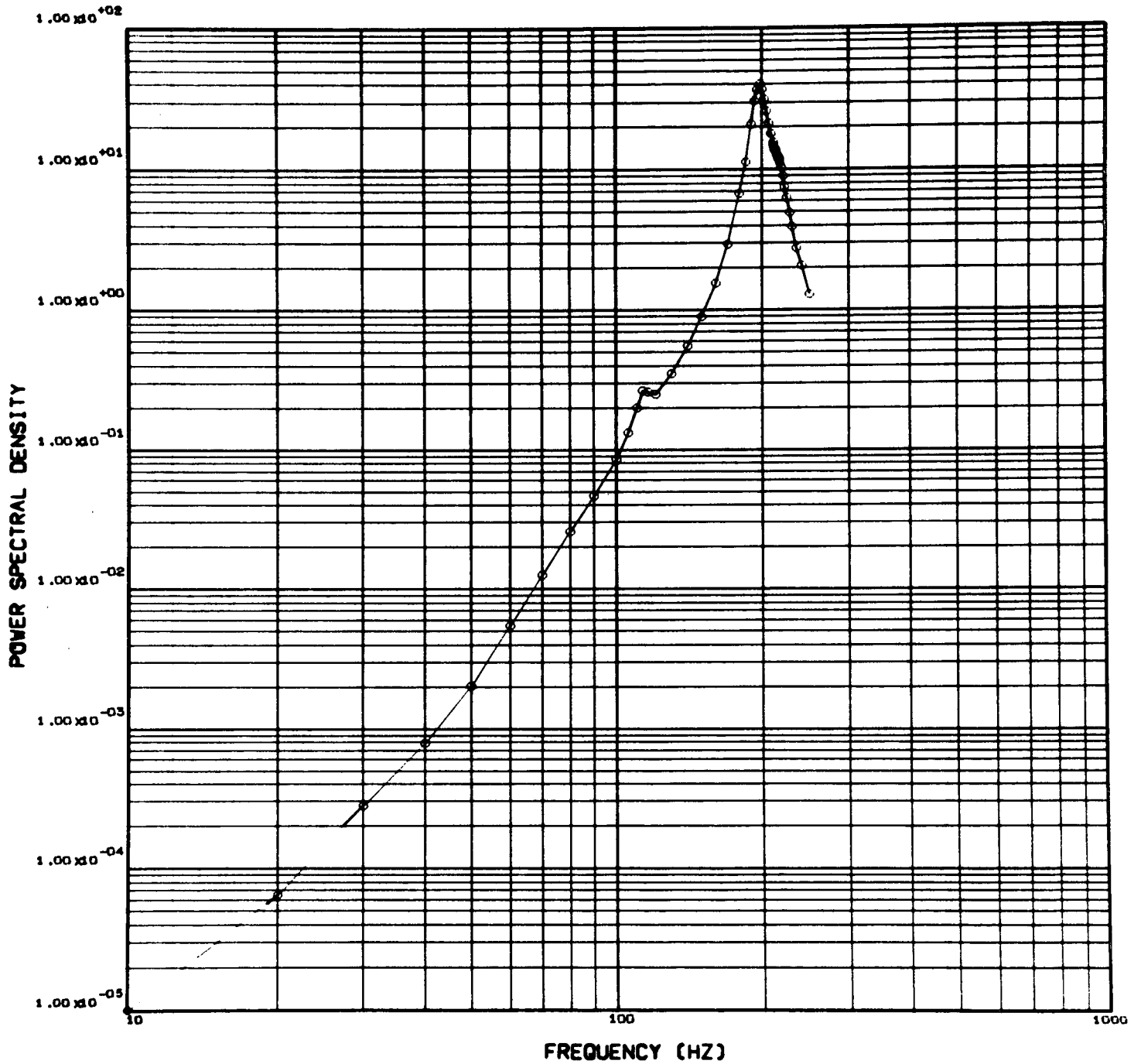


Fig. 46 - Power Spectral Density of the Response Acceleration at P, Log-Log Scale, 4% Modal Damping

TPS PANEL HAYNES 25 ALLOY L-605
DISPLACEMENT RESPONSE IN INCHES JOINT 53

VAR = 0.60338 E-04
RMS = 0.77678 E-02

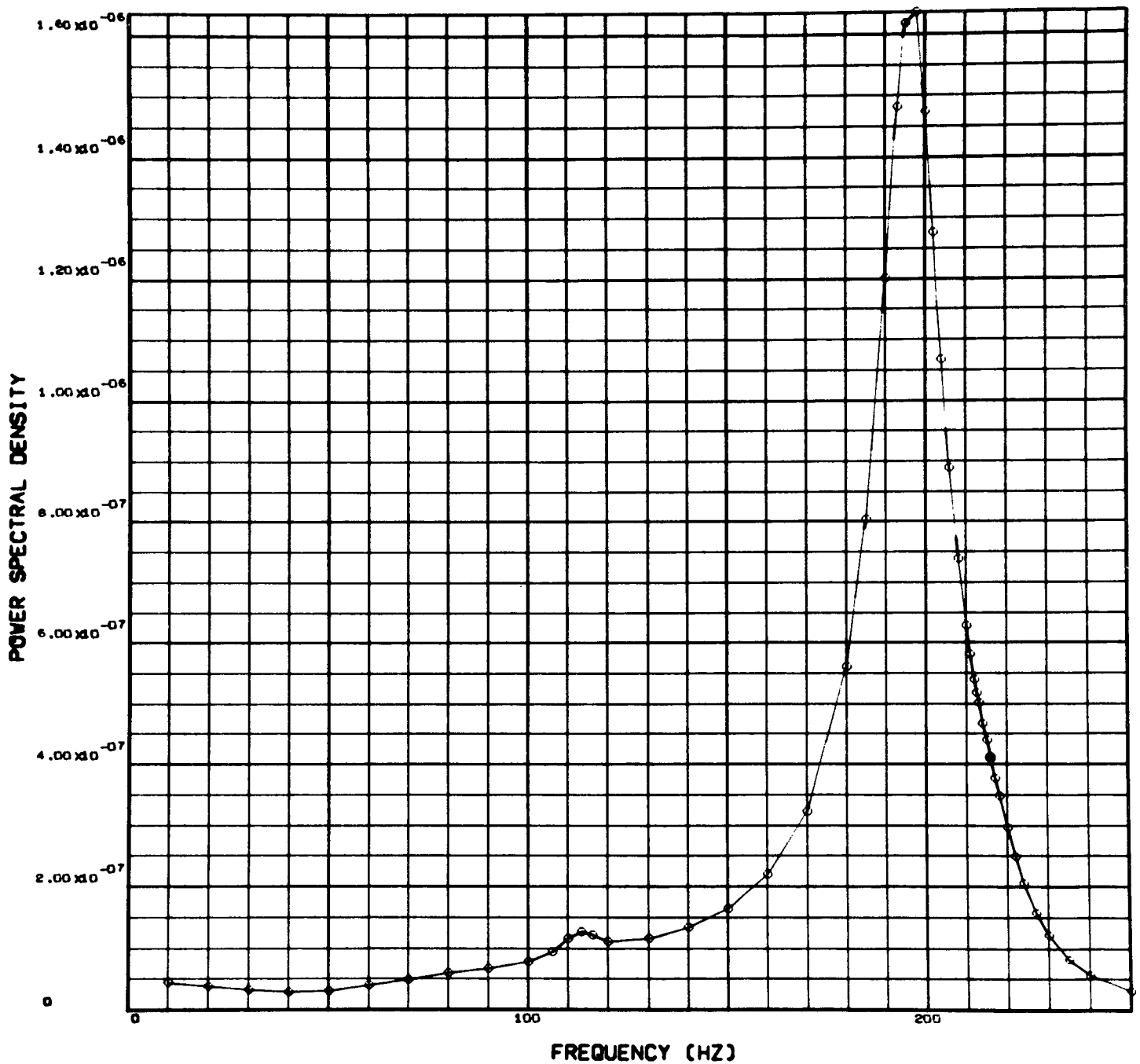


Fig. 47 - Power Spectral Density of the Response Displacement at P,
Linear Scale, 5% Modal Damping

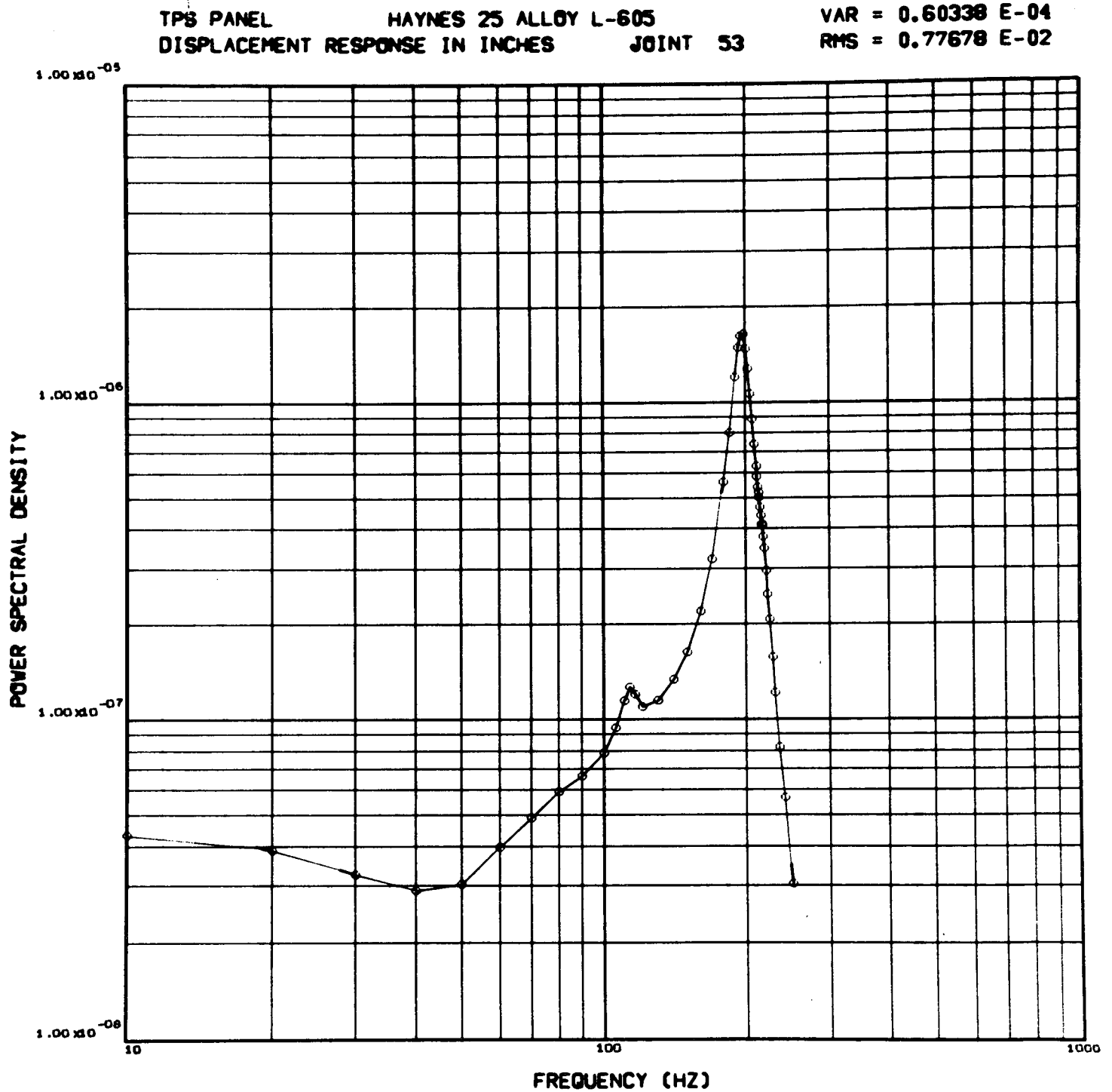


Fig. 48 - Power Spectral Density of the Response Displacement at P, Log-Log Scale, 5% Modal Damping

TPS PANEL

HAYNES 25 ALLOY L-605

VAR = 0.80825 E 03

ACCELERATION RESPONSE IN G'S

JOINT 53

RMS = 0.28429 E 02

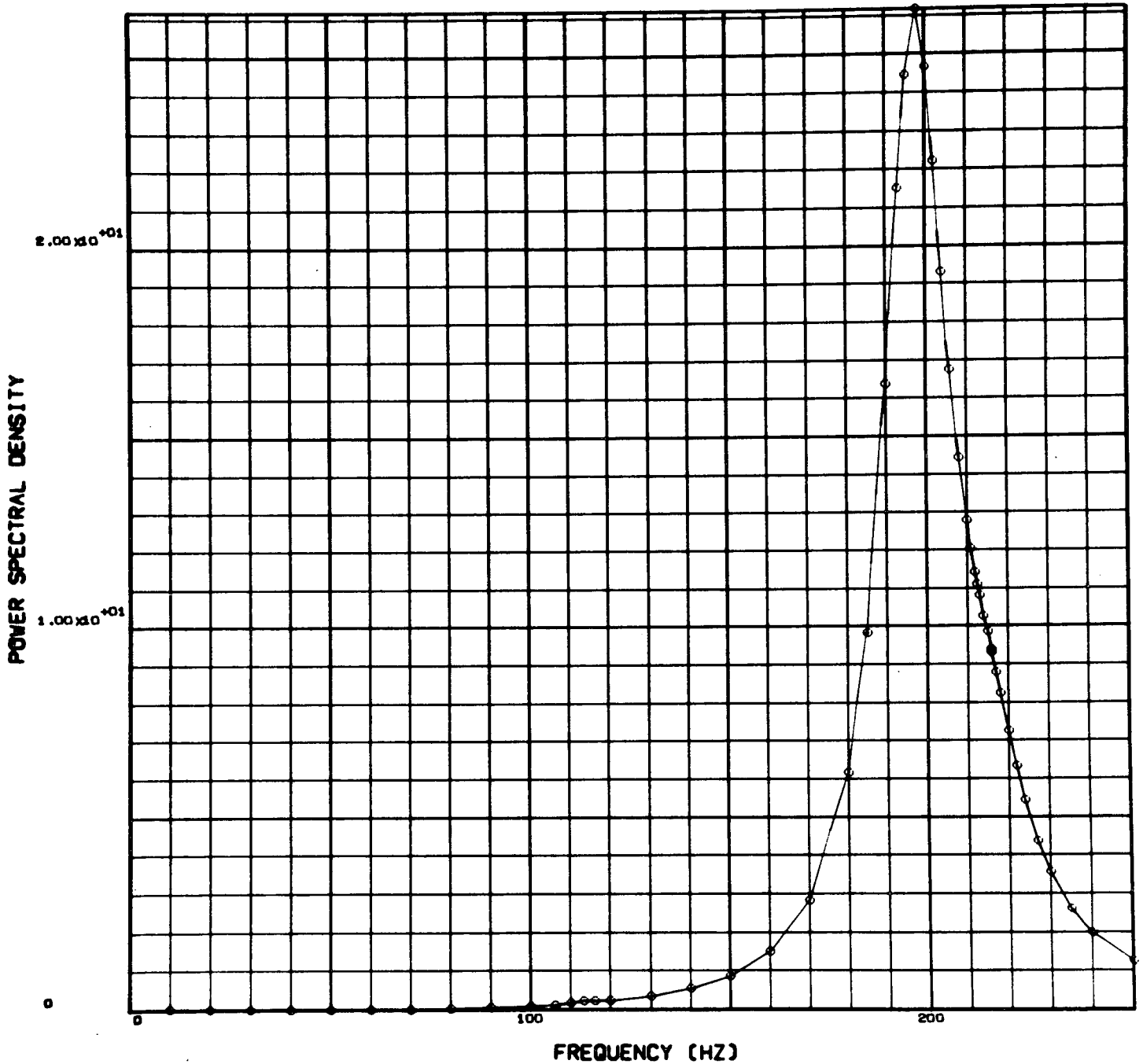


Fig. 49 - Power Spectral Density of the Response Acceleration at P, Linear Scale, 5% Modal Damping

TPS PANEL

HAYNES 25 ALLOY L-605

VAR = 0.80825 E 03

ACCELERATION RESPONSE IN G'S

JOINT 53

RMS = 0.28429 E 02

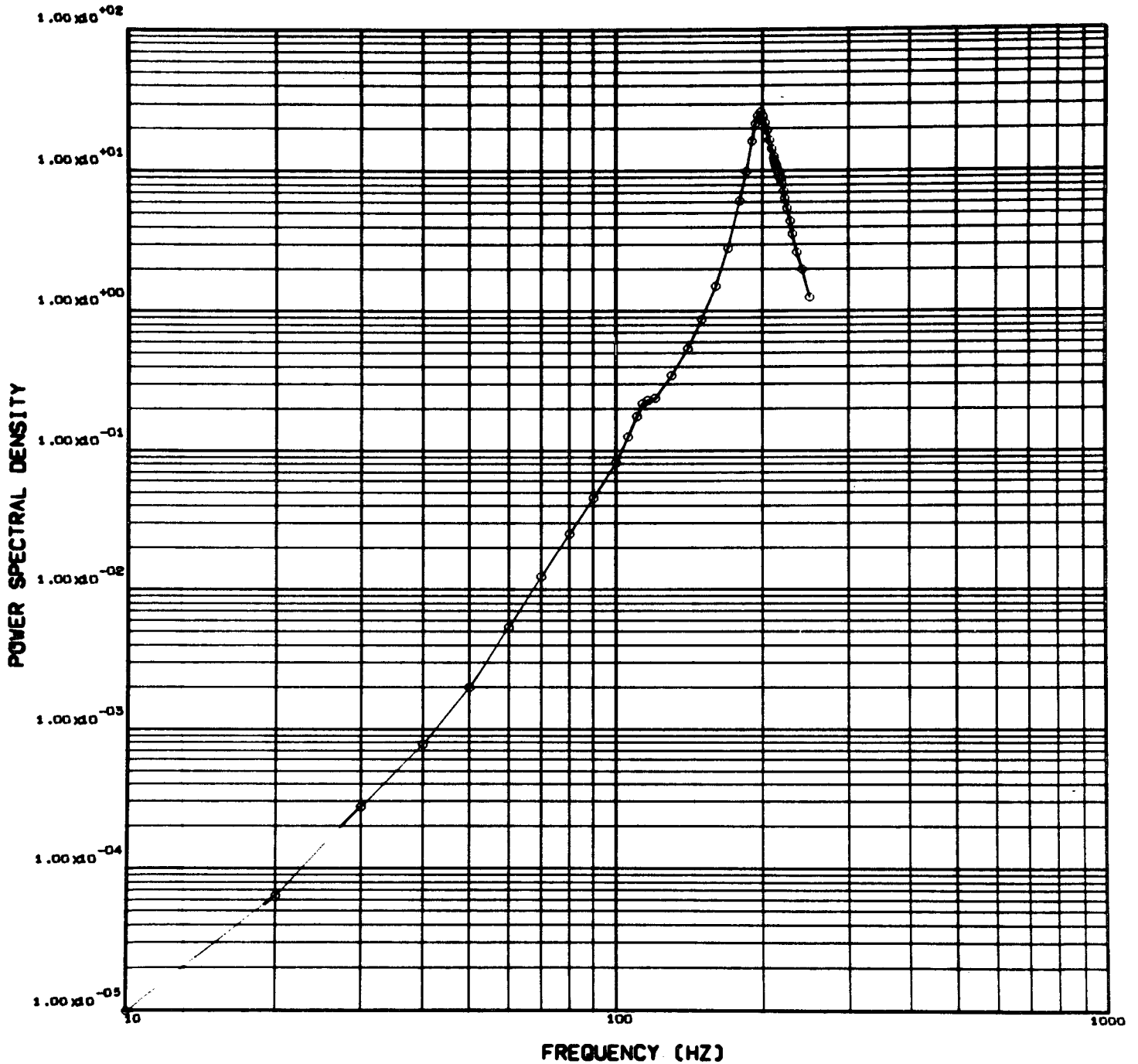


Fig. 50 - Power Spectral Density of the Response Acceleration at P, Log-Log Scale, 5% Modal Damping

Appendix A

ANALYSIS OF ATTACHED TURBULENT
BOUNDARY LAYER

Appendix A

A.1 INTRODUCTION

A large portion of the surface of space shuttle-type vehicles will be subjected to attached turbulent boundary layer during reentry into the earth's atmosphere. An investigation was made of the present state of knowledge of the turbulent boundary layer. A theoretical description of the boundary layer is presented. Problems encountered in measuring turbulent boundary layer parameters are discussed, along with results of experimental investigations.

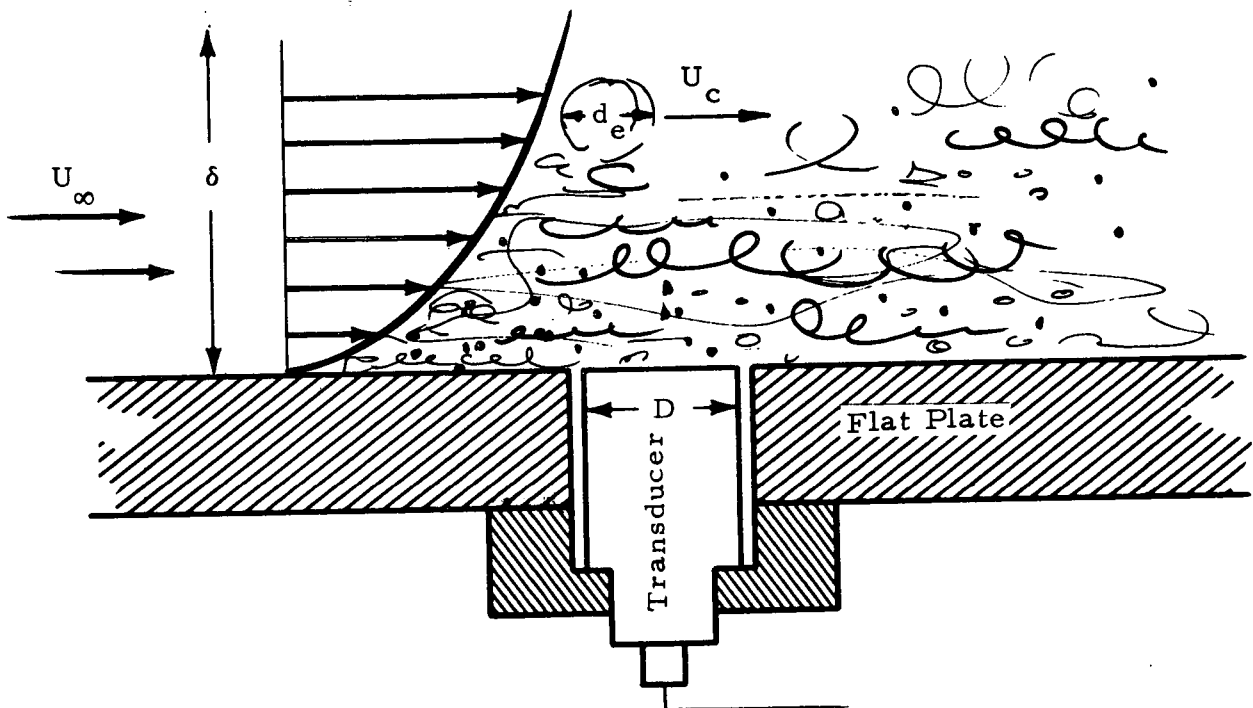
A.2 DISCUSSION

For a perfect fluid, i.e., frictionless and incompressible, motion does not create any tangential forces between contacting layers of fluid. Because of the absence of these forces, a slip condition must be assumed between the moving fluid and a solid boundary, i.e., a difference in relative velocities. For real fluids, however, tangential or shear forces can be transmitted between layers due to the viscosity. Then, because of the existence of intermolecular attractions, the fluid will adhere to a solid wall and give rise to a shearing stress which is transmitted through the fluid. In a thin region near the solid boundary the velocity increases from zero to its full value which corresponds to the external frictionless flow. The thickness of this layer increases along the boundary in the downstream direction and increases with an increase in viscosity (ν). Initially the particles of fluid move with a uniform velocity along straight paths. The flow is well ordered and the

moving particles can be visualized to form laminae. As the Reynolds number ($V_{\infty} \ell / \nu$) is increased the orderly pattern ceases and strong mixing of the particles occurs. The pattern of streamlines at a fixed point, as well as the velocity and pressure, becomes subjected to continuous fluctuations and there exists a continuous transport of energy from the main flow into the large eddies. Energy is dissipated, however, by the small eddies. This dissipation process occurs in a narrow strip inside the boundary layer in the region near the solid boundary. The eddies or balls of fluid that are formed have their own intrinsic motion which is superimposed on the main flow. The size of the eddies which are continually formed and dissipated determines the scale of the turbulence, i.e., the size is determined by the external condition of the flow.

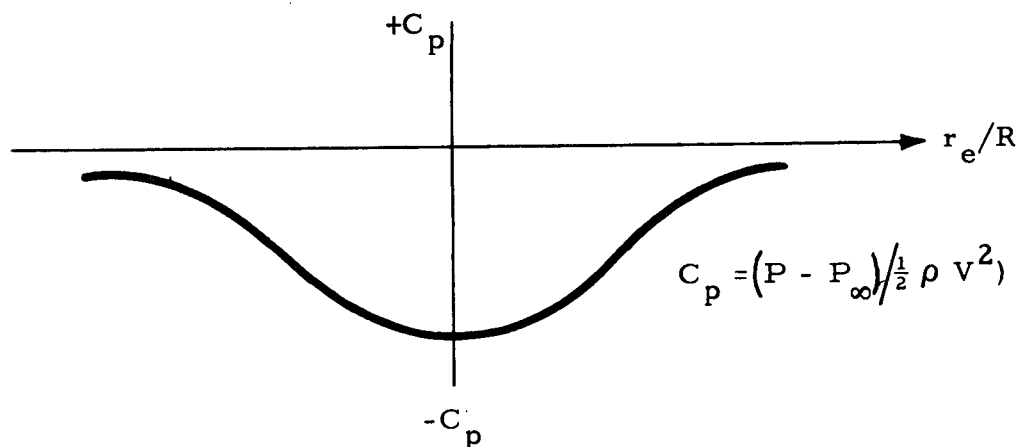
° As would be expected, the velocity at which the eddies are convected downstream varies through the boundary layer. Evidence of this is presented in Schlichting (Ref. A.1), from Nikuradse (Ref. A.2) and Tollmien (Ref. A.3), in photographs taken with a camera which moved with the flow at varying speeds. From correlation of velocity and pressure measurements Willmarth and Wooldridge (Ref. A.4), Bull (Ref. A.5), Serafini (Ref. A.6) and Blake (Ref. A.7) have shown that the convective velocity of the eddies varies with position in the boundary layer and can be associated with the eddy size. These data were obtained from measurements in the boundary layer on a flat plate with zero pressure gradient. The average convective velocity obtained from the broadband space-time correlations of a number of pressure transducers is presented in Fig. A-1 as a function of the separation distance (r) between transducers. For small values of r the convection velocity ratio U_c/U_{∞} begins to decrease significantly as r decreases. These results can be reasonably interpreted by considering that the smaller eddies have a shorter lifetime. Then as the distance between transducers increases, the correlation of the pressure fluctuations decreases, since these are only affected by the larger scale eddies. This implies that the small eddies are concentrated closer to the wall, since these are convected at slower velocities. The eddies in the boundary layer can then be visualized in two limiting regions; one near the wall which contains the smaller scale eddies that travel at low speeds and the other near the outer region which contain the larger scale eddies and move with a velocity approaching U_{∞} .

The physical description of the boundary layer is helpful in considering the results and problems that would occur in measuring the unsteady pressure. The sketch below shows a pressure transducer flush mounted to a flat plate immersed in a viscous flow. Typical nomenclature definitions are presented below.



- d_e = diameter of the eddy
- D = diameter of the transducer
- ω = circular frequency
- δ^* = displacement thickness of the boundary layer
- $k = \omega \delta^* / U_\infty$ (reduced frequency)
- U_c = convective eddy velocity

The pressure distribution in the eddy should be similar to the Rankine combined vortex shown on the following page.



Therefore, the velocity and diameter of the eddy as it moves across the pressure transducer should be related to the frequency of the output as

$$\omega = \frac{U_c}{d_e}$$

If the transducer diameter is larger than one-half the wave length, the measurement will be attenuated.

The energy at various frequencies can also be considered qualitatively by examining the expression for the reduced frequency ($k = \omega \delta^* / U_\infty$),

$$\text{assuming } \delta = O(10 \delta^*)$$

and letting

$$\omega = \frac{K_1 U_\infty}{d_e}$$

then

$$K_1 = 10 \frac{d_e}{\delta} k$$

if $k = 0.1$ then $K_1 = O(d_e/\delta)$. However, as k decreases, i.e., if $k \ll 1$ then d_e/δ must be larger than 1 for reasonable values of K_1 . This implies K_1 approaches 1. Therefore, setting $K_1 = 1$

$$\frac{d_e}{\delta} = \frac{1}{10k}$$

and for $k \ll 1$ implies $d_e > \delta$.

The probability of eddies with diameters larger than δ is relatively small and the energy measured by the transducer at these reduced frequencies should be much lower.

Also, $k \gg 1$ implies that d_e is very small for reasonable values of K_1 (i.e., $K_1 \ll 1$), and the energy content of these eddies sensed by the transducer should be significantly lower. Therefore, from this model, the PSD of the measured pressure should be a maximum between $0.1 \ll k \ll 1.0$ and orders of magnitude lower when $k > 10$ and $k < 0.01$.

The above examination of the physical description also aids in defining the similarity parameters for collapsing the available data. The above analysis suggests that the boundary layer thickness which is related to the eddy diameter (the displacement (δ^*) or momentum (δ_θ) thickness) should be used to nondimensionalize length. This leads to a reduced frequency defined as $k = \omega \delta^*/U$ where U is the local velocity of the external frictionless flow. Experimental and theoretical information on the pressure levels shows reasonably good correlation has been found using \bar{P}_{rms}/q as a parameter. Lilley (Ref. A.8) suggests that \bar{P}_{rms}/τ_w would be a suitable theoretical nondimensionalized parameter, where τ_w is the wall shear stress. This theoretical prediction is dependent on the similarity of the boundary layer velocity profiles. Neither the effects on pressure fluctuations of roughness (Refs. A.7 and A.9) nor those of pressure gradient (Ref. A.10) can be accurately predicted by using τ_w , although some improvement can be seen. Thus, use of τ_w increases the complexity of prediction without any significant advantages.

A number of both wind tunnel and flight test programs have been conducted to measure the fluctuating pressures beneath a turbulent boundary layer for subsonic flow. These data are inconsistent, however, and a number

of difficulties are presented in evaluating the cause of the anomalies. There is little or no uniformity in nondimensionalizing the data and in presenting the results. In most cases of the reported flight measurements no information is furnished about the boundary layer or local flow parameters. These data are normally nondimensionalized by calculated values of the boundary layer thickness and the freestream parameters independent of the body location. Flight measurements are also subject to background noise caused by the engines and turbulence generated by sections of the aircraft upstream of the measurement location. Although the flow conditions are well described for the wind tunnel measurements, the tunnel noise and turbulence can have large effects on the data and both flight and wind tunnel results are subject to errors caused by the frequency limitations of the instrumentation and the inherent loss in sensitivity of a finite size pressure transducer. A summary of the measured values of \bar{P}_{rms}/q_{∞} are presented in Table A-1.

After reviewing these reports and observing the scatter in the data, calculating an average value or performing statistical treatment of all the reported values would be meaningless. The scatter in these data far exceed the possible errors reported by any of the authors. The scatter in the data is not significantly reduced, even upon a selected compilation where data suspected to have attenuation of the high frequency components caused by the data acquisition equipment or transducer size are discarded. It was therefore concluded that the large scatter was either due to error or caused by a subtle difference in the testing techniques or conditions.

The results of the various investigations were further studied only if the following conditions were met

1. $D/\delta^* < 0.5$,
2. Data acquisition equipment with the capacity to accurately record results for large $k = \omega\delta^*/U_{\infty}$ was used,
3. Low background noise,
4. Known (measured) values of the local flow conditions were available, and
5. Details of experimental procedures were reported.

Table A-1
SUMMARY OF EXPERIMENTAL DATA

| Report | \bar{P}_{rms}/q_{∞} | M_{∞} | $\partial P/\partial S$ (psi/in.) | R_{δ}^* (Range) | D/δ^* | Corrected for Trans- ducer Size | $\left(\frac{\bar{P}(\omega) U_{\infty}}{q_{\infty}^2 \delta^*}\right) \left \frac{\omega \delta^*}{U_{\infty}} = 5 \right.$ | Comments |
|--|--|--------------------|--------------------------------------|--|--|---------------------------------------|---|--|
| Speaker & Ailman (Ref. A. 11) | 0.0058 0.0059 0.0070 0.0075 0.0044 | 0.42 | -9×10^{-4} | 4 to 5×10^4 | 3.40 0.66 0.66 0.60 8.00 | Yes | 7×10^{-7} | Wind Tunnel Test |
| | 0.0052 0.0057 0.0050 0.0070 0.0067 | 0.59 | -9×10^{-4} | 2.8 to 8×10^4 | 1.0 1.0 4.5 1.0 0.9 | Yes | 3 to 5×10^{-6} | |
| Serafini (Ref. A. 6) | 0.0074 0.0072 0.0077 0.0068 0.0058 0.0054 0.0048 0.0045 | 0.58 | -1.1×10^{-3} | 2.8 to 8×10^4 | 0.20 0.20 0.20 0.30 1.2 3.4 5.5 9.0 | No | 2×10^{-6} | Wind Tunnel Test |
| Bull (Ref. A. 5) | 0.0045 to 0.0053 | 0.3 | 0 | 1 to 6×10^4 | 0.3 to 1.0 | No | 8×10^{-7} | Wind Tunnel Test |
| Wilby, Bhat & Gloyne (Ref. A. 12) | 0.0053 | 0.78 | — | 1×10^5 | — | Yes | 5×10^{-7} | Flight Test |
| Schloemer (Ref. A. 10) | 0.0052 0.0046 | 0.07 to 0.09 | 0 | 10^4 | 0.406 | Yes No | 6×10^{-7} | Wind Tunnel Test High Frequency Cutoff at 10 kHz or $\omega \delta^*/U_{\infty} = 8$ and Low Cutoff $\omega \delta^*/U_{\infty} \approx 0.2$ |
| | 0.0075 0.00585 | 0.09 to 0.13 | -4.4×10^{-3} | 1.8×10^4 | 0.292 | Yes No | 6×10^{-7} | Low Frequency Cutoff at $\omega \delta^*/U_{\infty} = 0.12$ |
| | 0.00362 0.00502 | 0.14 0.14 | 9×10^{-3} | 3×10^3 | 2.36 | No Yes | 6×10^{-7} | Transducer Very Large |
| Ludwig (Ref. A. 13) | 0.008 to 0.011 | 0.17 to 0.02 | — | — | 0.092 to 0.74 | No | 1 to 8×10^{-4} | Channel or Duct Flow |
| Gibson (Ref. A. 14) | 0.0035 to 0.01 | 0.24 to 0.80 | — | — | 0.36 to 1.54 | No | — | Local Condition Un- known (Flight Test) Large Scatter in Data |
| Leech (Ref. A. 15) | 0.003 to 0.01 | 0.90 to 1.16 | — | — | — | No | — | Flight Test (F 102A Aircraft) Frequency Limited to 2 kHz |
| Willmarth & Wooldridge (Ref. A. 4) | 0.0056 0.0052 0.0049 0.0047 | 0.19 | 0 | 4 to 5.2×10^4 | 0.12 0.21 0.33 0.45 | No | 1×10^{-6} | Wind Tunnel Test Low Frequency Cutoff $\omega \delta^*/U_{\infty} = 0.13$ (High Low Frequency Noise Level) |
| Wiley & Seidl (Ref. A. 16) | 0.006 to 0.02 Sub- sonic Values ≈ 0.01 | 0.6 to 1.08 | — | 3 to 4×10^6 (Per Foot) | — | — | — | Wind Tunnel Test of X 20 Vehicle |

Results of those studies meeting most of the above conditions are tabulated below.

| Report | Mach No. | \bar{P}_{rms}/q_{∞} | Re_{δ^*} (Range) | D/δ^* | Corrected for Transducer Size |
|-----------------------|--------------|--|-----------------------------|-------------------------------|-------------------------------|
| Willmarth (Ref. 4) | 0.19 | 0.0056 0.0052 0.0049 0.0047 0.0050 | 4 to 5.2×10^4 | 0.122 0.21 0.35 0.45 | No |
| Bull (Ref. 5) | 0.3 0.5 | 0.0045 to 0.0053 | 1 to 6×10^4 | 1.0 to 0.3 | No |
| Blake (Ref. 7) | 0.07 0.15 | 0.00876 | 1 to 2×10^4 | 0.11 | No |
| Speaker (Ref. 11) | 0.42 0.59 | 0.0044 to 0.0075 | 2.1 to 2.4×10^4 | 8.0 to 0.60 | Yes |
| Serafini (Ref. 6) | 0.58 | 0.0045 to 0.0075 | 2.5 to 8×10^4 | 9.0 to 0.2 | No |

NOTE: $\partial P/\partial S \approx 0$ for all the above.

The wall pressure spectrum results with the exception of Blake* are presented in Fig. A-2.

As seen in the above table, there is much scatter in the \bar{P}_{rms}/q_{∞} values. Some of the scatter can be attributed to transducer size; however, if values of \bar{P}_{rms}/q_{∞} are compared with results of Willmarth, Bull, Blake and Serafini for D/δ^* of 0.1 to 0.2, \bar{P}_{rms}/q_{∞} still ranges from 0.005 to 0.00876. The only plausible explanation that could be found is the effect of surface roughness. Willmarth and Wooldridge (Ref. A.4) flush-mounted the transducers to a one-inch thick (oil-lapped) steel plate 20 inches in diameter, which was supported independently of the tunnel by a large pedestal. The instrumented plate was flush with the tunnel floor which was a newly installed, varnished and waxed

*The pressure spectrum presented by Blake was inconsistent with his results of \bar{P}_{rms}/q_{∞} . Blake also presented the spectrum obtained by Bull and Willmarth in the same figure and it appears as though all the data were plotted incorrectly.

sheet of masonite extending 14 feet upstream. The holes in the plate for mounting the transducers, which were not in use, were filled with brass plugs. These were fitted within ± 0.001 inches of the surface. On a second series of tests in which even greater care was taken to ensure smooth flush surfaces, a reduction of approximately 13% in the measured value of \bar{P}_{rms}/q_{∞} was noted. Bull (Ref. A.5) reported that the tunnel walls were ground and polished and the transducers mounted in six-inch diameter plugs which were attached to the wall so that the transducer and wall formed a continuous surface. The values of \bar{P}_{rms}/q_{∞} measured by both authors were nearly the same ($\bar{P}_{rms}/q_{\infty} \approx 0.0053 \pm 0.0003$). Serafini (Ref. A.6) does not describe the details of the tunnel nor the installation of the transducers other than that they are flush-mounted. He implies, however, that the tunnel walls were smooth, but not polished. Speaker and Ailman, also, do not describe the installation; however, from photographs presented, the transducers appear to be flush-mounted on an unpolished aluminum plate which had a number of fine scratches on the surface.

Blake (Ref. A.7) flush-mounted the transducers in an aluminum traverse which was flush-mounted with the test surface consisting of a sheet of formica-coated plywood. The aluminum traverse disc was drilled along a diameter for positioning the microphones at various locations. The holes were filled when the disc was not in use; the assembly was reportedly smooth to the touch. A more exact description of the conditions of the surface was not given. Blake also investigated the effect of surface roughness by adhering sand to the test surface and the transducer diaphragm. These results are presented in the table below.

| Wall Designation | \bar{k}_g | k_s | \bar{P}_{rms}/q_{∞} | \bar{P}_{rms}/τ_w |
|------------------|-------------|---------|----------------------------|------------------------|
| Smooth | — | — | 0.00876 | 3.59 |
| S-S | 0.0563" | 0.106" | 0.0202 | 3.83 |
| D-S | 0.0563" | 0.0736" | 0.01605 | 3.2 |
| D-L | 0.092" | 0.192" | 0.0184 | 2.87 |

NOTE: S-S = Small, sparsely packed sand particles
 D-S = Small, densely packed sand particles
 D-L = Large, densely packed sand particles
 \bar{k}_g = Mean geometric roughness height
 k_s = Equivalent hydrodynamic sand roughness height

Coe (Ref. A.17) shows large changes in the pressure fluctuations measured by a transducer as it was moved in and out from a flush position and pressures measured by a flush-mounted transducer positioned 0.118δ downstream. For a change in level of the variable transducer of $0.002 y/\delta$, the output changed approximately 60 to 70%, while the output of the fixed transducer changed approximately 10%. Results of Speaker and Ailman are again of interest since a large number of transducers were aligned in the direction of the flow and the surface was not polished. The \bar{P}_{rms}/q_∞ values are presented in Figs. A-3 and A-4 as a function of the downstream location. Although it can be argued that the increase in \bar{P}_{rms}/q_∞ with distance is due to the change in D/δ^* , the possibility of the progressive effects of the relatively rough surface and transducer misalignments also exist.

The narrow-band convection velocities as measured by Blake (Ref. A.7) and Bull (Ref. A.5) are presented in Fig. A-5. They agree well for $\omega\delta^*/U_\infty > 0.3$; however, for $\omega\delta^*/U_\infty < 0.3$, the pressure fluctuations have low phase velocities which are strongly dependent on the microphone separation distance used in their measurement. The association of these pressure disturbances with a particular eddy system within the boundary layer is difficult. Also, from the earlier analysis of the equation $K_1 = 10 d_e k/\delta$, for $k = O(0.1)$, both high- and low-velocity eddies could contribute to the pressure fluctuations, and large scatter in the measured narrowband convective velocities might be expected. However, it was also shown that as k decreases, the contribution should come from the large, high-speed eddies.

A.3 CONCLUSIONS

Results of the experimental investigations of the characteristics of the fluctuating pressure measured beneath a subsonic turbulent boundary layer are in relatively good agreement for measurements of the broad and narrow band convective velocities; unfortunately, however, in measurements of the spectrum and rms levels of the pressure, the data were scattered. Most of the scatter can be attributed to the attenuation or error caused by the finite size of the transducer or high frequency limitations of the data acquisition systems. However, there is still considerable scatter for data which were obtained when small and approximately equal transducers ($D/\delta^* = 0.1$ to 0.2) were used and which were recorded by equipment capable of obtaining the high-frequency components. The data obtained by Blake (Ref. A.7) show large effects due to surface roughness and data by Coe (Ref. A.17) demonstrate large effects caused by poor alignment of the transducer. This, combined with the variation in the smoothness of the surfaces used in the various investigations, indicates that the quality of the surface could have caused the observed scatter in the data.

REFERENCES

- A.1 Schlichting, H., Boundary Layer Theory, (6th ed.), McGraw-Hill, New York, 1968.
- A.2 Nikuradse, J., Kenematographische Aufnahme einer Turbulentin Strömung, ZAMN 9. 495-496 (1929).
- A.3 Tollmien, W., Turbulente Stromungen., Handb. der Experimentalphysik, Vol. 4, Part I, 291 (1931).
- A.4 Willmarth, W. W., and C. E. Wooldridge, "Measurements of the Correlation Between the Fluctuating Velocities and the Fluctuating Wall Pressure in a Thick Turbulent Boundary Layer," AGARD Report 456, Paris, France, April 1963.
- A.5 Bull, M. K., "Wall-Pressure Fluctuations Associated with Subsonic Turbulent Boundary Layer Flow," J. Fluid Mech., Vol. 28, Part 4, 1967, pp. 719-754.
- A.6 Serafini, J. S., "Wall Pressure Fluctuations and Pressure Velocity Correlations in Turbulent Boundary Layers," AGARD Report 453, Paris, France, April 1963.
- A.7 Blake, W. K., "Turbulent Boundary Layer Wall Pressure Fluctuations on Smooth and Rough Walls," Report No. 70208-1, Massachusetts Institute of Technology, Cambridge, Mass., January 1969.
- A.8 Lilley, G. M., "Pressure Fluctuations in an Incompressible Turbulent Boundary Layer," Rpt. 133, College of Aeronautics, Cranfield, England, 1960.
- A.9 Willmarth, W. W., "Turbulent Boundary Measurements of the Fluctuating Pressure at the Wall Beneath a Thick Turbulent Boundary Layer," J. Fluid Mech., Vol. 21, Part 1, January 1965, pp. 107-109.
- A.10 Schloemer, H. H., "Effects of Pressure Gradients on Turbulent Boundary-Layer Wall-Pressure Fluctuations," J. Acoust. Soc. Am., Vol. 42, July 1967, pp. 93-113.
- A.11 Speaker, W. V., and C. M. Ailman, "Spectra and Space-Time Correlations of the Fluctuating Pressures at a Wall Beneath a Supersonic Turbulent Boundary Layer Perturbed by Steps and Shock Waves," NASA CR-486, Washington, D. C., May 1966.

- A.12 Wilby, J. F., W. V. Bhat and F. L. Gloyna, "Airplane Fuselage Response to Turbulent Boundary Layers," 70-WA/DE-10, American Society of Mechanical Engineers, New York, N. Y., December 1970.
- A.13 Ludwig, G. R., "An Experimental Investigation of the Sound Generated by Thin Steel Panels Excited by Turbulent Flow (Boundary Layer Noise)," UTIA Report No. 87, Institute of Aerophysics, University of Toronto, Toronto, Canada, November 1962.
- A.14 Gibson, J. S., "Boundary Layer Noise Measurements on a Large Turbofan Aircraft," 70th Meeting of Acoustical Society of America, St. Louis, Mo., November 1965.
- A.15 Leech, F. J., and V. E. Sackschewsky, "Boundary Layer Noise Measurements of the F-102 Aircraft," MRL-TDR-62-71, Wright-Patterson Air Force Base, Ohio, August 1962.
- A.16 Wiley, D. R., and M. G. Seidl, "Aerodynamic Noise Tests on X-20 Scale Models, Volume II, Summary and Analysis Report," AFFDL-TR-65-192, Vol. II, Wright-Patterson Air Force Base, Ohio, November 1965.
- A.17 Coe, C. F., "Surface-Pressure Fluctuations Associated with Aerodynamic Noise," NASA SP-207, Washington, D. C., July 1969, pp. 409-424.

A-14

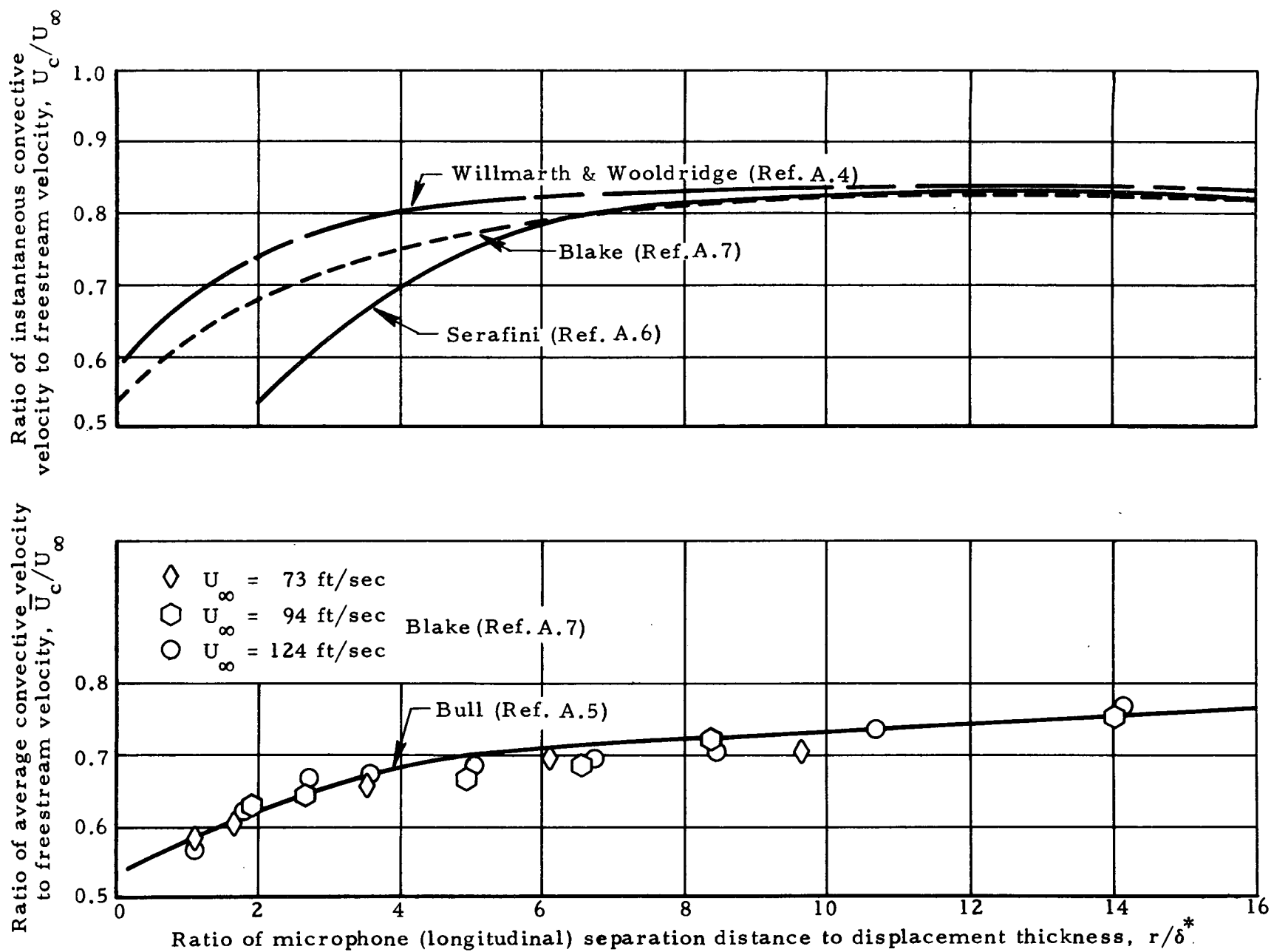


Fig. A-1 - Broad Band Convection Velocities

A-15

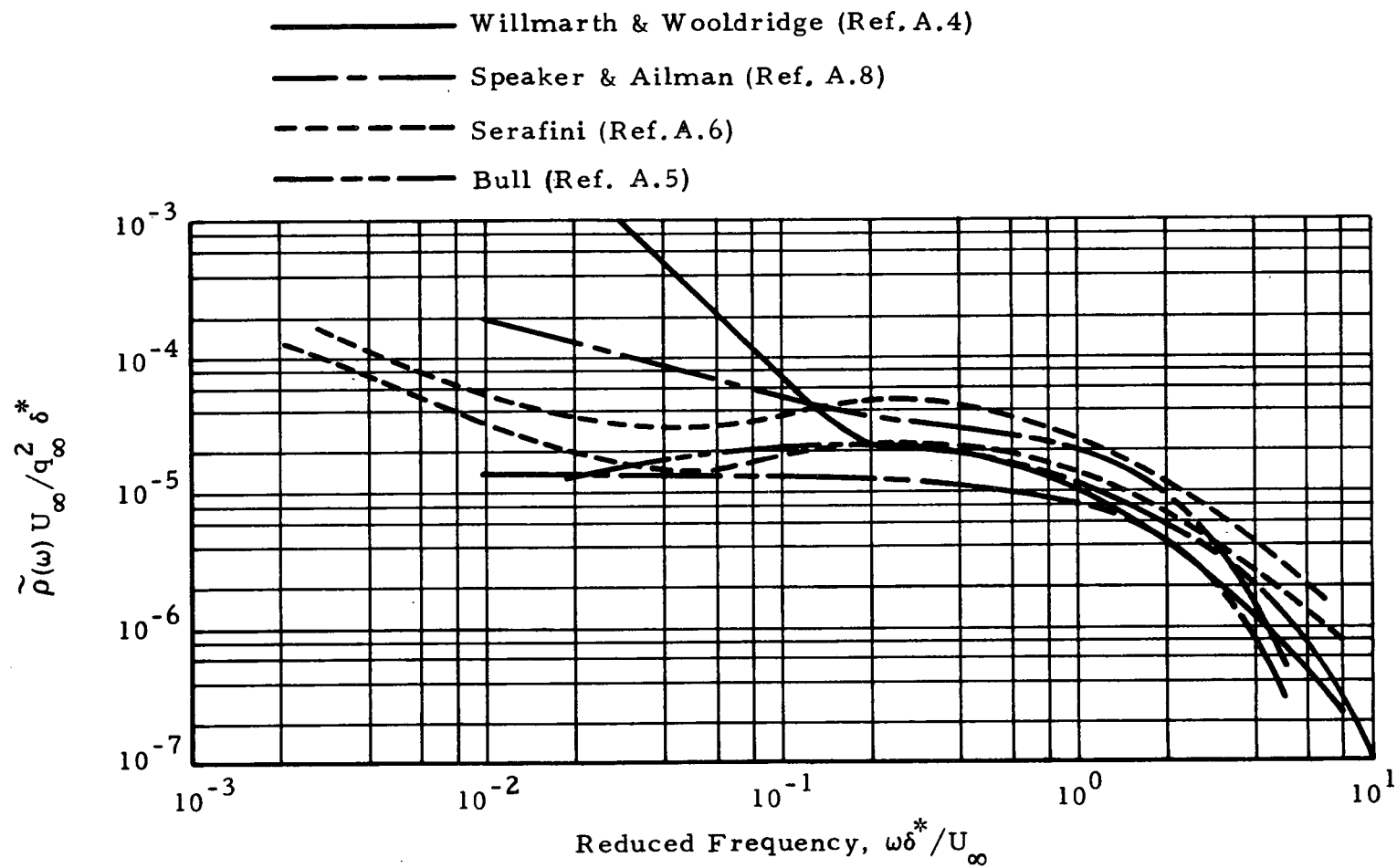
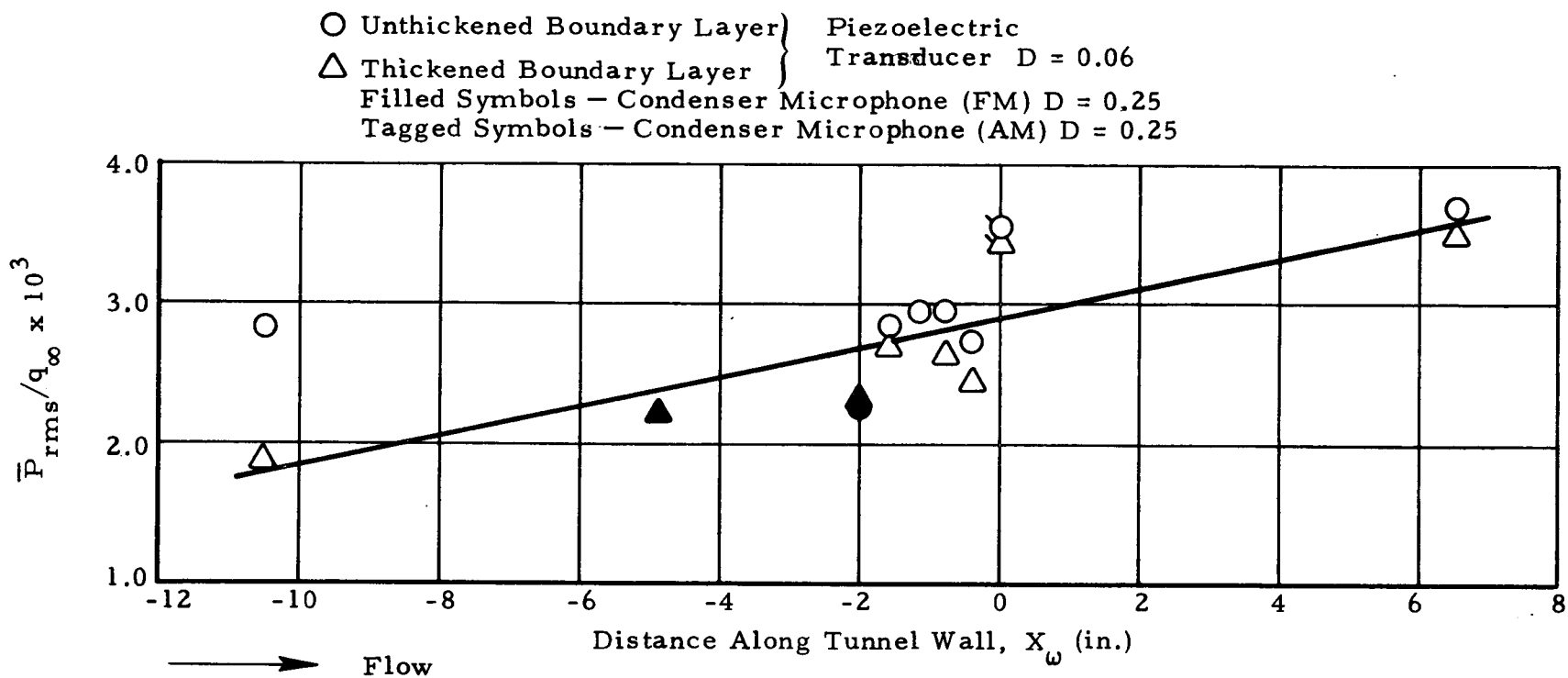
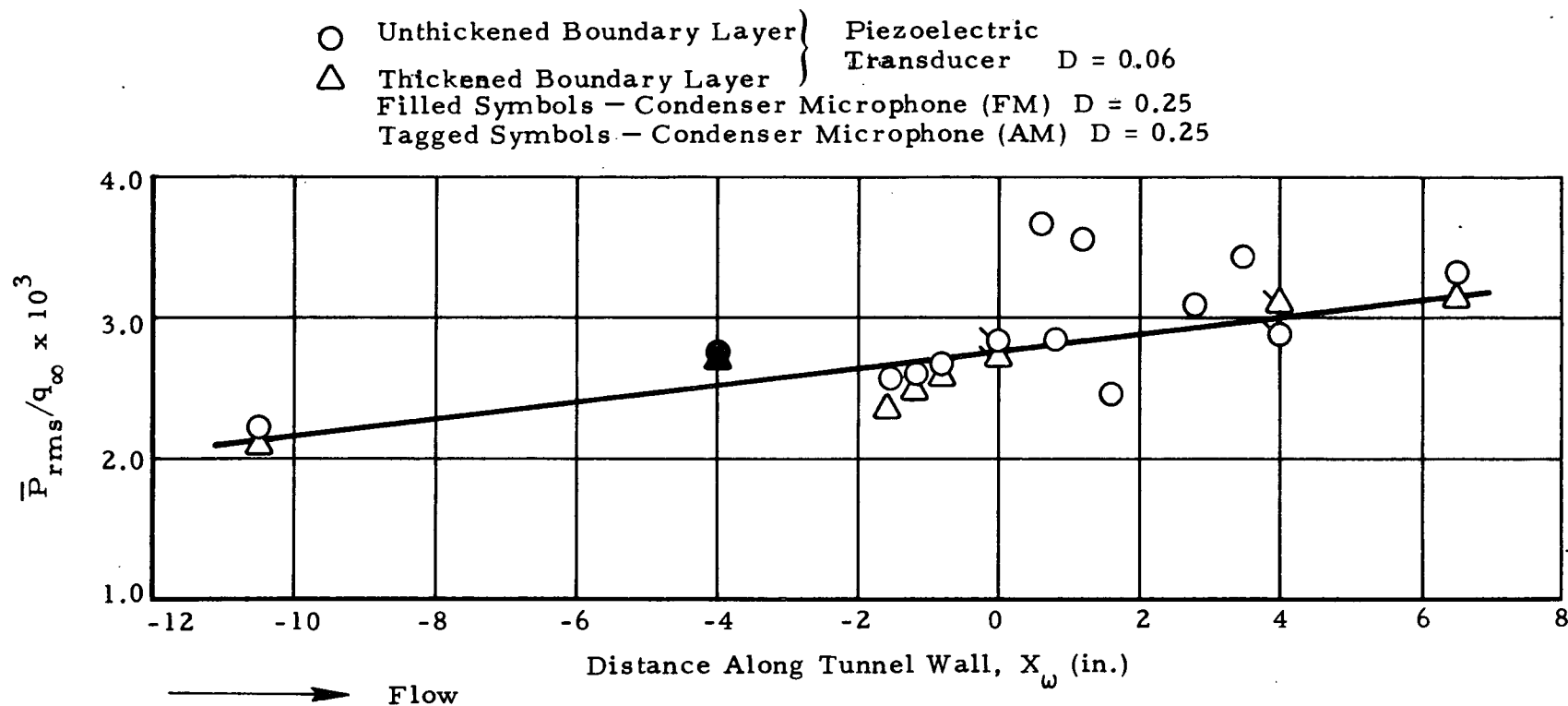


Fig. A-2 - Mean-Square Spectra of Wall Pressure Fluctuations

A-16

Fig. A-3 - Variation of the rms Pressure Fluctuations Along the Tunnel Wall, $M_{\infty} = 0.42$

A-17

Fig. A-4 - Variation of the rms Pressure Fluctuations Along the Tunnel Wall, $M_\infty = 0.59$

A-18

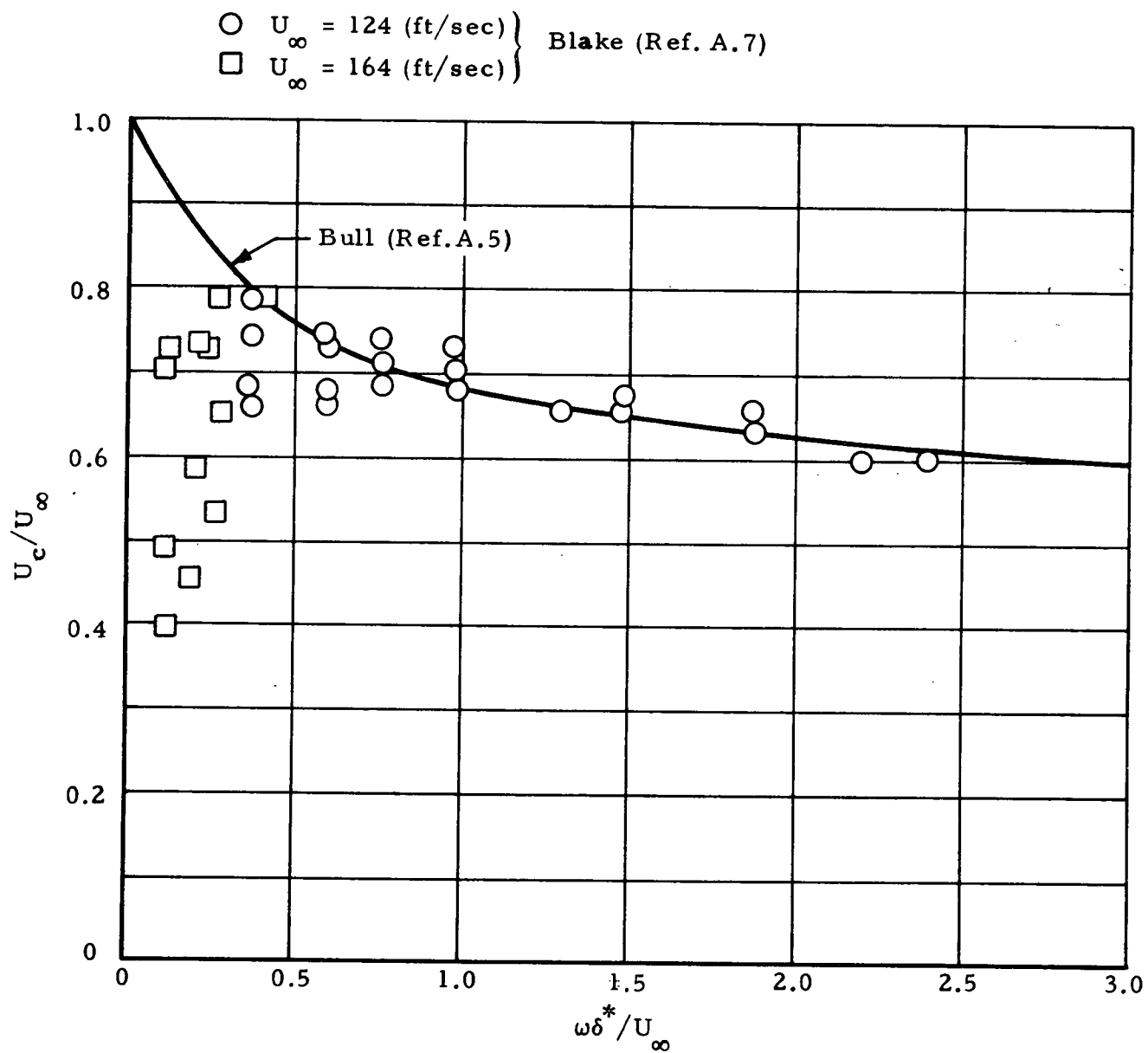


Fig. A-5 - Narrow Band Convective Velocities

Appendix B
RESPONSE COMPUTER PROGRAM

Appendix B

B.1 DISCUSSION

This program is written in Fortran V for the Univac 1108 computer at Marshall Space Flight Center. It uses as input the output tape from the Structural Network Analysis Program (SNAP) along with data cards. The SNAP output tape provides the natural frequencies and mode shapes, normalized to unit generalized mass, of a panel structure to be exposed to a reverberant acoustic field. The data cards provide the power spectral density of the acoustic field, the damping values of the panel modes, designation of the panel modes to be used in the analysis, designation of the joints in the finite element model to be used in the double area integration over the mode shapes, and designation of the joint where the response is to be determined. The primary output of the program is four SC 4020 plots, giving the power spectral densities of the response displacement and acceleration using both linear and log-log scales. Although the program was written for a reverberant acoustic field, it can be easily modified to handle other types of acoustic fields by changing the spatial correlation (designated SC in the program) calculation. However, the program is designed strictly for panel-type response and only determines response perpendicular to the plane of the panel.

B.2 ORIENTATION OF PANEL

In the SNAP analysis, the axis perpendicular to the plane of the panel must be of the first coordinate axis. The plane of symmetry, if used, must be the plane of the first and third coordinate axes.

B.3 MAIN PROGRAM LISTING

```

*FOR,LI  PSP,RSP
      INTEGER R
      DIMENSION RM(6,600) , RP(3,1200) , RC(3600) , S(546,10) , X(546)
1      , Y(546) , IL(546) , A(546) , F(500) , DS(500) , AS(500)
2      , WS(10) , IM(10) , WSQ(100) , GMAS(100) , D(10)
3      , P(500) , PR(500,2) , VS(2,2) , TL(6) , HD(6,2)
4      , HG1(12) , HG2(12) , IP(2) , HG(12,2) , TX(10)
5      , TY(10) , TLM(2,2) , BLM(2,2) , GLM(2) , RLM(2)
6      , SR(10)
      EQUIVALENCE (RM,RP,RC,F) , (RC(501),DS,PR) , (RC(1001),AS)
1      , (RC(2001),A) , (RC(3),JT)
2      , (RC(4),MT) , (RC(5),WSQ) , (RC(105),GMAS)
3      , (RC(1501),P) , (VS,VD) , (VS(1,2),VA)
4      , (HG,HG1) , (HG(1,2),HG2)
      NAMELIST /JNTS/NJ,IL,NM,IM,JTN,R,NS
1      /FREQ/NF,F,A,D,P,TL
      DATA PI/3.14159265/P21/6.2831853/P41/12.5663706/IP/0,1/CBF/'00000
10'/' HD/72HDISPLACEMENT RESPONSE IN INCHES ACCELERATION RESPO
2NSE IN G'S /
3      HG1/72HTPS PANEL VA
4R = 0. F /
5      HG2/72H JOINT RM
6S = 0. E /BZM/' 00--'/BLM(1,1),BLM(1,2),GLM(1)/3*0.0/
7TY/' POWER SPECTRAL DENSITY '/'
8TX/' FREQUENCY (HZ) '/'
      READ (5,JNTS)
      WRITE (6,JNTS)
      IF (NS.LT.0) NS = 0
      IF (NS.GT.NJ) NS = NJ
      NZ = NS + 1
      CALL NTRAN (10,10)
      CALL NTRAN (10,2,204,RC,LSTA)
      CALL NTRAN (10,22)
      IF (LSTA) 9000
      WRITE (6,2) RC(1),RC(2),JT,MT,(WSQ(I),I=1,MT),(GMAS(I),I=1,MT)
2 FORMAT ('1DATE ',A6,' , TIME ',A6,' , JT = ',I6,' , MT = ',I6/
1      (10X,5E20.8))
      IF (MT-IM(NM)) 9999
      IF (JT-JTN) 9999,.9999
      J3T = 3*JT
      J6T = 6*JT
      DO 4 I=1,NM
      J = IM(I)
      WS(I) = WSQ(J)
4 CONTINUE
      CALL NTRAN (10,2,J3T,RC,LSTA)
      CALL NTRAN (10,22)
      IF (LSTA) 9000

```

NOT REPRODUCIBLE

```

DO 6 K=1,NJ
  J = II(K)
  X(K) = RP(2,J)
  Y(K) = RP(3,J)
6 CONTINUE
  CALL NTRAN (10,7,IM(1))
  DO 12 M=1,NM
    CALL NTRAN (10,2,J6T,RC,LSTA)
    CALL NTRAN (10,22)
    IF (LSTA) 9000
  DO 10 J=1,NJ
    I = IL(J)
    S(J,M) = RM(1,I)
10 CONTINUE
    SR(M) = RM(1,R)
    IF (NM-M) 12,12
    I = IM(M+1) - IM(M) - 1
    IF (I) 12,12
    CALL NTRAN (10,7,I)
12 CONTINUE
  READ (5,FRFQ)
  DO 16 M=1,NM
    D(M) = 4.0*D(M)*D(M)
16 CONTINUE
  DO 60 L=1,NF
    DA = 0.0
    W = P2I*F(L)
    W2 = W*W
    WDC = W/13400.0
  DO 50 M=1,NM
    AJ = 0.0
    IF (NS) ,41
  DO 40 J=1,NS
    AJ = AJ + (S(J,M)*A(J))**2
    NK = J - 1
    IF (NK) ,40
  DO 30 K=1,NK
    DL = SQRT ((X(J)-X(K))**2 + (Y(J)-Y(K))**2) * WDC
    SC = SIN (DL) / DL
    AJ = AJ + SC*S(J,M)*S(K,M)*A(J)*A(K)*2.0
30 CONTINUE
40 CONTINUE
    IF (NS-NJ) ,46
41 CONTINUE
  DO 45 J=NZ,NJ
    DL = 2.0 * X(J) * WDC
    SC = SIN (DL) / DL
    AJ = AJ + 0.5 * (1.0+SC) * (S(J,M)*A(J))**2

```

NOT REPRODUCIBLE

```

      IF (NS) .43
DO 42 K=1,NS
      DL = SQRT ((X(J)-X(K))**2 + (Y(J)-Y(K))**2) * WDC
      SC = SIN (DL) / DL
      AJ = AJ + SC*S(J,M)*S(K,M)*A(J)*A(K)*2.0
42 CONTINUE
43 CONTINUE
      NK = J - 1
      IF (NK-NZ) 45
DO 44 K=NZ,NK
      DL = SQRT ((X(J)-X(K))**2 + (Y(J)-Y(K))**2) * WDC
      SC1= SIN (DL) / DL
      DL = SQRT ((X(J)+X(K))**2 + (Y(J)-Y(K))**2) * WDC
      SC2= SIN (DL) / DL
      SC = SC1 + SC2
      AJ = AJ + SC*S(J,M)*S(K,M)*A(J)*A(K)
44 CONTINUE
45 CONTINUE
46 CONTINUE
      DA = DA + AJ* (SR(M)**2) / ((WS(M)-W2)**2 + D(M)*WS(M)*W2)
50 CONTINUE
      DS(L) = P(L) * DA
      AS(L) = 0.6709E-5 * W2 * W2 * DS(L)
60 CONTINUE
      FI = F(2) - F(1)
      FIV = F(NF) - F(NF-1)
      VD = DS(1)*FI + DS(NF)*FIV
      VA = AS(1)*FI + AS(NF)*FIV
DO 64 L=3,NF
      FI = F(L) - F(L-2)
      VD = VD + DS(L-1)*FI
      VA = VA + AS(L-1)*FI
64 CONTINUE
      VD = 0.5*VD
      VA = 0.5*VA
      VS(2,1) = SQRT(VD)
      VS(2,2) = SQRT(VA)
      WRITE (6,66) TL,R,VS,(DS(I),I=1,NF)
66 FORMAT ('1TPS PANEL',6A6,6X,'JOINT',15,'0DISPLACEMENT RESPON
1E',6X,'VAR = ',E16.8,6X,'RMS = ',E16.8,' INCHES',10'ACCELERATION RE
2SPONSE',6X,'VAR = ',E16.8,6X,'RMS = ',E16.8,4H G'S',10'DISPLACEMENT
3SPECTRUM',10'5E20.8))
      WRITE (6,68) (AS(I),I=1,NF)
68 FORMAT ('1ACCELERATION SPECTRUM',10'5E20.8))
      WRITE (6,70) (F(I),I=1,NF)
70 FORMAT ('1FREQUENCIES',10'5E20.8))
DO 72 I=1,6
      HG1(I+2) = TL(I)

```

NOT REPRODUCIBLE

```

72 CONTINUE
  CALL PLOTIN (9)
  CALL BNBCDV((FLOAT(R)+0.01),NPR,NDS)
    NPR = OR(NPR,CBF)
    K1 = 46 - NDS
  CALL MOVST (NDS,K1,HG2,0,NPR)
    RLM(1) = F(NF)
  CALL MXMNLG (NF,DS,BLM(2,1),TLM(1,1))
  CALL MXMNLG (NF,AS,BLM(2,2),TLM(1,2))
  CALL LOGLIM (1.0,F(1),F(NF),GLM(2),RLM(2))
  CALL LOGLIM (1.0,BLM(2,1),TLM(1,1),BLM(2,1),TLM(2,1))
  CALL LOGLIM (1.0,BLM(2,2),TLM(1,2),BLM(2,2),TLM(2,2))
  DO 90 K=1,2
  DO 78 I=1,6
    HG2(I) = HD(I,K)
78 CONTINUE
  DO 80 I=1,2
    CALL BNBCDV (VS(I,K),NPR,NDS)
      NPR = OR(NPR,CBF)
    CALL MOVST (5,60,HG(1,I),0,NPR)
    CALL BNBCDV((FLOAT(NDS)),NPR,K1)
      NPR = OR(NPR,CBF)
    CALL MOVST (3,67,HG(1,I),1,BZM)
      IF (NDS) ,80
      K2 = 70 - K1
    CALL MOVST (K1,K2,HG(1,I),0,NPR)
      IF (NDS) ,80
    CALL MOVST (1,67,HG(1,I),5,BZM)
80 CONTINUE
  DO 82 I=1,2
    CALL GRIDPL (IP(I),IP(I),20,1,NF,F,PR(1,K),GLM(I),RLM(I),BLM(I,K),
1      TLM(I,K),TX,TY,HG1,HG2)
82 CONTINUE
90 CONTINUE
  CALL ENDPLT
  GO TO 9999
9000 WRITE (6,9001) LSTA
9001 FORMAT ('ONTRAN READ ERROR , LSTA = ',I4)
  CALL FRROFF
9999 STOP
  END

```

NOT REPRODUCIBLE

B.4 SUBROUTINE PROGRAM LISTINGS

```

*FOR,LI PTN,PTN
SUBROUTINE PLOTIN (IC)
EXTERNAL TABLIV
DIMENSION ADARY(22)
DATA ADARY/6HONF HA,6HRDCOPY,20*6H /
DATA DL/20.0/
CALL IDENT (IC,ADARY)
CALL SFTMIV (24,0,30,54)
CALL CHSIV (2,2)
CALL RITSTV (12,18,TABLIV)
RETURN
ENTRY GRIDPL (LX,LY,IP,IL,N,X,Y,XL,XR,YB,YT,TX,TY,H1,H2)
DIMENSION H1(12) , H2(12) , TX(10) , TY(10) , X(N) , Y(N)
CALL SMXYV (LX,LY)
CALL DXDYV (1,XL,XR,DX,LVR,LVL,NX,DL,IER)
CALL DXDYV (2,YB,YT,DY,LHR,LHL,NY,DL,IER)
IF (LX) ,2
  DX = 1.0
  LVR = 10.0
  LVL = 10.0
2 IF (LY) ,4
  DY = 1.0
  LHR = 10.0
  LHL = 10.0
4 CALL GRIDIV (4,XL,XR,YB,YT,DX,DY,LVR,LHR,-LVL,-LHL,NX,-3)
CALL RITE2V (148,1015,1023,90,1,72,1,H1,IER)
CALL RITE2V (148,991,1023,90,1,72,1,H2,IER)
CALL RITE2V (220,8,1023,90,1,60,1,TX,IER)
CALL RITE2V (8,140,1023,180,1,60,1,TY,IER)
ENTRY ADLINE (IP,IL,N,X,Y)
CALL XSCLV1 (X(1),NX1,IER)
CALL YSCLV1 (Y(1),NY1,IER)
CALL PLOTV (NX1,NY1,IP,0)
DO 10 K=2,N
  CALL XSCLV1 (X(K),NX2,IER)
  CALL YSCLV1 (Y(K),NY2,IER)
  CALL PLOTV (NX2,NY2,IP,0)
IF (IL) 8,8
  CALL LINEV (NX1,NY1,NX2,NY2)
8 NX1 = NX2
  NY1 = NY2
10 CONTINUE
RETURN
ENTRY ENDPLT
CALL ENDJOB
RETURN
END

```

NOT REPRODUCIBLE

```

*FOR,LI  MML,MML
  SUBROUTINE MXMNLG (N,X,B,T)
  DIMENSION X(N)
    T = X(1)
    B = T
  DO 1 K=2,N
    IF (X(K).LT.1.0E-38) X(K) = 1.0E-38
    IF (X(K).GT.T) T = X(K)
    IF (X(K).LT.B) B = X(K)
1 CONTINUE
  RETURN
  END

```

```

*FOR,LI  LGM,LGM
  SUBROUTINE LOGLIM (F,B,T,BL,TL)
    BL = ALOG10 (B) / F
    IF (BL.LT.0.0) BL = BL - 1.0
    BL = F*AIN(T)(BL)
    TL = ALOG10 (T) / F
    IF (TL.GT.0.0) TL = TL + 1.0
    TL = F*AIN(T)(TL)
    IF ((TL-BL).GT.7.0) BL = TL - 7.0
    BL = 10.0 ** BL
    TL = 10.0 ** TL
  RETURN
  END

```

NOT REPRODUCIBLE

B.5 DATA CARD INPUT

This input data is read in Namelist format. Namelist JNTS contains

| | | |
|-----|---|--|
| JTN | = | total number of joints in the finite element model |
| R | = | joint number where response prediction is desired |
| NJ | = | number of joints to be used in the double area integration |
| IL | = | array of NJ joint numbers to be used in the double area integration (If the plane-of-symmetry method was used in SNAP, any joint numbers located in the plane of symmetry must precede the other joint numbers.) |
| NS | = | number of joints in the IL array that are located in the plane of symmetry, if the plane-of-symmetry method was used in SNAP (If the plane-of-symmetry method was not used, NS must be equal to NJ.) |
| NM | = | number of panel modes to be used in the analysis |
| IM | = | array of NM mode numbers to be used in the analysis. |

Namelist FREQ contains

| | | |
|----|---|---|
| TL | = | 36 character title that will appear on the plots and printout |
| A | = | array of NJ areas that contain the panel area represented by the corresponding joint number in the IL array |
| D | = | array of NM damping values for the corresponding modes in the IM array |
| NF | = | number of frequencies for power spectral density calculations |
| F | = | array of NF frequencies where power spectral densities are to be calculated |
| P | = | array of NF values of the power spectral density of the acoustic excitation field for the corresponding frequencies in the F array. |

B.6 SAMPLE DATA CARDS

\$UNTS JTN = 594, R = 53, NS = 8,

NJ = 96,

IL = 5, 7, 9, 11, 12, 14, 16, 18,
47, 49, 51, 53, 54, 56, 58, 60,
89, 91, 93, 95, 96, 98, 100, 102,
131, 133, 135, 137, 138, 140, 142, 144,
173, 175, 177, 179, 180, 182, 184, 186,
215, 217, 219, 221, 222, 224, 226, 228,
257, 259, 261, 263, 264, 266, 268, 270,
299, 301, 303, 305, 306, 308, 310, 312,
341, 343, 345, 347, 348, 350, 352, 354,
383, 385, 387, 389, 390, 392, 294, 396,
425, 427, 429, 431, 432, 434, 436, 438,
446, 448, 450, 452, 453, 455, 457, 459,

NM = 5, IM = 1, 2, 3, 4, 5,

\$END

\$FREQ TL = 36H HAYNES 25 ALLOY L-605 ,

A = 3*1.5, 2*1.125, 3*1.5,
3*3.0, 2*2.25, 3*3.0,
3*3.0, 2*2.25, 3*3.0,
3*3.0, 2*2.25, 3*3.0,
3*3.0, 2*2.25, 3*3.0,
3*3.0, 2*2.25, 3*3.0,
3*3.0, 2*2.25, 3*3.0,
3*3.0, 2*2.25, 3*3.0,
3*3.0, 2*2.25, 3*3.0,
3*2.5, 2*1.875, 3*2.5,
3*2.0, 2*1.5, 3*2.0,

D = 5*0.05

NF = 51,

F = 10, 20, 30, 40, 50, 60, 70, 80, 90, 100, 106, 110,
113.09774,

116, 120, 130, 140, 150, 160, 170, 180, 185, 190, 193,
195, 197.75882,

200, 202, 204, 206, 208, 210, 211, 212,
212.65793, 213, 214, 215,
215.82162, 215.90176, 215.98190,

217, 218, 220, 222, 224, 227, 230, 235, 240, 250,
P = 20.5E-5, 18.2E-5, 15.0E-5, 12.9E-5, 12.9E-5, 16.0E-5,
18.5E-5, 5*20.5E-5,
3*20.5E-5, 20.0E-5, 19.0E-5, 17.5E-5,
16.3E-5, 14.8E-5, 13.3E-5, 12.5E-5, 11.8E-5, 11.4E-5,
11.1E-5, 10.7E-5, 10.3E-5, 10.1E-5, 9.9E-5, 9.8E-5,
9.6E-5, 9.5E-5, 9.4E-5, 2*9.3E-5, 9.2E-5, 9.1E-5,
9.1E-5, 3*9.0E-5, 8.9E-5, 8.8E-5, 8.7E-5, 8.6E-5,
8.4E-5, 8.2E-5, 8.0E-5, 7.6E-5, 7.2E-5, 6.5E-5,

\$END

NOT REPRODUCIBLE